$\mathcal{L}_1$ Adaptive Control for Safety-Critical Systems

NASA LANGLEY/SEAN SMITH

GUARANTEED ROBUSTNESS WITH FAST ADAPTATION

NAIRA HOVAKIMYAN, CHENGYU CAO, EVGENY KHARISOV, ENRIC XARGAY, and IRENE M. GREGORY

Digital Object Identifier 10.1109/MCS.2011.941961
Date of publication: 16 September 2011

Safety-critical systems appear in several application areas, such as transportation and air-traffic control systems, nuclear plants, space systems, and operating rooms in hospitals. Reliable control of these systems requires not only meeting performance specifications in the presence of multiple constraints, which together ensure predictable response of the overall system and safe operation, but also graceful performance degradation when the

1066-033X/11/$26.00©2011IEEE

underlying assumptions are violated. Figure 1 explains this requirement for flight control applications. The green region for angle of attack and sideslip represents the normal flight envelope, where the airplane usually flies in the absence of abnormalities. The light blue area represents configurations for which high-fidelity nonlinear aerodynamic models of the aircraft are available from wind-tunnel data. Outside this wind-tunnel data envelope, the aerodynamic models available are typically obtained by extrapolating wind-tunnel test data and hence are highly uncertain. This fact suggests that pilots might not be adequately trained to fly the aircraft in these regimes. Moreover, it is not reasonable to rely on a flight control system to compensate for the uncertainty in these flight conditions, since aircraft controllability is not guaranteed in such regimes. The main objective of the flight control system therefore, from safety considerations, is to ensure that an aircraft, suddenly experiencing an adverse flight regime or an unexpected failure, does not "escape" its α–β wind-tunnel data envelope, provided that enough control authority remains. This objective requires that the control system quickly adapt to the failure with guaranteed and uniform transient performance specifications to ensure the safety of the aircraft.

Typical performance specifications in control applications include transient and steady-state performance, as well as robustness margins that the control engineer must be able to trade off in a systematic way subject to hardware constraints, such as CPU, sampling rates of sensors and actuators, and control channel bandwidth. This viewpoint has led to certification of flight control laws for commercial aviation, where the certification protocols rely on the gain and phase margins of the gain-scheduled controllers computed for all operating points [1]. This process is repeated for each aircraft, rendering the overall verification and validation (V&V) expensive. The price of this process increases with growing system complexity.

$\mathcal{L}_1$ adaptive-control theory is motivated by the emerging need to certify advanced adaptive flight critical systems with a more affordable V&V process. On the one hand, this objective requires the development of a control architecture with a priori quantifiable transient and steady-state performance specifications and robustness margins. On the other hand, achieving this objective appears to be possible with an architecture that enables fast and robust adaptation with uniform performance bounds [2, Def. 4.6] without losing robustness. In this context, *fast adaptation* indicates that the adaptation rate in $\mathcal{L}_1$ architectures is to be selected so that the time scale of the adaptation process is faster than the time scales associated with plant parameter variations and the underlying closed-loop dynamics. *Robust adaptation* indicates that, despite fast adaptation in $\mathcal{L}_1$ architectures, the robustness properties of the closed-loop adaptive system can be adjusted independently of the adaptation rate. Because the emphasis is on uniform performance bounds for transient and steady-state operation, a sufficient condition for stability and performance is derived in terms of $\mathcal{L}_1$-norms of the underlying transfer functions, which leads to uniform bounds on the $\mathcal{L}_\infty$-norms of the input-output signals. Therefore, the underlying theory is named $\mathcal{L}_1$ *adaptive-control theory*. For the definition and properties of the $\mathcal{L}_1$-norm of a system see "$\mathcal{L}_1$-Norm of a System."

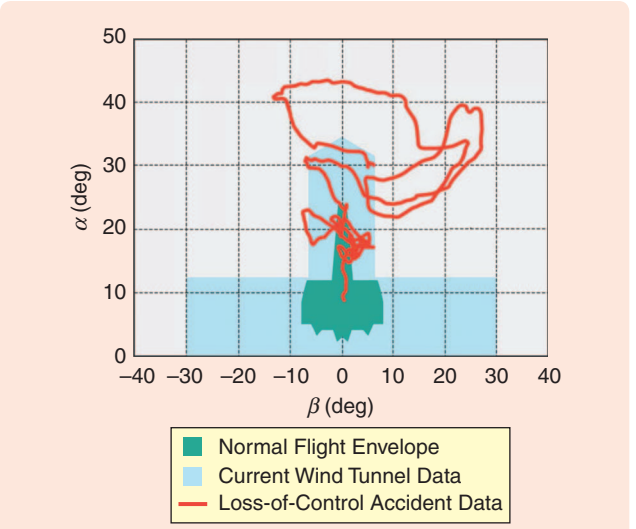

FIGURE 1 Loss of control accident data relative to angle of attack α and sideslip β (from [77]). Angle of attack α and angle of sideslip β are two of the state variables describing aircraft dynamics. The green region is the combination of these variables associated with the normal flight envelope. The light blue area corresponds to configurations for which there are accurate models based on wind-tunnel data. The gray area corresponds to configurations for which the aerodynamic data are extrapolated from the light blue area and are highly uncertain. This fact suggests that pilots might not be correctly trained to fly the aircraft in these $\alpha-\beta$ conditions and can potentially cause dangerous oscillations, known as pilot-induced oscillations.

The key feature of $\mathcal{L}_1$ adaptive-control architectures is guaranteed robustness in the presence of fast adaptation, which leads to uniform performance bounds both in transient and steady-state operation, thereby eliminating the need for gain scheduling of the adaptation rates [3]. These properties can be achieved by appropriate formulation of the control objective with the understanding that uncertainty in a feedback loop cannot be compensated outside of the control channel bandwidth. By explicitly building the robustness specification into the problem formulation, it is possible to decouple adaptation from robustness and increase the speed of adaptation, subject only to hardware limitations. With $\mathcal{L}_1$ adaptive-control architectures, large learning gains appear to be beneficial both for performance and robustness, while the tradeoff between the two is resolved by selecting the underlying filter structure. The latter is a linear problem and thus can be addressed using conventional methods from classical and robust control. Moreover, the performance bounds of $\mathcal{L}_1$ adaptive-control

$\mathcal{L}_1$-Norm of a System

The $\mathcal{L}_1$-norm of a system sets the relation between the peak values of the system's input and output. The $\mathcal{L}_1$-norm is also called the peak-to-peak gain of a system.

Let $G(s)$ be a proper and exponentially stable system. Assume zero initial conditions. Then, for the bounded input $u(t)$, its output $y(t)$ can be written as

$$y(t) = g(t) * u(t) = \int_0^t g(t-\tau)u(\tau)d\tau,$$

where "$*$" denotes the convolution operator, and $g(t)$ is the impulse response of $G(s)$. Letting

$$\|y\|_{\mathcal{L}_\infty} \triangleq \sup_{t\geq 0}|y(t)|,$$

we obtain the bound

$$\begin{aligned}|y(t)| &= \left|\int_0^t g(\tau)u(t-\tau)d\tau\right| \\ &\leq \int_0^t |g(\tau)\|u(t-\tau)|\,d\tau \\ &\leq \int_0^\infty |g(\tau)|\,d\tau\,\|u\|_{\mathcal{L}_\infty}.\end{aligned}$$

The $\mathcal{L}_1$-norm of $G(s)$ is defined as

$$\|G(s)\|_{\mathcal{L}_1} \triangleq \int_0^\infty |g(\tau)|d\tau,$$

which leads to the bound

$$\|y\|_{\mathcal{L}_\infty} \leq \|G(s)\|_{\mathcal{L}_1}\|u\|_{\mathcal{L}_\infty}. \tag{S1}$$

Notice that the bound in (S1) holds if and only if the system $G(s)$ is exponentially stable and proper [4]. For unstable or improper systems the $\mathcal{L}_1$-norm does not exist, since the impulse response is unbounded.

For the m-input, l-output exponentially stable, proper system $G(s)$, the $\mathcal{L}_1$-norm is defined by

$$\|G(s)\|_{\mathcal{L}_1} \triangleq \max_{i=1,\ldots,l}\left(\sum_{j=1}^m \int_0^\infty |g_{ij}(\tau)|d\tau\right),$$

where $g_{ij}(t)$ is the (i,j) entry of the impulse-response matrix of the system $G(s)$. If $G_1(s)$ and $G_2(s)$ are exponentially stable proper systems, then

$$\|G(s)\|_{\mathcal{L}_1} \leq \|G_2(s)\|_{\mathcal{L}_1}\|G_1(s)\|_{\mathcal{L}_1},$$

where $G(s) = G_2(s)G_1(s)$ [4].

architectures can be analyzed to determine the extent of the modeling of the system required for the given hardware.

This article uses a scalar example to explain the key concept of this theory in terms of decoupling adaptation from robustness. Additional details are given in [4]. We also describe extensions for a broader class of systems involving unknown input gain and unmodeled dynamics. A simpler version of this analysis is presented in [5] for a scalar example. Here we extend the discussion from [5] to systems of arbitrary dimension with unknown input gain. Two benchmark examples are used to illustrate robustness and performance tradeoffs, Rohrs's example, and the two-cart system. For more details we refer the reader to [4] and [6]. Key theorems and lemmas that support the theoretical results are stated in sidebars with appropriate references, without the details of proofs. Several flight test examples are included as real-world applications. Additional detail on the flight test results is given in [7] and [8].

FROM THE "BRAVE ERA" TO $\mathcal{L}_1$ ADAPTIVE CONTROL

Research in adaptive control was motivated in the 1950s by the design of autopilots for highly agile aircraft that need to operate over a wide range of speeds and altitudes, experiencing large parametric variations. In the early 1950s, adaptive control was conceived and put forward as a technology for automatically adjusting the controller parameters in the face of changing aircraft dynamics [9], [10]. In [11], that period is called the *brave era* because "there was a very short path from idea to flight test with very little analysis in between." The tragic flight test of the X-15 confirms this view [12].

The initial results in adaptive control were motivated by system identification [13], which led to an architecture consisting of an online parameter estimator combined with automatic control design [14], [15]. Two architectures of adaptive control emerged, namely, the direct method, where controller parameters are estimated, and the indirect method, where process parameters are estimated and the controller parameters are obtained using a design procedure. The relationships between these architectures are clarified in [16].

Progress in systems theory has led to fundamental results for the development of adaptive-control architectures [16]–[26]. Along the same lines, Rohrs's example challenged the robustness of adaptive controllers in the presence of unmodeled dynamics [27]. Although [27] includes a proof of the existence of two infinite-gain operators in the closed-loop adaptive system, the explanation given for the phenomenon observed in the simulations, which was based on qualitative considerations, was not complete. Further details can be found in [28] and [29]. Nevertheless, [27] emphasizes a key point, namely, the available adaptive-control algorithms to that date were not able to limit the bandwidth of the closed-loop system and guarantee its robustness. The results and conclusions of [27] motivated numerous investigations of robustness and

stability issues of adaptive-control systems. In [30]–[35], the causes of instability are analyzed, and damping-type modifications of adaptation laws are suggested to prevent them. The basic idea of these modifications is to limit the gain of the adaptation loop and eliminate its integral action. Examples of these modifications are the σ-modification [32] and the e-modification [35]. Although these modifications address the problem of parameter drift, they do not directly address the architectural problem identified in [27]. An overview of robustness and stability issues of adaptive controllers can be found in [29].

In adaptive control, the nature of the adaptation process plays a central role in both robustness and performance. Ideally, adaptation is expected to correctly respond to all changes in initial conditions, reference inputs, and uncertainties by quickly identifying a set of control parameters that provide a satisfactory system response. This fact demands fast estimation schemes with high adaptation rates and, as a consequence, leads to the fundamental question of determining an upper bound on the adaptation rate that does not result in poor robustness characteristics. We notice that the results of [36, p. 549] limit the rate of variation of uncertainty by providing examples of destabilization due to fast adaptation, while the transient performance analysis is reduced to a persistency of excitation assumption [37], which cannot be verified a priori. The lack of analytical quantification of the relationship between the rate of adaptation, the transient response, and the robustness margins led to gain-scheduled designs of adaptive controllers, examples of which are the flight tests of the late 1990s by the U.S. Air Force and Boeing [38], [39]. These flight tests relied on intensive Monte Carlo analysis for determining the "best" rate of adaptation for various flight conditions. It was apparent that fast adaptation led to high frequencies in control signals and increased sensitivity to time delays. The fundamental question was thus reduced to determining an architecture that would allow for fast adaptation without losing robustness. It was understood that this architecture can reduce the amount of gain scheduling and possibly eliminate gain scheduling, since fast adaptation—in the presence of guaranteed robustness—can compensate for the negative effects of rapidly time-varying uncertainty on the system response.

$\mathcal{L}_1$ adaptive-control theory addresses this question by setting in place an architecture for which the estimation loop is decoupled from the control loop. This decoupling allows for an arbitrary increase of the estimation rate, limited by only the available hardware, that is, the CPU clock speed, while robustness is limited by the available control channel bandwidth and can be addressed by conventional methods from classical and robust control. The architectures of $\mathcal{L}_1$ adaptive-control theory have guaranteed transient performance and guaranteed robustness in the presence of fast adaptation, without introducing or requiring persistence of excitation, without gain scheduling of the controller parameters, without control reconfiguration, and without resorting to high-gain feedback. With an $\mathcal{L}_1$ adaptive controller in the feedback loop, the response of the closed-loop system can be predicted a priori, thus reducing the amount of Monte Carlo analysis required to verify and validate these systems. These features of $\mathcal{L}_1$ adaptive-control theory are exhibited by flight tests and in mid-to-high fidelity simulation environments [7], [8], [40]–[60].

In the remaining sections of this article we present the two basic architectures of adaptive control, direct and indirect, and use the indirect architecture for transition to $\mathcal{L}_1$ adaptive control. We discuss various insights and properties by analyzing two benchmark problems, specifically, Rohrs's example and the two-cart system. Flight tests of NASA's Airborne Subscale Transport Aircraft Research (AirSTAR) testbed conclude the article.

LIMITATIONS AND OPPORTUNITIES INDUCED BY ARCHITECTURES

In this section we place the focus on the architecture. We first present the direct model reference adaptive control (MRAC) architecture using a scalar system. We proceed by considering its state-predictor-based reparameterization, and we preview the $\mathcal{L}_1$ adaptive controller. We emphasize the role of the predictor in the architecture.

Consider the first-order plant

$$\dot{x}(t) = -a_m x(t) + b(u(t) + \theta x(t)), \quad x(0) = x_0, \tag{1}$$

where $x(t) \in \mathbb{R}$ is the state of the system, $u(t) \in \mathbb{R}$ is the control input, $a_m \in (0, \infty)$ defines the desired pole location, $b \in (0, \infty)$ is the known system input gain, and $\theta \in \mathbb{R}$ is a constant uncertainty with the known bound

$$|\theta| \leq \theta_{\max}. \tag{2}$$

The control objective is to define the feedback signal $u(t)$ such that $x(t)$ tracks a given bounded piecewise continuous input $r(t) \in \mathbb{R}$ with desired performance specifications. We assume that $\|r\|_{\mathcal{L}_\infty} \leq \bar{r}$.

The MRAC architecture proceeds by considering the *ideal controller*

$$u_{\mathrm{id}}(t) = -\theta x(t) + k_g r(t), \tag{3}$$

where

$$k_g \triangleq \frac{a_m}{b} \tag{4}$$

is the inverse of the dc gain of the plant (1), which yields unit dc gain of the closed-loop system (1), (3) with $u(t) = u_{\mathrm{id}}(t)$. Thus, the choice of k_g in (4) ensures that $x(t)$ tracks step reference inputs $r(t)$ with zero steady-state error. In fact, (3) provides perfect cancellation of the uncertainty in (1) and leads to the *ideal system*

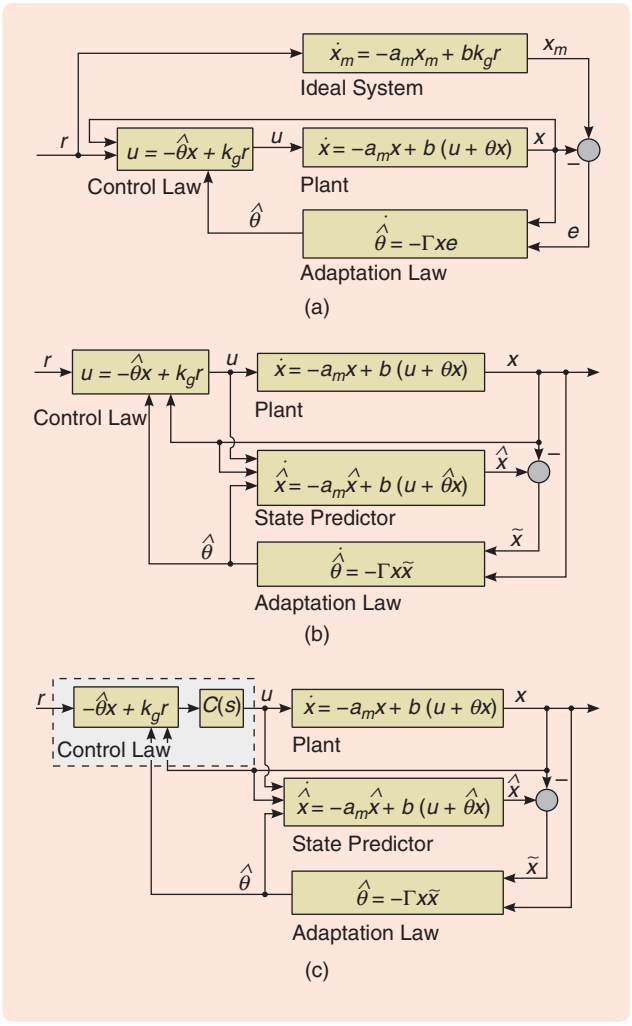

FIGURE 2 Adaptive-control architectures for the scalar case. The model reference adaptive-control (MRAC) architecture with (b) state predictor is equivalent to the (a) conventional MRAC architecture. The (c) $\mathcal{L}_1$ controller is based on the MRAC architecture with state predictor but has a lowpass filter $C(s)$ in the control channel.

$$\dot{x}_m(t) = -a_m x_m(t) + a_m r(t), \quad x_m(0) = x_0, \tag{5}$$

with state $x_m(t) \in \mathbb{R}$. However, the ideal controller (3) is not implementable since this controller explicitly uses the uncertain plant parameter θ in its definition.

Model Reference Adaptive Control

The model reference adaptive controller is obtained by replacing the unknown parameter θ in the ideal controller (3) by its estimate $\hat{\theta}(t)$ yielding the implementable control law

$$u(t) = -\hat{\theta}(t)x(t) + k_g r(t), \tag{6}$$

where $\hat{\theta}(t) \in \mathbb{R}$ is an estimate of θ. Substituting (6) into (1) yields the closed-loop system

$$\dot{x}(t) = -a_m x(t) - b\tilde{\theta}(t)x(t) + bk_g r(t), \quad x(0) = x_0,$$

where $\tilde{\theta}(t) \triangleq \hat{\theta}(t) - \theta$ denotes the parametric estimation error.

Defining the tracking error signal $e(t) \triangleq x_m(t) - x(t)$, the tracking error dynamics can be written as

$$\dot{e}(t) = -a_m e(t) + b\tilde{\theta}(t)x(t), \quad e(0) = 0. \tag{7}$$

The update law for the parametric estimate is given by

$$\dot{\hat{\theta}}(t) = -\Gamma x(t)e(t), \quad \hat{\theta}(0) = \hat{\theta}_0, \tag{8}$$

where $\Gamma \in (0, \infty)$ is the adaptation gain, and the initial conditions for the parametric estimate $\hat{\theta}_0$ are selected according to (2). The architecture of the closed-loop system is given in Figure 2(a).

To analyze the asymptotic properties of this adaptive scheme, consider the Lyapunov-function candidate

$$V(e(t), \tilde{\theta}(t)) = \frac{1}{2}e^2(t) + \frac{b}{2\Gamma}\tilde{\theta}^2(t). \tag{9}$$

The time-derivative $\dot{V}(t)$ of $V(e(t), \tilde{\theta}(t))$ along the system trajectories (7)–(8) is given by

$$\begin{aligned}\dot{V}(t) &= \frac{\partial V(e, \tilde{\theta})}{\partial e}\dot{e}(t) + \frac{\partial V(e, \tilde{\theta})}{\partial \tilde{\theta}}\dot{\tilde{\theta}}(t)\\ &= e(t)(-a_m e(t) + b\tilde{\theta}(t)x(t)) + \frac{b}{\Gamma}\tilde{\theta}(t)\dot{\tilde{\theta}}(t)\\ &= -a_m e^2(t) + b\tilde{\theta}(t)x(t)e(t) + \frac{b}{\Gamma}\tilde{\theta}(t)\dot{\hat{\theta}}(t).\end{aligned}$$

Using the adaptation law (8), we obtain

$$\dot{V}(t) = -a_m e^2(t) \leq 0.$$

Hence, the equilibrium of (7)–(8) is Lyapunov stable, and thus the signals $e(t)$, $\tilde{\theta}(t)$ are bounded. Since $x(t) = x_m(t) - e(t)$ and $x_m(t)$ is the state of the exponentially stable ideal system (5), it follows that $x(t)$ is bounded. To show that the tracking error converges to zero, we compute the second derivative

$$\ddot{V}(t) = -2a_m e(t)\dot{e}(t).$$

It follows from (7) that $\dot{e}(t)$ is uniformly bounded [2, Def. 4.6], and hence $\ddot{V}(t)$ is bounded, implying that $\dot{V}(t)$ is uniformly continuous. Application of Barbalat's lemma, stated in "Barbalat's Lemma," yields

$$\lim_{t\to\infty} \dot{V}(t) = 0,$$

which implies that $e(t) \to 0$ as $t \to \infty$. Thus, $x(t) - x_m(t)$ converges to zero, and $x(t)$ follows $x_m(t)$ as $t \to \infty$ with desired specifications given with the help of the ideal system (5).

Barbalat's Lemma

For a continuous function $f:\mathbb{R}\to\mathbb{R}$, the convergence of the integral

$$\int_0^t f(\tau)d\tau$$

to a finite number as $t\to\infty$ does not imply that the function $f(t)\to 0$ as $t\to\infty$. For example, consider the function $f(t)$ shown in Figure S1, which contains triangular spikes of equal height one and area $1/i!$, where $i=0,1,2,\ldots$ is the number of the spike. Then $f(t)$ is continuous and

$$\int_0^\infty f(\tau)d\tau=\sum_0^\infty \frac{1}{i!}=\mathrm{e}.$$

However, from Figure S1 we see that $f(t)$ does not have a limit as $t\to\infty$.

Barbalat's lemma invokes an additional assumption on $f(t)$, which ensures that $f(t)$ converges to zero as $t\to\infty$.

LEMMA S1 [2, LEMMA 8.2]

Let $f:\mathbb{R}\to\mathbb{R}$ be a uniformly continuous function on $[0,\infty)$ and assume that

$$\lim_{t\to\infty}\int_0^t f(\tau)d\tau$$

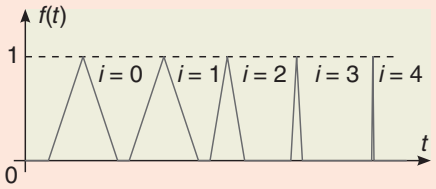

FIGURE S1 Barbalat's lemma. The function $f(t)$ contains triangular spikes of equal height one and area $1/i!$, This function is continuous and $\int_0^\infty f(\tau)d\tau=\mathrm{e}$. However, $f(t)$ does not have a limit as $t\to\infty$.

exists. Then

$$\lim_{t\to\infty} f(t)=0\,.$$

The assumption on uniform continuity, rather than only continuity, is critical for convergence of $f(t)$. In the example in Figure S1, the function $f(t)$ is continuous but not uniformly continuous because the slope of $f(t)$ tends to infinity as $i\to\infty$.

Notice that convergence of the parametric estimation error $\tilde{\theta}(t)$ to zero is not guaranteed. The parametric estimation errors are guaranteed only to be bounded.

MRAC with State Predictor

Next, we consider a reparameterization of the architecture (6), (8) using the state predictor

$$\dot{\hat{x}}(t)=-a_m\hat{x}(t)+b(u(t)+\hat{\theta}(t)x(t)),\quad \hat{x}(0)=x_0, \tag{10}$$

where $\hat{x}(t)\in\mathbb{R}$ is the state of the predictor. System (10) replicates the plant structure (1), with the unknown parameter θ replaced by its estimate $\hat{\theta}(t)$. Notice that, since the state of the plant (1) is measured, we can initialize the state predictor with $\hat{x}(0)=x_0$. By subtracting (1) from (10), we obtain the *prediction error dynamics*

$$\dot{\tilde{x}}(t)=-a_m\tilde{x}(t)+b\tilde{\theta}(t)x(t),\quad \tilde{x}(0)=0, \tag{11}$$

where $\tilde{x}(t)\triangleq\hat{x}(t)-x(t)$ and $\tilde{\theta}(t)\triangleq\hat{\theta}(t)-\theta$. Notice that (11) is identical to the error dynamics (7) and is independent of the control signal $u(t)$.

Let the adaptation law for $\hat{\theta}(t)$ be given by

$$\dot{\hat{\theta}}(t)=-\Gamma x(t)\tilde{x}(t),\quad \hat{\theta}(0)=\theta_0, \tag{12}$$

where $\Gamma\in(0,\infty)$, and the initial conditions for the parameter estimate $\hat{\theta}_0$ are selected according to (2). The adaptation law (12) is similar to (8) in its structure, except that the tracking error $e(t)$ is replaced by the prediction error $\tilde{x}(t)$. The choice of the Lyapunov-function candidate

$$V(\tilde{x}(t),\tilde{\theta}(t))=\frac{1}{2}\tilde{x}^2(t)+\frac{1}{2\Gamma}\tilde{\theta}^2(t) \tag{13}$$

leads to

$$\dot{V}(t)=-a_m\tilde{x}^2(t)\le 0,$$

implying that the errors $\tilde{x}(t)$ and $\tilde{\theta}(t)$ are uniformly bounded. Consider the Lyapunov function (13) evaluated along the system trajectories (11)–(12), which is denoted as $V(t)\triangleq V(\tilde{x}(t),\tilde{\theta}(t))$. Since $\dot{V}(t)\le 0$ for all $t\ge 0$, we obtain

$$\frac{1}{2}\tilde{x}^2(t)\le V(t)\le V(0)=\frac{\tilde{\theta}^2(0)}{2\Gamma}, \tag{14}$$

which leads, for all $t\ge 0$,

$$|\tilde{x}(t)|\le\frac{|\tilde{\theta}(0)|}{\sqrt{\Gamma}}. \tag{15}$$

Taking into account that

$$|\tilde{\theta}(0)|=|\hat{\theta}(0)-\theta|\le 2\theta_{\max},$$

bound (15) can be rewritten, for all $t\ge 0$, as

$$|\tilde{x}(t)|\le\frac{2\theta_{\max}}{\sqrt{\Gamma}}. \tag{16}$$

Available Bandwidth of Control Systems

In classical control the *bandwidth* of a system is defined as the frequency range $[0, \omega_b]$, where ω_b is the frequency at which the magnitude of the frequency response is 3 dB less than the magnitude at zero frequency. The frequency ω_b is also called the *cutoff frequency*.

One of the key characteristics of a control system is the *available bandwidth*, which is defined as the frequency range over which the unstructured multiplicative perturbations are less than unity [14]. The digital nature of control implementations, sensor and actuator uncertainties, and the presence of unmodeled dynamics in the plant limit the fidelity of the frequency response model of the plant, especially for high frequencies. These limitations on the ability to obtain a model of the plant impose constraints on the frequency range in which a controller can achieve performance improvement. The available bandwidth of a control system refers to this frequency range. Thus, the available bandwidth does not depend on the compensator. Rather, the available bandwidth is an a priori constraint imposed by the available plant model used for the control design. Most importantly, the available bandwidth is finite [14].

Notice, however, that without introducing the feedback signal $u(t)$ we cannot apply Barbalat's lemma to conclude convergence of $\tilde{x}(t)$ to zero. Both $x(t)$ and $\hat{x}(t)$ can diverge at the same rate, keeping $\tilde{x}(t)$ uniformly bounded.

If we use the control law (6) in (10), we obtain

$$\dot{\hat{x}}(t) = -a_m\hat{x}(t) + bk_s r(t), \quad \hat{x}(0) = x_0, \tag{17}$$

which shows that the closed-loop state predictor replicates the bounded ideal system of (5). Hence, Barbalat's lemma can be invoked to conclude that $\tilde{x}(t) \to 0$ as $t \to \infty$. The architecture of the closed-loop system with the predictor is given in Figure 2(b).

Comparing the closed-loop state predictor (17) with the ideal system (5) and the error dynamics (7) with (11), we see that the state-predictor parameterization of MRAC is equivalent to the MRAC architecture. However, Figure 2(a) and (b) illustrates the fundamental difference between the MRAC and the predictor-based MRAC; in (b), the control signal is provided as the input to both systems, the plant and the predictor, while in (a), the control signal serves as the input only to plant (1). Therefore, in the predictor-based MRAC (10), (12), control signal (6) can be redefined without affecting the proof of stability of the prediction error dynamics (11). This feature is used in [61] to obtain the $\mathcal{L}_1$ adaptive-control architecture.

Tuning Challenges

From (16) it follows that the tracking error can be arbitrarily reduced for all $t \geq 0$, including the transient phase, by increasing the adaptation gain Γ. However, from the control law (6) and the adaptation laws in (8) and (12) it follows that large adaptive gains result in high-gain feedback control, which manifests itself by high-frequency oscillations in the control signal and reduced tolerance to time delays. Moreover, applications requiring identification schemes with time scales comparable with those of the closed-loop dynamics tend to be challenging due to undesirable interactions between the two processes [29]. Due to the lack of systematic design guidelines for selecting an adequate adaptation gain, tuning such applications is done by either computationally expensive Monte Carlo simulations or trial-and-error methods following empirical guidelines or engineering intuition. As a consequence, efficient tuning of MRAC architectures represents a major challenge.

$\mathcal{L}_1$ ADAPTIVE CONTROL

The $\mathcal{L}_1$ adaptive controller is obtained from the predictor-based MRAC by letting the control be given by

$$u(s) = C(s)\hat{\eta}(s), \tag{18}$$

where $C(s)$ is an exponentially stable, strictly proper low-pass filter, while $\hat{\eta}(s)$ is the Laplace transform of the signal

$$\hat{\eta}(t) \triangleq -\hat{\theta}(t)x(t) + k_g r(t). \tag{19}$$

The architecture of the $\mathcal{L}_1$ adaptive controller is shown in Figure 2(c).

Unlike the predictor-based MRAC, the closed-loop system (1), (10) with the $\mathcal{L}_1$ adaptive controller (18) does not behave similarly to the ideal system (5) due to the limited bandwidth of the control channel enforced by $C(s)$. To derive the dynamics of the reference system for the $\mathcal{L}_1$ controller, consider the case where the parameter θ is known. Then, the controller in (18) takes the form of the *reference controller*

$$u_{\text{ref}}(s) = C(s)(k_g r(s) - \theta x_{\text{ref}}(s)). \tag{20}$$

Notice that this control law, as compared to the ideal control law (3), aims for partial compensation of the uncertainty $\theta x(s)$, namely, by compensating for only low-frequency content of $\theta x(s)$ within the bandwidth of the control channel. Substituting the reference controller (20) into the plant dynamics (1) leads to the $\mathcal{L}_1$ *reference system*

$$x_{\text{ref}}(s) = H(s)C(s)k_g r(s) + H(s)(1-C(s))\theta x_{\text{ref}}(s) + x_{\text{in}}(s), \tag{21}$$

Bridging Adaptive and Robust Control

Consider plant (1). In the frequency domain, we can rewrite (1) as

$$x(s) = H(s)(u(s) + \theta x(s)) + x_{\text{in}}(s). \tag{S2}$$

For simplicity of explanation, we consider zero initial conditions, which yields $x_{\text{in}}(s) \equiv 0$. With this assumption, multiplying (S2) by $C(s)$ and then dividing by $H(s)$, we obtain

$$C(s)\theta x(s) = \frac{C(s)}{H(s)}x(s) - C(s)u(s). \tag{S3}$$

Substituting (S3) into the equation for the reference control signal (20) and isolating $u(s)$, we obtain the reference controller

$$u_{\text{ref}}(s) = \frac{C(s)}{1-C(s)}k_g r(s) - \frac{1}{1-C(s)}\frac{C(s)}{H(s)}x_{\text{ref}}(s). \tag{S4}$$

Notice that $(1/1-C(s))\ (C(s)/H(s))$ is proper for all strictly proper $C(s)$. A block diagram of the closed-loop $\mathcal{L}_1$ reference system is shown in Figure S2. Notice that all elements of the controller implementation in Figure S2 are proper and stable. This representation of the $\mathcal{L}_1$ reference system is structurally similar to the disturbance observer architecture, analyzed in [S1]–[S3]. Disturbance observer control design is based on the internal model principle, which assumes that the control system encapsulates either implicitly or explicitly a model of the system to be controlled. The $\mathcal{L}_1$ reference controller, similar to disturbance observers, compensates for the mismatch between the ideal system and the plant within the frequency range specified by the bandwidth of the lowpass filter $C(s)$. This structural similarity of these architectures facilitates application of robust control design methods to the design of the filter $C(s)$ of the $\mathcal{L}_1$ adaptive controller [S4].

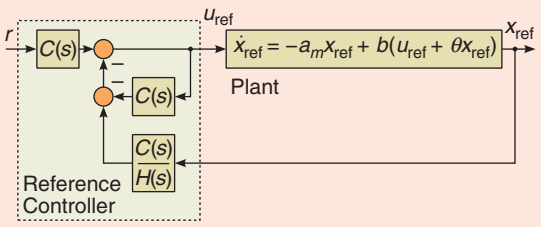

FIGURE S2 Reference controller for the $\mathcal{L}_1$ architecture. The $\mathcal{L}_1$ reference system can be equivalently represented in this form. This representation is structurally similar to the disturbance observer architecture considered in [S1]–[S3].

REFERENCES

[S1] K. Ohnishi, "A new servo method in mechatronics," *Trans. Jpn. Soc. Elect. Eng.*, vol. 107-D, pp. 83–86, 1987.

[S2] T. Umeno and Y. Hori, "Robust servo system design with two degrees of freedom and its application to novel motion control of robust manipulators," *IEEE Trans. Ind. Electron.*, vol. 40, no. 5, pp. 473–485, 1993.

[S3] W. C. Yang and M. Tomizuka, "Disturbance rejection through an external model for non-minimum phase systems," *ASME J. Dynamic Syst., Meas. Contr.*, vol. 116, no. 1, pp. 39–44, 1994.

[S4] E. Kharisov, K.-K. Kim, X. Wang, and N. Hovakimyan, "Limiting behavior of $\mathcal{L}_1$ adaptive controllers," in *Proc. AIAA Guidance, Navigation and Control Conf.*, Portland, OR, Aug. 2011, AIAA-2011-6441.

where $x_{\text{ref}}(t) \in \mathbb{R}^n$ is the state, and

$$H(s) \triangleq \frac{b}{s+a_m}, \qquad x_{\text{in}}(s) \triangleq \frac{1}{s+a_m}x_0.$$

We notice that $x_{\text{in}}(s)$ is the Laplace transform of the ideal system's response to the initial condition. The first term in (21) contains the ideal system (5) and the filter, which corresponds to the desired behavior of the system in the absence of uncertainty. The second term depends on the uncertainty $\theta x(s)$. The transfer function $1-C(s)$ is a high-pass filter, which attenuates the low-frequency content of the uncertainty $\theta x(s)$. This approach differs from the MRAC schemes (6), (8), (10), (12), where the ideal controller (3) attempts to follow the ideal system and compensate for the uncertainty $\theta x(s)$ in the entire frequency range. The $\mathcal{L}_1$ adaptive controller pursues a less ambitious, yet practically achievable, objective, namely, compensation of only the low-frequency content of the uncertainty $\theta x(s)$ within the bandwidth of the control channel. More details about the bandwidth of the control system are given in "Available Bandwidth of Control Systems." We notice that the $\mathcal{L}_1$ reference system is equivalent to a disturbance observer type closed-loop system as shown in "Bridging Adaptive and Robust Control."

Notice, however, that the consequence of the lowpass filter in the control channel is that the stability of the $\mathcal{L}_1$ reference system is not guaranteed a priori as it is for the ideal system (5). Taking the $\mathcal{L}_1$-norm of the transfer functions in (21), we obtain the bound

$$\|x_{\text{ref}}\|_{\mathcal{L}_\infty} \le \|H(s)C(s)k_g\|_{\mathcal{L}_1}\|r\|_{\mathcal{L}_\infty} + \|H(s)(1-C(s))\theta\|_{\mathcal{L}_1}\|x_{\text{ref}}\|_{\mathcal{L}_\infty} + \|x_{\text{in}}\|_{\mathcal{L}_\infty}. \tag{22}$$

Let

$$G(s) \triangleq H(s)(1-C(s)). \tag{23}$$

Then assuming that

$$\|G(s)\theta\|_{\mathcal{L}_1} < 1, \tag{24}$$

the bound (22) can be solved for $\|x_{\text{ref}}\|_{\mathcal{L}_\infty}$ to obtain

$$\|x_{\text{ref}}\|_{\mathcal{L}_\infty} \le \frac{\|H(s)C(s)k_g\|_{\mathcal{L}_1}\|r\|_{\mathcal{L}_\infty} + \|x_{\text{in}}\|_{\mathcal{L}_\infty}}{1-\|G(s)\theta\|_{\mathcal{L}_1}}. \tag{25}$$

Verifying the $\mathcal{L}_1$-Norm Bound

The stability of the $\mathcal{L}_1$ reference system is reduced to verifying the $\mathcal{L}_1$-norm condition in (24). For simplicity, let

$$C(s) = \frac{\omega_c}{s+\omega_c},$$

where $\omega_c > 0$ is the filter bandwidth. From (23) it follows that

$$G(s) = (1-C(s))H(s) = \frac{s}{s+\omega_c}H(s).$$

Therefore

$$\begin{aligned}\|G(s)\theta\|_{\mathcal{L}_1} &= \|(1-C(s))H(s)\theta\|_{\mathcal{L}_1}\\ &\le \left\|\frac{1}{s+\omega_c}\right\|_{\mathcal{L}_1}\|sH(s)\theta\|_{\mathcal{L}_1}\\ &= \frac{1}{\omega_c}\|sH(s)\theta\|_{\mathcal{L}_1}.\end{aligned}$$

Since $H(s)$ is strictly proper and exponentially stable, it follows that $sH(s)$ is proper and exponentially stable, and therefore $\|sH(s)\theta\|_{\mathcal{L}_1}$ is bounded. Therefore,

$$\lim_{\omega_c\to\infty}\|G(s)\theta\|_{\mathcal{L}_1} \le \lim_{\omega_c\to\infty}\frac{1}{\omega_c}\|sH(s)\theta\|_{\mathcal{L}_1} = 0,$$

and hence the $\mathcal{L}_1$-norm condition can be satisfied for a given plant (1) by choosing the filter $C(s)$ with sufficiently large bandwidth. However, in $\mathcal{L}_1$ adaptive-control architectures, increasing the bandwidth of the filter leads to high-gain control with a reduced time-delay margin [3]. Therefore, the allowed bandwidth of the filter is limited by robustness considerations.

Notice that the sufficient condition for stability of the $\mathcal{L}_1$ reference system (24) ensures that (25) is meaningful. The question of the filter design to satisfy the condition in (24) is discussed in "Verifying the $\mathcal{L}_1$-Norm Bound."

Next, we rewrite the control signal (18) as

$$u(s) = C(s)(k_g r(s) - \theta x(s) - \tilde{\eta}(s)), \tag{26}$$

where $\tilde{\eta}(t) \triangleq \tilde{\theta}(t)x(t)$. Rewriting the plant dynamics (1) in the frequency domain, we obtain

$$\begin{aligned}x(s) &= \frac{b}{s+a_m}(u(s)+\theta x(s)) + x_{\text{in}}(s)\\ &= H(s)(C(s)k_g r(s) + (1-C(s))\theta x(s) - C(s)\tilde{\eta}(s)) + x_{\text{in}}(s).\end{aligned} \tag{27}$$

Subtracting (27) from (21) gives

$$x_{\text{ref}}(s) - x(s) = G(s)\theta(x_{\text{ref}}(s) - x(s)) + H(s)C(s)\tilde{\eta}(s),$$

which can be solved for $x_{\text{ref}}(s) - x(s)$ to obtain

$$x_{\text{ref}}(s) - x(s) = \frac{C(s)}{1-G(s)\theta}H(s)\tilde{\eta}(s).$$

Since the $\mathcal{L}_1$ adaptive controller uses the same state predictor (10) and adaptation law (12) as the MRAC with state predictor, the $\mathcal{L}_1$ controller has the same prediction error dynamics as in (11). Thus, it follows that

$$\tilde{x}(s) = \frac{b}{s+a_m}\tilde{\eta}(s), \tag{28}$$

which leads to

$$x_{\text{ref}}(s) - x(s) = \frac{C(s)}{1-G(s)\theta}\tilde{x}(s).$$

Using the bound on $|\tilde{x}(t)|$ in (16), we obtain the bound

$$\|x_{\text{ref}} - x\|_{\mathcal{L}_\infty} \le \left\|\frac{C(s)}{1-G(s)\theta}\right\|_{\mathcal{L}_1}\|\tilde{x}\|_{\mathcal{L}_\infty} \le \left\|\frac{C(s)}{1-G(s)\theta}\right\|_{\mathcal{L}_1}\frac{2\theta_{\max}}{\sqrt{\Gamma}}. \tag{29}$$

This bound implies that the error between the states of the closed-loop system with the $\mathcal{L}_1$ adaptive controller and the $\mathcal{L}_1$ reference system, which uses the reference controller, can be uniformly bounded by a constant inversely proportional to the square root of the adaptation gain Γ.

Similarly, using (20), (26), and (28), we can derive

$$\begin{aligned}u_{\text{ref}}(s) - u(s) &= C(s)(-\theta(x_{\text{ref}}(s)-x(s)) + \tilde{\eta}(s))\\ &= -C(s)\theta(x_{\text{ref}}(s)-x(s)) + C(s)\frac{s+a_m}{b}\tilde{x}(s).\end{aligned} \tag{30}$$

Because $C(s)$ is strictly proper and exponentially stable, it follows that $C(s)(s+a_m)/b$ is proper and exponentially stable, and thus the $\mathcal{L}_1$ norms of both $C(s)$ and $C(s)(s+a_m)/b$ are bounded. Thus, we obtain the uniform bound for the difference in the control signals given by

$$\|u_{\text{ref}} - u\|_{\mathcal{L}_\infty} \le \|C(s)\theta\|_{\mathcal{L}_1}\|x_{\text{ref}} - x\|_{\mathcal{L}_\infty} + \left\|C(s)\frac{s+a_m}{b}\right\|_{\mathcal{L}_1}\frac{2\theta_{\max}}{\sqrt{\Gamma}}. \tag{31}$$

Notice that without the lowpass filter, that is, with $C(s) = 1$, the transfer function $C(s)(s+a_m)/b$ reduces to $(s+a_m)/b$, which is improper, and, hence, in the absence of the filter $C(s)$, we cannot uniformly bound $|u_{\text{ref}}(t) - u(t)|$ as in (31).

This analysis illustrates the role of $C(s)$ toward obtaining a uniform performance bound for the control signal of the $\mathcal{L}_1$ adaptive-control architecture, as compared to its nonadaptive version. We further notice that this uniform

bound is inversely proportional to the square root of the adaptation gain, similar to the tracking error. Thus, both performance bounds can be systematically reduced by increasing the rate of adaptation.

Performance and Robustness Analysis Using a Simplified Scalar System

Because a large adaptation rate in the case of MRAC leads to poor robustness characteristics, we conduct a preliminary robustness analysis of the $\mathcal{L}_1$ controller (18). For this purpose, we assume that $a_m = 1$ and $b = 1$ in (1), and we analyze the performance of the closed-loop adaptive system in the presence of input disturbances and measurement noise. In this case both the MRAC and $\mathcal{L}_1$ adaptive controller specialize to a linear model-following controller, the performance and robustness of which can be analyzed using classical control techniques. Thus, consider the scalar plant

$$\dot{x}(t) = -x(t) + u(t) + \sigma(t), \quad x(0) = x_0, \tag{32}$$

$$z(t) = x(t) + n(t), \tag{33}$$

where $z(t) \in \mathbb{R}$ is the measurement of the state $x(t) \in \mathbb{R}$, corrupted with noise $n(t) \in \mathbb{R}$, and $\sigma(t) \in \mathbb{R}$ is the unknown signal to be rejected by the control input $u(t) \in \mathbb{R}$.

Model Reference Adaptive Control

Having shown that the state predictor parameterization of MRAC (10), (12), (8) is equivalent to the MRAC (6), (8), we now focus on robustness and performance analysis of the MRAC architecture described in (6) and (8). For the plant with input disturbance (32), this architecture specializes to the integral controller

$$u(t) = -\hat{\sigma}(t) + r(t), \tag{34}$$

where $\hat{\sigma}(t) \in \mathbb{R}$ is an estimate of $\sigma(t)$, given by

$$\dot{\hat{\sigma}}(t) = -\Gamma e(t) = -\Gamma(x_m(t) - z(t)), \quad \sigma(0) = \sigma_0, \tag{35}$$

$\Gamma \in (0, \infty)$, and $x_m(t) \in \mathbb{R}$ is the state of the ideal system (5), which in this case becomes

$$\dot{x}_m(t) = -x_m(t) + r(t), \quad x_m(0) = x_0. \tag{36}$$

The block diagram of the closed-loop system is shown in Figure 3.

Figure 3 shows that, in the absence of input disturbance and measurement noise, the closed-loop system response is identical to the response of the ideal system (36). Next, for the performance analysis we consider the transfer functions from the input disturbance and the measurement noise to the plant control input and output. From Figure 3 we obtain

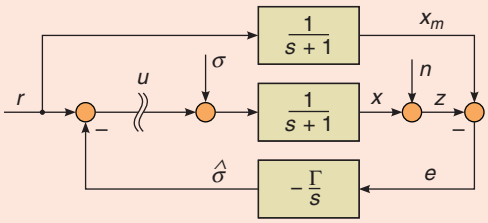

FIGURE 3 Closed-loop system with a model reference adaptive-control-type integral controller. The adaptation gain Γ is located in the feedback loop of the control system. Hence, the loop gain and bandwidth of the closed-loop system are determined by Γ.

$$H_{x\sigma}(s) = \frac{s}{s^2 + s + \Gamma}, \qquad H_{xn}(s) = -\frac{\Gamma}{s^2 + s + \Gamma}, \tag{37}$$

$$H_{u\sigma}(s) = -\frac{\Gamma}{s^2 + s + \Gamma}, \qquad H_{un}(s) = -\Gamma\frac{s + 1}{s^2 + s + \Gamma}. \tag{38}$$

We notice that all of the transfer functions in (37)–(38) have the same denominator, which gives a Hurwitz pair of closed-loop poles with the damping inversely proportional to $\sqrt{\Gamma}$ and natural frequency proportional to $\sqrt{\Gamma}$. Hence, in the presence of fast adaptation, the MRAC scheme (34)–(36) may develop high-frequency oscillations. Further analysis shows that increasing the adaptation gain, on the one hand, reduces the gain of $H_{x\sigma}(s)$ at low frequencies, which improves disturbance rejection, whereas, on the other hand, a larger adaptation gain shifts the pair of the closed-loop system poles closer to the imaginary axis. This fact implies that $H_{un}(s)$ acts similarly to a differentiator and thus leads to undesirable amplification of the measurement noise in the control channel. Consequently, the adaptation gain Γ in (35) resolves the performance tradeoff between disturbance rejection and noise attenuation.

Next we investigate the robustness properties of MRAC. For this purpose we consider the loop transfer function of the system in Figure 3 with negative feedback given by

$$L_1(s) = \frac{\Gamma}{s(s + 1)}, \tag{39}$$

from which gain and phase margins can be computed. Figure 4(a) shows that the Nyquist plot of $L_1(s)$ does not cross the negative part of the real line; therefore, the closed-loop system has infinite gain margin $g_m = \infty$. The gain-crossover frequency ω_{gc} can be computed from

$$|L_1(j\omega_{gc})| = \frac{\Gamma}{\omega_{gc}\sqrt{\omega_{gc}^2 + 1}} = 1,$$

which leads to the phase margin

$$\phi_m = \pi + \angle L_1(j\omega_{gc}) = \arctan\left(\frac{1}{\omega_{gc}}\right).$$

It can be shown [5] that increasing Γ leads to higher gain-crossover frequency and thus reduced phase margin. The

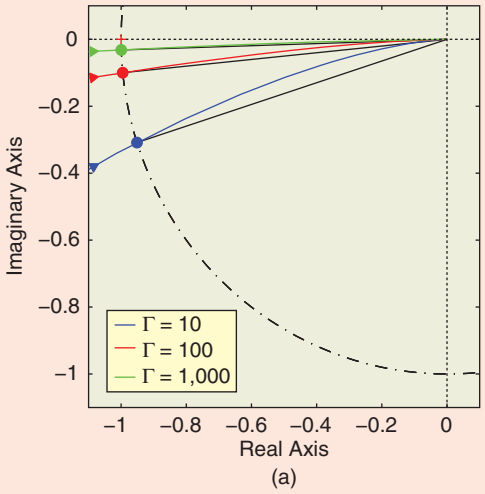

FIGURE 4 Nyquist plots of the loop transfer functions. Plot (a) shows that the phase margin of the model reference adaptive-control-type integral controller vanishes as the adaptation gain Γ is increases. On the other hand, plot (b) shows that the phase margin of the $\mathcal{L}_1$ adaptive controller approaches $\pi/2$ as the adaptation gain Γ increases.

reduction of phase margin with large Γ can also be observed in Figure 4(a). Thus, if increasing Γ improves the tracking performance for all $t \geq 0$, including the transient phase, then robustness degrades. Hence, the adaptation rate Γ is the key to the tradeoff between performance and robustness in the design of MRAC.

$\mathcal{L}_1$ Adaptive Control

The state predictor of the $\mathcal{L}_1$ adaptive controller, given by (10), takes the form

$$\dot{\hat{x}}(t) = -\hat{x}(t) + u(t) + \hat{\sigma}(t), \quad \hat{x}(0) = x_0. \tag{40}$$

The parametric estimate, given by (12), is thus replaced by

$$\dot{\hat{\sigma}}(t) = -\Gamma \tilde{x}(t), \quad \sigma(0) = \sigma_0, \tag{41}$$

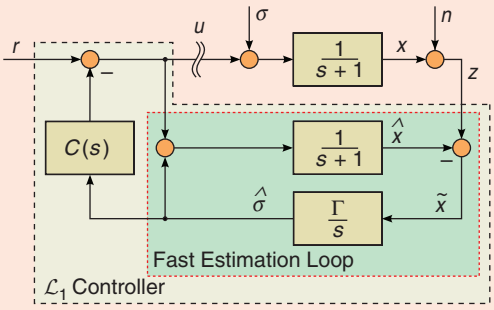

FIGURE 5 Closed-loop system with an $\mathcal{L}_1$ adaptive controller. The adaptation gain Γ affects only the fast estimation loop (red), while the bandwidth of the control loop is determined by the lowpass filter $C(s)$.

where $\tilde{x}(t) \triangleq \hat{x}(t) - z(t)$ and $\Gamma \in (0, \infty)$. Next, similar to (18), we use a lowpass-filtered version of $\hat{\sigma}(t)$ for the control law given by

$$u(s) = -C(s)\hat{\sigma}(s) + r(s). \tag{42}$$

The block diagram of the closed-loop system is given in Figure 5.

From Figure 5 we see that, similar to MRAC in Figure 3, in the absence of input disturbance and measurement noise, the closed-loop system recovers the ideal system in (36). From the block diagram in Figure 5 we derive the transfer functions from the input disturbance and the measurement noise to the plant input and the output given by

$$H_{x\sigma}(s) = \frac{1}{s+1}\left(1 - \frac{\Gamma C(s)}{s^2+s+\Gamma}\right), \quad H_{xn}(s) = -\frac{\Gamma}{s^2+s+\Gamma}C(s), \tag{43}$$

$$H_{u\sigma}(s) = -\frac{\Gamma}{s^2+s+\Gamma}C(s), \qquad H_{un}(s) = -\Gamma\frac{s+1}{s^2+s+\Gamma}C(s). \tag{44}$$

Notice that the transfer functions (43)–(44) have the same denominator. Moreover, in the absence of the filter, that is, $C(s) \equiv 1$, controller (42) reduces to the MRAC-type integral controller introduced in (34), and transfer functions (43)–(44) reduce to (37)–(38). This fact implies that the $\mathcal{L}_1$ controller also results in lightly damped closed-loop poles in the presence of fast adaptation. However, for the $\mathcal{L}_1$ controller, transfer functions (43)–(44) containing this pole are followed by the lowpass filter $C(s)$. Hence, the effect of the lightly damped pole can be compensated or even canceled by an appropriate choice of $C(s)$, avoiding the undesired transient behavior, which is observed in MRAC. This compensation allows for safe increase of the adaptation gain Γ without degrading the noise-attenuation properties of the system and without causing high-frequency oscillations in the control channel. Notice that the fast, lightly damped poles arise in the estimation loop shown in Figure 5, which is implemented inside the controller block. Hence

the compensation of these poles with the help of the filter occurs inside the controller and cannot be affected by the uncertainty or unmodeled dynamics possibly present in the plant. On the other hand, from Figure 3 we can see that for MRAC the lightly damped poles due to large adaptation gain are generated by the loop, which involves the plant. Therefore, in the presence of fast adaptation, even small plant uncertainty may cause these poles to drift to the right-hand side of the complex plane, causing closed-loop system instability. This observation explains how the low-pass filter in $\mathcal{L}_1$ adaptive controller helps to decouple the estimation performance from the robustness of the adaptive controller, which consequently enables fast adaptation.

In the foregoing analysis, we further consider the first-order lowpass filter

$$C(s) = \frac{\omega_c}{s + \omega_c}, \tag{45}$$

although similar results can be obtained using higher order filters. The loop-transfer function of the system in Figure 5 is given by

$$L_2(s) = \frac{\Gamma C(s)}{s(s+1) + \Gamma(1 - C(s))}. \tag{46}$$

In the absence of the filter, that is, with $C(s) = 1$, the loop-transfer function (46) reduces to (39), that is, $L_2(s) = L_1(s)$. Although (46) has a more complex structure compared to (39), the Nyquist plot in Figure 4(b) shows that the phase and the gain margins of the $\mathcal{L}_1$ controller are not significantly affected by large values of Γ. The effect of the adaptive gain on the robustness margins of the two closed-loop systems, MRAC and $\mathcal{L}_1$, is presented in Figure 6. While the phase margin of the MRAC-type integral controller vanishes as the adaptation gain Γ is increased, Figure 6 shows that the $\mathcal{L}_1$ adaptive controller has guaranteed phase and gain margins that are bounded away from zero in the presence of fast adaptation.

Furthermore, as $\Gamma \to \infty$, the expression (46) leads to the limiting loop-transfer function

$$L_{2l}(s) = \frac{C(s)}{1 - C(s)} = \frac{\omega_c}{s}. \tag{47}$$

The transfer function (47) represents the loop transfer function of the $\mathcal{L}_1$ reference system, which in the case of the scalar plant (32) specializes to

$$x_{\text{ref}}(s) = \frac{1}{s+1}(u_{\text{ref}}(s) + \sigma(s)), \tag{48}$$

$$u_{\text{ref}}(s) = -C(s)\sigma(s) + r(s). \tag{49}$$

Transfer function (47) has an infinite gain margin, that is, $g_m = \infty$, and a phase margin of $\phi_m = \pi/2$. However, Figure 6(a) shows that the gain margin of the $\mathcal{L}_1$ controller is finite and converges to $g_m = 6.02$ dB with the increase of Γ. We note that the dynamics of the adaptation loop in Figure 5 do not appear in the limiting loop transfer function (47). Then, since the phase-crossover frequency tends to infinity as the adaptation gain Γ increases, this limiting loop transfer function cannot be used to analyze the gain margin of the closed-loop system with the $\mathcal{L}_1$ adaptive controller (40)–(42). However, the gain-crossover frequency stays in the low-frequency range, where the limiting loop transfer function (47) approximates the loop transfer function (46). Consequently, the limiting loop transfer function can be used to analyze the phase margin of the closed-loop adaptive system.

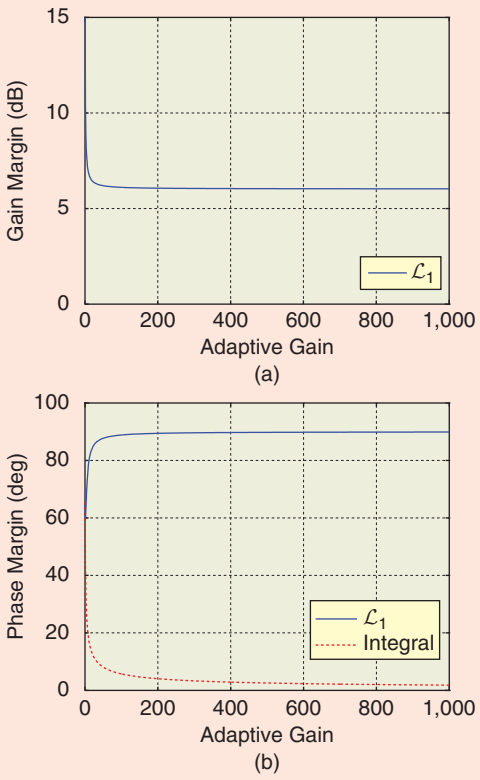

FIGURE 6 Effect of high adaptation gain on the stability margins. The (a) gain and (b) phase margins of the $\mathcal{L}_1$ adaptive controller are bounded away from zero. The model reference adaptive-control-type integral controller has infinite gain margin while the phase margin diminishes as the adaptation gain increases. These results are consistent with Figure 4.

ADAPTIVE CONTROL IN THE PRESENCE OF UNKNOWN INPUT GAIN

In this section we revisit the main adaptive architectures for a class of multivariable systems with time-varying uncertainties, disturbances, and an unknown input gain. We consider direct and indirect MRAC architectures, as given in Figure 7(a) and (b) [62]. In the direct architecture, the controller parameters are directly updated, while in the indirect architecture the plant parameters are estimated and used in the feedback law. We present in this section the indirect architecture using the state-predictor parameterization of

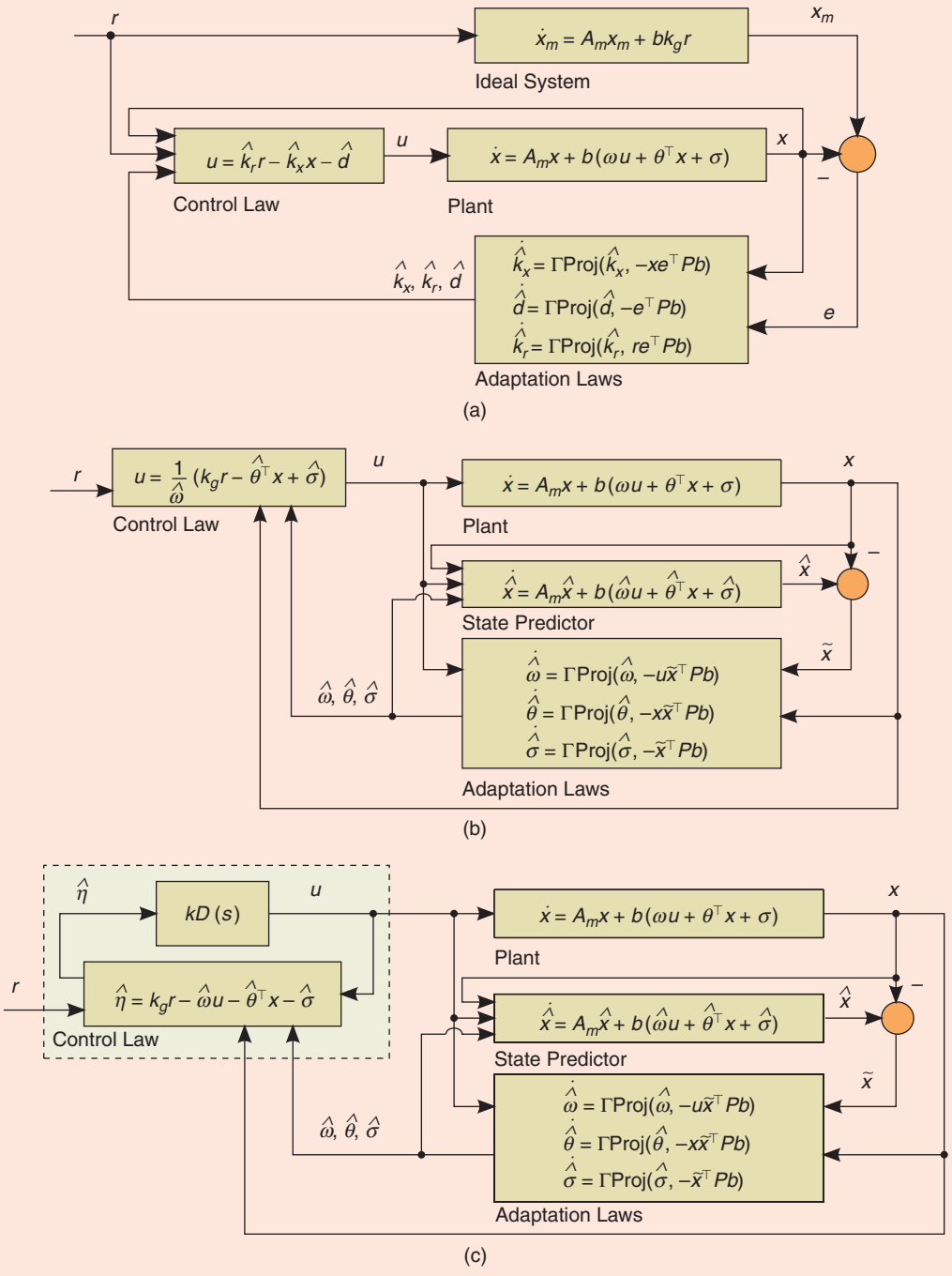

FIGURE 7 Block diagrams of the adaptive-control architectures: (a) direct model reference adaptive control (MRAC), (b) indirect MRAC, and (c) $\mathcal{L}_1$ adaptive controller. The indirect MRAC architecture is based on a state predictor. The $\mathcal{L}_1$ adaptive-control architecture has the same state predictor and adaptation laws as the indirect MRAC architecture but a different control law.

MRAC, and, similar to (18)–(19), use this architecture to develop the $\mathcal{L}_1$ adaptive controller.

Thus, consider the plant dynamics given by

$$\dot{x}(t) = A_m x(t) + b(\omega u(t) + \theta^\top(t) x(t) + \sigma(t)), \quad x(0) = x_0, \tag{50}$$

$$y(t) = c^\top x(t), \tag{51}$$

where $x(t) \in \mathbb{R}^n$ is the measured state of the plant; $A_m \in \mathbb{R}^{n \times n}$ is a known Hurwitz matrix that defines the desired dynamics for the closed-loop system; $b, c \in \mathbb{R}^n$ are known constant vectors; $u(t) \in \mathbb{R}$ is the control input; $y(t) \in \mathbb{R}$ is the regulated output; $\sigma(t) \in \mathbb{R}$ is the unknown disturbance; $\theta(t) \in \mathbb{R}^n$ is the vector of unknown time-varying parameters; and $\omega \in (0, \infty)$ is the unknown plant

input gain. The unknown quantities are subject to the bounds

$$\omega \in \Omega \triangleq [\omega_{\min}, \omega_{\max}],\ \theta(t) \in \Theta,\ \ \sigma(t) \in \Delta \triangleq [-\sigma_b, \sigma_b], \tag{52}$$

$$\|\dot{\theta}(t)\| \le d_\theta, \quad |\dot{\sigma}(t)| \le d_\sigma, \tag{53}$$

for all $t \ge 0$, where Θ is a given convex compact set,

$$0 < \omega_{\min} < \omega_{\max} < \infty,$$

and σ_b, d_θ, d_σ are known bounds. The control objective is to determine a state feedback controller $u(t)$ such that $y(t)$ follows a given bounded piecewise continuous input $r(t) \in \mathbb{R}$, $\|r\|_{\mathcal{L}_\infty} \le \bar{r}$, with the desired specifications given according to the ideal system

$$\dot{x}_m(t) = A_m x_m(t) + b k_g r(t), \quad x_m(0) = x_0, \tag{54}$$

$$y_m(t) = c^\top x_m(t), \tag{55}$$

where $x_m(t) \in \mathbb{R}^n$ is the state, and

$$k_g \triangleq -\frac{1}{c^\top A_m^{-1} b} \tag{56}$$

ensures that $y_m(t)$ tracks step reference inputs with zero steady-state error. We notice that the ideal system (54)–(55) is obtained from the plant (50)–(51) by applying the ideal controller

$$u_{\mathrm{id}}(t) = \frac{1}{\omega}(k_g r(t) - \theta^\top(t)x(t) - \sigma(t)), \tag{57}$$

which, similar to (3), assumes cancellation of uncertainties in the plant (50)–(51).

Direct MRAC

The direct MRAC law uses the estimates of the unknown controller parameters in (57) and takes the form

$$u(t) = \hat{k}_r(t) r(t) - \hat{k}_x^\top(t) x(t) - \hat{d}(t), \tag{58}$$

where $\hat{k}_x(t) \in \mathbb{R}^n$ is an estimate of $k_x(t) \triangleq \theta(t)/\omega$, $\hat{d}(t) \in \mathbb{R}$ is an estimate of $d(t) \triangleq \sigma(t)/\omega$, and $\hat{k}_r(t) \in \mathbb{R}$ is an estimate of $k_r \triangleq k_g/\omega$ in (57). Substituting (58) into (50) yields the closed-loop system dynamics

$$\dot{x}(t) = (A_m - \omega b \tilde{k}_x^\top(t))x(t) - \omega b \tilde{d}(t) + \omega b \hat{k}_r(t) r(t),\ x(0) = x_0,$$
$$y(t) = c^\top x(t),$$

where $\tilde{k}_x(t) \triangleq \hat{k}_x(t) - k_x(t)$ and $\tilde{d}(t) \triangleq \hat{d}(t) - d(t)$ denote the parametric estimation error.

The tracking error signal $e(t) \triangleq x_m(t) - x(t)$ satisfies

$$\dot{e}(t) = A_m e(t) + \omega b \tilde{k}_x^{\mathrm{T}}(t) x(t) + \omega b \tilde{d}(t) - b\omega \tilde{k}_r(t) r(t),$$
$$e(0) = 0, \tag{59}$$

where $\tilde{k}_r(t) \triangleq \hat{k}_r(t) - k_r$. In the case of time-varying plant parameters, the update laws for the parametric estimates use the projection operator, which ensures boundedness of the adaptive estimates $\hat{k}_x(t)$, $\hat{d}(t)$, $\hat{k}_r(t)$ by definition. The projection operator plays a crucial role in ensuring robustness and avoiding parameter drift. For more details, see "Projection Operator." Thus, the adaptation laws are given by

$$\dot{\hat{k}}_x(t) = \Gamma \mathrm{Proj}(\hat{k}_x(t), -x(t)e^\top(t)Pb), \hat{k}_x(0) = \hat{k}_{x0}, \tag{60}$$

$$\dot{\hat{d}}(t) = \Gamma \mathrm{Proj}(\hat{d}(t), -e^\top(t)Pb), \hat{d}(0) = \hat{d}_0, \tag{61}$$

$$\dot{\hat{k}}_r(t) = \Gamma \mathrm{Proj}(\hat{k}_r(t), r(t)e^\top(t)Pb), \hat{k}_r(0) = \hat{k}_{r0}, \tag{62}$$

where $\Gamma \in (0, \infty)$ is the adaptation gain, $\hat{k}_{x0}$, $\hat{d}_0$, $\hat{k}_{r0}$ represent the "best possible guess" of the ideal values of the unknown parameters, the projection bounds are set according to the available conservative bounds (52), and $P = P^\top > 0$ solves the algebraic Lyapunov equation

$$A_m^\top P + P A_m = -Q$$

for arbitrary $Q = Q^\top > 0$.

Next we examine boundedness and asymptotic properties of the error dynamics (59) by considering the Lyapunov-function candidate

$$V(e(t), \tilde{k}_x(t), \tilde{d}(t), \tilde{k}_r(t)) = e^\top(t)Pe(t) + \frac{1}{\Gamma}\Big(\tilde{k}_x^\top(t)\tilde{k}_x(t) + \tilde{d}^2(t) + \tilde{k}_r^2(t)\Big)\omega. \tag{63}$$

Using the property of the projection operator (S5), we obtain a bound on the time-derivative of the Lyapunov function along the system trajectories (59)–(62)

$$\begin{aligned}
\dot{V}(t) &= \dot{e}^\top(t)Pe(t) + e^\top(t)P\dot{e}(t) \\
&\quad + \frac{1}{\Gamma}\Big(2\tilde{k}_x^\top(t)\dot{\tilde{k}}_x(t) + 2\tilde{d}(t)\dot{\tilde{d}}(t) + 2\tilde{k}_r(t)\dot{\tilde{k}}_r(t)\Big)\omega \\
&= e^\top(t)(A_m^\top P + P A_m)e(t) + 2e^\top(t)P\omega b\big(\tilde{k}_x^\top(t)x(t) \\
&\quad + \tilde{d}(t) - \tilde{k}_r(t)r(t)\big) + \frac{2}{\Gamma}\Big(\tilde{k}_x^\top(t)\dot{\hat{k}}_x(t) + \tilde{d}(t)\dot{\hat{d}}(t) \\
&\quad + \tilde{k}_r(t)\dot{\hat{k}}_r(t)\Big)\omega - \frac{2}{\Gamma}\Big(\tilde{k}_x^\top(t)\dot{k}_x(t) + \tilde{d}(t)\dot{d}(t)\Big)\omega \\
&= -e^\top(t)Qe(t) + 2\tilde{k}_x^\top(t)\Big(e^\top(t)P\omega b x(t) \\
&\quad + \mathrm{Proj}(\hat{k}_x(t), -x(t)e^\top(t)Pb)\Big) \\
&\quad + 2\tilde{d}(t)\Big(e^\top(t)P\omega b + \mathrm{Proj}(\hat{d}(t), -e^\top(t)Pb)\Big) \\
&\quad - 2\tilde{k}_r(t)\Big(e^\top(t)P\omega b r(t) - \mathrm{Proj}(\hat{k}_r(t), r(t)e^\top(t)Pb)\Big) \\
&\quad - \frac{2}{\Gamma}\Big(\tilde{k}_x^\top(t)\dot{k}_x(t) + \tilde{d}(t)\dot{d}(t)\Big)\omega \\
&\le -e^\top(t)Qe(t) - \frac{2}{\Gamma}\Big(\tilde{k}_x^\top(t)\dot{k}_x(t) + \tilde{d}(t)\dot{d}(t)\Big)\omega.
\end{aligned}$$

Projection Operator

The projection operator ensures boundedness of the parametric estimates by definition. The definition of the projection operator proceeds by considering a compact convex set with a smooth boundary given by

$$\Omega_c \triangleq \{\theta \in \mathbb{R}^n | f(\theta) \le c\}, \quad 0 \le c \le 1,$$

where $f: \mathbb{R}^n \to \mathbb{R}$ is the smooth convex function

$$f(\theta) \triangleq \frac{(\epsilon_\theta + 1)\theta^\top \theta - \theta_{\max}^2}{\epsilon_\theta \theta_{\max}^2},$$

$\theta_{\max}$ is the norm bound imposed on the vector θ, and $\epsilon_\theta > 0$ is the projection tolerance bound of the choice. As shown in Figure S3, the projection operator is defined as

$$\text{Proj}(\theta, y) \triangleq \begin{cases} y, & \text{if } f(\theta) < 0, \\ y, & \text{if } f(\theta) \ge 0 \text{ and } \nabla f^\top y \le 0, \\ y - \dfrac{\nabla f}{\|\nabla f\|} \left\langle \dfrac{\nabla f}{\|\nabla f\|}, y \right\rangle f(\theta), & \text{if } f(\theta) \ge 0 \text{ and } \nabla f^\top y > 0. \end{cases}$$

Notice that the projection operator $\text{Proj}(\theta, y)$ does not alter y if θ belongs to the set $\Omega_0 \triangleq \{\theta \in \mathbb{R}^n | f(\theta) \le 0\}$. In the set $\{\theta \in \mathbb{R}^n | 0 \le f(\theta) \le 1\}$, if $\nabla f^\top y > 0$, the $\text{Proj}(\theta, y)$ operator subtracts a vector normal to the boundary $\overline{\Omega}_{f(\theta)} = \{\overline{\theta} \in \mathbb{R}^n | f(\overline{\theta}) = f(\theta)\}$ so that we obtain a smooth transformation from the original vector field y to an inward or tangent vector field for Ω_1. As a result of this transformation, the projection operator verifies the property

$$(\theta - \theta^*)^\top (\text{Proj}(\theta, y) - y) \le 0, \tag{S5}$$

for given vectors $y \in \mathbb{R}^n$, $\theta^* \in \Omega_0 \subset \Omega_1 \subset \mathbb{R}^n$, and $\theta \in \Omega_1$ [64]. The proofs of ultimate boundedness of the adaptive errors rely on (S5).

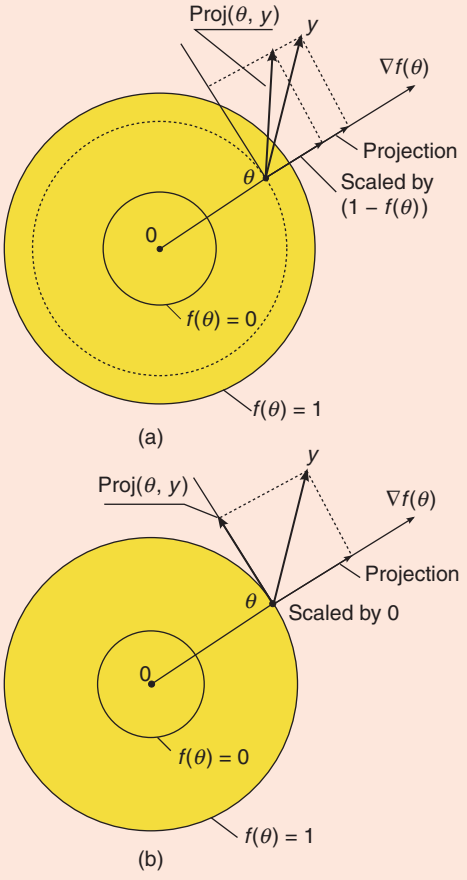

FIGURE S3 Illustration of the projection operator. Inside the set bounded by $f(\theta) = 0$, the projection operator does not modify the vector. In the set between $f(\theta) = 0$ and $f(\theta) = 1$, the projection operator scales down the normal component of the vector as shown in (a). The scaling factor is given by $1 - f(\theta)$. On the boundary $f(\theta) = 1$, the normal component of the vector is canceled.

Notice that $\dot{V}(t) \le 0$, if

$$e^\top(t) Q e(t) \ge \frac{4\omega_{\max}}{\Gamma \omega_{\min}^2} (\theta_{\max} d_\theta + \sigma_b d_\sigma),$$

where

$$\theta_{\max} \triangleq \max_{\theta \in \Theta} \|\theta\|. \tag{64}$$

Therefore, if

$$\|e(t)\|^2 \ge e_{\max}^2 \triangleq \frac{4\omega_{\max}}{\lambda_{\min}(Q) \Gamma \omega_{\min}^2} (\theta_{\max} d_\theta + \sigma_b d_\sigma),$$

then $\dot{V}(t) \le 0$, where $\lambda_{\min}(\cdot)$ denotes the minimum eigenvalue of the matrix. From (63) it follows that $\dot{V}(t) \le 0$ if $V(t) \ge V_{\max}$, where

$$\begin{aligned} V_{\max} &\triangleq \lambda_{\max}(P) e_{\max}^2 + \frac{\omega_{\max}}{\Gamma \omega_{\min}^2} \left(4\theta_{\max}^2 + 4\sigma_b^2 + \frac{k_g^2}{\omega_{\max}^2} \right. \\ &\quad \left. \times (\omega_{\max} - \omega_{\min})^2 \right) \\ &= \frac{\omega_{\max}}{\Gamma \omega_{\min}^2} \left(\frac{4\lambda_{\max}(P)}{\lambda_{\min}(Q)} (\theta_{\max} d_\theta + \sigma_b d_\sigma) + 4\theta_{\max}^2 + 4\sigma_b^2 \right. \\ &\quad \left. + \frac{k_g^2}{\omega_{\max}^2} (\omega_{\max} - \omega_{\min})^2 \right) \\ &= \frac{\omega_{\max}}{\Gamma \omega_{\min}^2} \theta_{md}, \end{aligned}$$

where $\lambda_{\max}(\cdot)$ denotes the maximum eigenvalue of the matrix, and

$$\theta_{md} \triangleq \frac{4\lambda_{\max}(P)}{\lambda_{\min}(Q)}(\theta_{\max}d_\theta+\sigma_b d_\sigma) + 4\theta_{\max}^2 + 4\sigma_b^2 + k_g^2\frac{(\omega_{\max}-\omega_{\min})^2}{\omega_{\max}^2}.$$

Since $V(0) \le V_{\max}$, we obtain that $V(t) \le V_{\max}$, and therefore, for all $t \ge 0$,

$$\lambda_{\min}(P)\|e(t)\|^2 \le V_{\max},$$

which, for all $t \ge 0$, yields the bound

$$\|e(t)\| \le \sqrt{\frac{\omega_{\max}\theta_{md}}{\lambda_{\min}(P)\omega_{\min}^2\Gamma}}.$$

Hence, the signals $e(t)$, $\widetilde{k}_x(t)$, $\widetilde{d}(t)$, $\widetilde{k}_r(t)$ are uniformly bounded. Since $x(t) = x_m(t) - e(t)$, and $x_m(t)$ is the state of an exponentially stable ideal system, it follows that $x(t)$ is uniformly bounded. We note that in the presence of time-varying plant parameters $\theta(t)$ and $\sigma(t)$ asymptotic stability cannot be achieved.

Indirect MRAC

The indirect MRAC scheme given in Figure 7(b) uses estimates $\hat{\omega}(t) \in \mathbb{R}$, $\hat{\theta}(t) \in \mathbb{R}^n$, and $\hat{\sigma}(t) \in \mathbb{R}$ of the plant parameters but not the controller parameters. To derive the adaptation laws we consider a reparameterization of the direct MRAC architecture in Figure 7(a) using the state predictor

$$\dot{\hat{x}}(t) = A_m\hat{x}(t) + b(\hat{\omega}(t)u(t) + \hat{\theta}^\top(t)x(t) + \hat{\sigma}(t)), \quad \hat{x}(0) = x_0, \tag{65}$$

$$\hat{y}(t) = c^\top\hat{x}(t), \tag{66}$$

with state $\hat{x}(t) \in \mathbb{R}^n$. System (65)–(66) replicates the plant structure from (50)–(51), with the unknown parameters replaced by their estimates. The error in the indirect control scheme is the estimation error $\widetilde{x}(t) \triangleq \hat{x}(t) - x(t)$, which is governed by

$$\dot{\widetilde{x}}(t) = A_m\widetilde{x}(t) + b(\widetilde{\omega}(t)u(t) + \widetilde{\theta}^\top(t)x(t) + \widetilde{\sigma}(t)), \quad \widetilde{x}(0) = 0, \tag{67}$$

where

$$\widetilde{\omega}(t) \triangleq \hat{\omega}(t) - \omega, \quad \widetilde{\theta}(t) \triangleq \hat{\theta}(t) - \theta(t), \quad \widetilde{\sigma}(t) \triangleq \hat{\sigma}(t) - \sigma(t).$$

The indirect MRAC control law uses the estimates $\hat{\omega}(t)$, $\hat{\theta}(t)$, $\hat{\sigma}(t)$ of the plant parameters to achieve the control objective. The control law is obtained by replacing the values of the unknown plant parameters in (57) by their estimates

$$u(t) = \frac{1}{\hat{\omega}(t)}(k_g r(t) - \hat{\theta}^\top(t)x(t) - \hat{\sigma}(t)). \tag{68}$$

This definition of the control law requires that the estimate $\hat{\omega}(t)$ remain bounded away from zero. This property is achieved by the projection-based adaptation laws, similar to (60)–(62)

$$\dot{\hat{\omega}}(t) = \Gamma\,\mathrm{Proj}(\hat{\omega}(t), -u(t)\widetilde{x}^\top(t)Pb), \quad \hat{\omega}(0) = \hat{\omega}_0, \tag{69}$$

$$\dot{\hat{\theta}}(t) = \Gamma\,\mathrm{Proj}(\hat{\theta}(t), -x(t)\widetilde{x}^\top(t)Pb), \quad \hat{\theta}(0) = \hat{\theta}_0, \tag{70}$$

$$\dot{\hat{\sigma}}(t) = \Gamma\,\mathrm{Proj}(\hat{\sigma}(t), -\widetilde{x}^\top(t)Pb), \quad \hat{\sigma}(0) = \hat{\sigma}_0, \tag{71}$$

where $\Gamma \in (0, \infty)$ is the adaptation gain, and $\omega_{\max} > \hat{\omega}_0 > \omega_{\min}$, $\hat{\theta}_0$, $\hat{\sigma}_0$ are the initial conditions for the plant parameter estimates selected according to conservative knowledge of their ideal values. In the case of known plant input gain ω, the indirect MRAC in Figure 7(a) and the direct MRAC in Figure 7(b) architectures are identical, and therefore we do not distinguish them in the previous section as direct and indirect, but we refer to the difference due to the predictor.

The choice of the Lyapunov-function candidate

$$V(\widetilde{x}(t), \widetilde{\omega}(t), \widetilde{\theta}(t), \widetilde{\sigma}(t)) = \widetilde{x}^\top(t)P\widetilde{x}(t) + \frac{1}{\Gamma}(\widetilde{\omega}^2(t) + \widetilde{\theta}^\top(t)\widetilde{\theta}(t) + \widetilde{\sigma}^2(t)) \tag{72}$$

leads to

$$\dot{V}(t) \le -\widetilde{x}^\top(t)Q\widetilde{x} - \frac{2}{\Gamma}(\widetilde{\theta}^\top(t)\dot{\theta}(t) + \widetilde{\sigma}(t)\dot{\sigma}(t)). \tag{73}$$

Similar to the direct MRAC, from this inequality we obtain the uniform bound

$$\|\widetilde{x}(t)\| \le \frac{\gamma_0}{\sqrt{\Gamma}}, \quad \text{for all } t \ge 0, \tag{74}$$

where

$$\gamma_0 \triangleq \sqrt{\frac{\theta_{mi}}{\lambda_{\min}(P)}}, \quad \theta_{mi} \triangleq 4\theta_{\max}^2 + 4\sigma_b^2 + (\omega_{\max} - \omega_{\min})^2 + 4\frac{\lambda_{\max}(P)}{\lambda_{\min}(Q)}(\theta_{\max}d_\theta + \sigma_b d_\sigma), \tag{75}$$

and $\theta_{\max}$ is defined in (64). We notice that the Lyapunov function (72) and its derivative (73) are independent of the choice of the control signal. Hence, the uniform bound for $\widetilde{x}(t)$ (74) is independent of the control choice.

Notice that substitution of (68) into (65) leads to the same ideal system as in (54)

$$\dot{\hat{x}}(t) = A_m\hat{x}(t) + bk_g r(t), \quad \hat{x}(0) = x_0.$$

Hence, the state predictor with the indirect control law (68) is equivalent to the ideal system in (54). Since $x(t) = \hat{x}(t) - \widetilde{x}(t)$, and $\hat{x}(t) = x_m(t)$, where $x_m(t)$ is the state of an exponentially stable ideal system, then $x(t)$ is uniformly bounded. Finally, bound (74) implies that the

tracking error can be arbitrarily reduced if we increase the adaptation gain Γ.

$\mathcal{L}_1$ Adaptive Control

The $\mathcal{L}_1$ adaptive-control architecture for an unknown plant input gain is presented in Figure 7(c) [61]. Consider the plant (50), and assume that (52) holds. The $\mathcal{L}_1$ adaptive controller uses the same state predictor and adaptation laws as the indirect MRAC given by (65)–(66) and (69)–(71), respectively. Therefore, the $\mathcal{L}_1$ controller has the same prediction error dynamics as the indirect MRAC (67), and the uniform bound on the prediction error given in (74) also holds. The key difference between the indirect MRAC and the $\mathcal{L}_1$ adaptive controller lies in the definition of the control law. Recall that, in the case of known plant input gain, the $\mathcal{L}_1$ adaptive controller considers a lowpass filter in the definition of the control law (18). However, in the presence of an unknown plant input gain, the lowpass filter cannot be directly applied to the control signal. To show where the problem lies, consider the filtered version of the control signal in (68)

$$u_f(s) = C_f(s)u(s),$$

where $u(s)$ is the Laplace transform of $u(t)$ in (68), and $C_f(s)$ is a lowpass filter. Let $c_f(t)$ be the impulse response of the transfer function $C_f(s)$. Then

$$u_f(t) = c_f(t) * u(t) = c_f(t) * \left(\frac{k_g r(t) - \hat{\theta}^\top(t)x(t) - \hat{\sigma}(t)}{\hat{\omega}(t)} \right),$$

where $*$ denotes the convolution operator. Substituting this expression in the state predictor (65), we obtain

$$\dot{\hat{x}}(t) = A_m \hat{x}(t) + b \left(\hat{\omega}(t) c_f(t) * \left(\frac{k_g r(t) - \hat{\theta}^\top(t)x(t) - \hat{\sigma}(t)}{\hat{\omega}(t)} \right) + \hat{\theta}^\top(t)x(t) + \hat{\sigma}(t) \right). \tag{76}$$

Notice that the parameter estimate $\hat{\omega}(t)$ may change rapidly due to the fast adaptation that, along with the fact that the convolution operator does not allow cancellation of $\hat{\omega}(t)$, may result in unpredictable consequences on the system's performance. The $\mathcal{L}_1$ adaptive controller instead generates the control $u(t)$ from

$$u(s) = kD(s)\hat{\eta}(s), \tag{77}$$

where k is a positive feedback gain, $\hat{\eta}(s)$ is the Laplace transform of

$$\hat{\eta}(t) \triangleq k_g r(t) - \hat{\omega}(t)u(t) - \hat{\theta}^\top(t)x(t) - \hat{\sigma}(t),$$

and $D(s)$ is a strictly proper transfer function such that, for all $\omega \in [\omega_{\min}, \omega_{\max}]$, the strictly proper transfer function

$$C(s) = \frac{\omega k D(s)}{1 + \omega k D(s)} \tag{78}$$

is exponentially stable and has unit dc gain $C(0) = 1$ [61]. The choice $D(s) = 1/s$ with $k > 0$ results in an exponentially stable strictly proper transfer function

$$C(s) = \frac{k\omega}{s + k\omega}.$$

Notice that in (77), $\hat{\omega}(s)$ does not multiply $kD(s)$. Therefore, in this approach $\hat{\omega}(t)$ can be viewed as a time-varying gain of the filter (78), which compensates for $\hat{\omega}(t)$ in (76).

To better understand the nature of the control law (77), notice that the requirement $C(0) = 1$ implies that $D(s)$ must contain an integrator. Hence, for the case of slowly varying parameters $\theta(t)$ and $\sigma(t)$, in steady state, when $u(t)$ is approximately a constant, the input to the filter must be $\hat{\eta}(t) \approx 0$. Therefore, control law (77) leads to

$$k_g r(t) - \hat{\omega}(t)u(t) - \hat{\theta}^\top(t)x(t) - \hat{\sigma}(t) \approx 0. \tag{79}$$

Comparing (79) to the indirect MRAC control law (68), we find that the $\mathcal{L}_1$ control law avoids division by $\hat{\omega}(t)$. The filter in the $\mathcal{L}_1$ control law (77) solves the design equation dynamically by driving $\hat{\eta}(t)$ in (77) to zero [5].

$\mathcal{L}_1$ Reference System

Similar to the scalar case with known plant input gain, the closed-loop system with the $\mathcal{L}_1$ adaptive controller does not follow the ideal system (54)–(55) due to the limited bandwidth of the control channel enforced by $C(s)$. To derive the dynamics of the reference system for the plant (50)–(51), consider the case of known plant parameters. Then the controller (77) takes the form

$$u_{\text{ref}}(s) = kD(s)(k_g r(s) - \eta_{\text{ref}}(s) - \omega u_{\text{ref}}(s)), \tag{80}$$

where $\eta_{\text{ref}}(s)$ is the Laplace transform of

$$\eta_{\text{ref}}(t) \triangleq \theta^\top(t)x_{\text{ref}}(t) + \sigma(t).$$

Thus, the reference control law can be represented as

$$u_{\text{ref}}(s) = \frac{1}{\omega} C(s)(k_g r(s) - \eta_{\text{ref}}(s)), \tag{81}$$

where $C(s)$ is defined in (78). Substituting the reference controller from (81) into the plant dynamics (50) leads to the $\mathcal{L}_1$ reference model

$$\dot{x}_{\text{ref}}(t) = A_m x_{\text{ref}}(t) + b(\omega u_{\text{ref}}(t) + \theta^\top(t)x_{\text{ref}}(t) + \sigma(t)), \quad x_{\text{ref}}(0) = x_0. \tag{82}$$

Reference Controller for Multivariable Systems

The ideas discussed in "Bridging Adaptive and Robust Control" for the scalar case can be extended to the vector case. To this end, we consider the reference system (82) for zero initial conditions. In frequency domain (82) can be written as

$$x_{\text{ref}}(s) = H(s)(\omega u_{\text{ref}}(s) + \eta_{\text{ref}}(s)). \tag{S6}$$

We choose a constant vector $c_0^\top$ satisfying the conditions of Lemma S2, which ensures that the transfer function $c_0^\top H(s)$ is minimum phase and has relative degree one. Therefore, the transfer function $kD(s)\,c_0^\top/(c_0^\top H(s))$ is proper. Hence, multiplying (S6) by this transfer function, we obtain

$$\frac{kD(s)c_0^\top}{c_0^\top H(s)}\, x_{\text{ref}}(s) = kD(s)(\omega u_{\text{ref}}(s) + \eta_{\text{ref}}(s)).$$

Substituting this expression into (80) for the reference control signal and isolating $u(s)$, we obtain the reference controller

$$u_{\text{ref}}(s) = kD(s)k_g\, r(s) - \frac{kD(s)c_0^\top}{c_0^\top H(s)}\, x_{\text{ref}}(s),$$

which further can be rewritten as

$$u_{\text{ref}}(s) = \frac{kD(s)}{c_0^\top H(s)}\left(c_0^\top\, H(s)k_g\, r(s) - c_0^\top x_{\text{ref}}(s)\right). \tag{S7}$$

Control law (S7) produces the same control signal as (80), however, compared to (80), control law (S7) does not depend on the unknown plant parameters and the disturbance.

The lowpass filter $C(s)$ can thus be viewed as a means for resolving the ambiguity in (76) due to the convolution, which also deviates from the ideal system, by leading to the $\mathcal{L}_1$ reference system (81)–(82). Setting the bandwidth of $C(s)$ to be comparable with the control channel bandwidth, the reference system in (81)–(82) achieves partial compensation of the uncertainty within the bandwidth of the control channel. For more details about the bandwidth of the control system refer to "Available Bandwidth of Control Systems."

The closed-loop $\mathcal{L}_1$ reference system can be written in the frequency domain as

$$x_{\text{ref}}(s) = H(s)\,C(s)k_g r(s) + H(s)(1-C(s))\eta_{\text{ref}}(s) + x_{\text{in}}(s), \tag{83}$$

where $H(s) \triangleq (s\mathbb{I} - A_m)^{-1}b$, and

$$x_{\text{in}}(s) \triangleq (s\mathbb{I} - A_m)^{-1}x_0$$

is the Laplace transform of the ideal system response due to the initial conditions. From (83) we obtain the bound

$$\begin{aligned}\|x_{\text{ref}}\|_{\mathcal{L}_\infty} \le\ & \|H(s)C(s)\|_{\mathcal{L}_1}\|k_g\|r\|_{\mathcal{L}_\infty}\| \\ & + \|G(s)\|_{\mathcal{L}_1}(L\|x_{\text{ref}}\|_{\mathcal{L}_\infty} + \sigma_b) + \|x_{\text{in}}\|_{\mathcal{L}_\infty},\end{aligned} \tag{84}$$

where

$$L \triangleq \max_{\theta\in\Theta}\|\theta\|_1, \qquad G(s) \triangleq H(s)(1-C(s)).$$

Assuming

$$\|G(s)\|_{\mathcal{L}_1} < \frac{1}{L}, \tag{85}$$

we can rewrite the bound (84) as

$$\|x_{\text{ref}}\|_{\mathcal{L}_\infty} \le \frac{\|H(s)C(s)\|_{\mathcal{L}_1}\|k_g\|r\|_{\mathcal{L}_\infty} + \|G(s)\|_{\mathcal{L}_1}\sigma_b + \|x_{\text{in}}\|_{\mathcal{L}_\infty}}{1 - \|G(s)\|_{\mathcal{L}_1}L}.$$

Notice that (85) is consistent with the stability condition obtained for the scalar case (24) and can be satisfied for arbitrary $H(s)$ by choosing $C(s)$ with sufficiently large bandwidth.

Notice that the reference control signal (80) depends on the unknown parameters ω, $\theta(t)$, and the disturbance $\sigma(t)$. In "Reference Controller for Multivariable Systems," an alternative form of this controller is derived, which facilitates implementation.

Uniform Performance Bounds

To derive the performance bounds, we follow the steps similar to the scalar case, described in (26)–(31) and obtain [61]

$$\|x_{\text{ref}} - x\|_{\mathcal{L}_\infty} \le \frac{\gamma_1}{\sqrt{\Gamma}}, \tag{86}$$

$$\|u_{\text{ref}} - u\|_{\mathcal{L}_\infty} \le \frac{\gamma_2}{\sqrt{\Gamma}}, \tag{87}$$

where

$$\gamma_1 \triangleq \frac{\|C(s)\|_{\mathcal{L}_1}}{1 - \|G(s)\|_{\mathcal{L}_1}L}\,\gamma_0, \tag{88}$$

$$\gamma_2 \triangleq \frac{1}{\omega}\,\|C(s)\|_{\mathcal{L}_1}L\gamma_1 + \frac{1}{\omega}\left\|\frac{C(s)c_0^\top}{c_0^\top H(s)}\right\|_{\mathcal{L}_1}\gamma_0, \tag{89}$$

γ_0 is given by (75), and $c_0 \in \mathbb{R}^n$ is an arbitrary vector that makes $c_0^\top H(s)$ minimum phase and relative degree one. For more details on the role of c_0, see "Special Form of State-to-Input Stability." Notice that the performance bounds (86)–(87) are inversely proportional to $\sqrt{\Gamma}$. Increasing the adaptation gain Γ is limited by the available CPU and high-frequency sensor noise. Notice that these performance bounds are derived in the case where the initial conditions of state predictor (65)–(66) are equal to the initial conditions of plant (50)–(51). However, similar performance bounds can be derived for the case of their initialization mismatch. For details, see "Performance Bounds and Time-Delay Margin in the Presence of Nonzero Trajectory Initialization Errors."

Special Form of State-to-Input Stability

Consider the system

$$\dot{x}(t) = A_m x(t) + bu(t), \quad x(0) = 0, \tag{S8}$$

where $x(t) \in \mathbb{R}^n$ is the state, $u(t) \in \mathbb{R}$ is the control input, which is assumed to be bounded and piecewise-continuous, $A_m \in \mathbb{R}^{n\times n}$, and $b \in \mathbb{R}^n$. Let $H(s) \triangleq (s\mathbb{I}-A_m)^{-1}b$, so that

$$x(s) = H(s)u(s).$$

The norm of the system state for all $\tau \geq 0$ satisfies the bound

$$\|x_\tau\|_{\mathcal{L}_\infty} \leq \|H(s)\|_{\mathcal{L}_1}\|u_\tau\|_{\mathcal{L}_\infty}.$$

It follows that, for an exponentially stable proper linear system with zero initial conditions, it is possible to bound the norm of the output by a function of the norm of the input. The opposite question can also be asked, namely, whether it is possible to find a bound on the system input in terms of its output, without invoking the derivatives of the output. While for system (S8) the answer to this question is negative [S5], we show that a bound can be derived for the lowpass-filtered input signal. For this purpose, let

$$H(s) = \frac{N(s)}{D(s)}, \tag{S9}$$

where $D(s) = \det(s\mathbb{I}-A)$, and $N(s)$ is the $n \times 1$ vector whose ith component is the polynomial function of the form

$$N_i(s) = \sum_{j=1}^{n} W_{ij}s^{j-1}. \tag{S10}$$

LEMMA S2

If the pair (A_m, b) in (S8) is controllable, then there exists $c_o \in \mathbb{R}^n$ such that $c_o^\top N(s)/D(s)$ has relative degree one, that is, $\deg(D(s))-\deg(c_0^\top N(s)) = 1$ and $N(s)$ has all its zeros in the open left-half plane.

Proof

It follows from (S9) that for arbitrary $c_o \in \mathbb{R}^n$

$$c_o^\top H(s) = \frac{c_o^\top W[s^{n-1}\cdots 1]^\top}{D(s)},$$

where $W \in \mathbb{R}^{n\times n}$ is the matrix whose (i,j) entry W_{ij} is introduced in (S10).

Controllability of (A_m, b) implies that W has full rank. Indeed, if the system is controllable, then for a given initial condition $x(0) = 0$ and arbitrary t_1 and x_{t_1}, there exists $u(\tau)$, $\tau \in [0, t_1]$ such that $x(t_1) = x_{t_1}$. If W is not full rank, then there exists nonzero $\mu \in \mathbb{R}^n$ such that $\mu^\top N(s) = 0$. Thus, for $x(0) = 0$ and for all $u(s)$ we have

$$\mu^\top x(s) = \mu^\top \frac{N(s)}{D(s)}\, u(s) = 0,$$

which implies that, in particular, $x(t) \neq \mu$ for all t. This conclusion contradicts the fact that $x(t_1) = x_{t_1}$ can be an arbitrary point in $\mathbb{R}^n$. Thus, W must be full rank.

Consider an arbitrary vector $\bar{c} \in \mathbb{R}^n$ such that $\bar{c}^\top[s^{n-1}\cdots 1]^\top$ is a Hurwitz polynomial of degree $n-1$, and let $c_o = (W^{-1})^\top \bar{c}$. Then

$$c_o^\top(s\mathbb{I}-A)^{-1}b = \frac{\bar{c}^\top[s^{n-1}\cdots 1]^\top}{D(s)}$$

has relative degree one with all its zeros in the open left-half plane. □

Next, let $C(s)$ be a strictly proper exponentially stable transfer function. Lemma S2 implies that there exists $c_o \in \mathbb{R}^n$ such that $c_o^\top H(s)$ has relative degree one, and $c_o^\top H(s)$ has all its zeros in the open left-half plane. Hence, we can write

$$C(s)u(s) = \frac{C(s)}{c_o^\top H(s)}\, c_o^\top H(s)u(s) = H_1(s)x(s),$$

where

$$H_1(s) \triangleq \frac{C(s)}{c_o^\top H(s)}c_o^\top$$

is proper and exponentially stable. Next, letting $\nu(s) \triangleq C(s)u(s)$, we have the bound

$$\|\nu_\tau\|_{\mathcal{L}_\infty} \leq \|H_1(s)\|_{\mathcal{L}_1}\|x_\tau\|_{\mathcal{L}_\infty}.$$

The filtered input signal $\nu(t)$ can thus be bounded in terms of the $\mathcal{L}_\infty$-norm of the system output.

REFERENCE

[S5] D. Liberzon, A. S. Morse, and E. D. Sontag, "Output-input stability and minimum-phase nonlinear systems," *IEEE Trans. Automat. Contr.*, vol. 47, no. 3, pp. 422–436, 2002.

BENCHMARK PROBLEM: ROHRS'S EXAMPLE

In this section we analyze Rohrs's example from [27] and [63], which illustrates the robustness features of the MRAC architectures. Specifically, this example demonstrates that, in the absence of specific modifications for bounding the adaptive parameters, such as projection [64], σ-modification [32], and e-modification [35], standard MRAC architecture can be destabilized due to unmodeled dynamics at the plant input. The fact that arbitrarily small disturbances can lead to instability in adaptive-control schemes that do not have a protection for preventing parameter drift is illustrated in [65, Ex. 9]. The following discussion highlights properties of the $\mathcal{L}_1$ adaptive controller that help to prevent this type of instability.

The plant under consideration in [63] is the first-order exponentially stable system with unknown time-constant and dc gain and with two heavily damped, high-frequency unmodeled poles given by

Performance Bounds and Time-Delay Margin in the Presence of Nonzero Trajectory Initialization Errors

In the design of state-feedback $\mathcal{L}_1$ controllers, the state predictor is initialized identically to the plant. Next, we analyze the degradation of the performance bounds due to initialization errors.

For simplicity consider the plant (50)–(51) with constant uncertain parameters $\theta(t) = \theta$, while retaining the time-varying disturbance $\sigma(t)$. We consider the state-predictor (65)–(66) with initial conditions that are different from the initial conditions of the plant, that is, $\hat{x}(0) = \hat{x}_0 \neq x_0$. This control system results in the prediction dynamics (67) but with the nonzero initial condition $\tilde{x}(0) = \hat{x}_0 - x_0$. Next, we consider the same adaptation laws as in (69)–(71) and the $\mathcal{L}_1$ control law given by (77). To derive the performance bounds for the closed-loop adaptive system with the $\mathcal{L}_1$ adaptive controller, we require the following notation. For an m-input, n-output exponentially stable proper transfer function $F(s)$ with impulse-response matrix $f(t)$, let

$$\Psi_F(t) \triangleq \max_{i=1,\ldots,n} \sqrt{\sum_{j=1}^{m} f_{ij}^2(t)},$$

where $f_{ij}(t)$ is the (i,j) entry of the impulse-response matrix $f(t)$. Then for the prediction error dynamics in (67) with nonzero initial conditions $\tilde{x}(0) \neq 0$, the bound in (74) becomes

$$\|\tilde{x}(t)\| \leq \rho(t), \quad \text{for all} \quad t \geq 0, \tag{S11}$$

where

$$\rho(t) \triangleq \sqrt{\frac{\left(V(0) - \frac{\theta_n}{\Gamma}\right)e^{-\alpha t}}{\lambda_{\min}(P)} + \frac{\theta_n}{\lambda_{\min}(P)\Gamma}}, \quad \alpha \triangleq \frac{\lambda_{\min}(Q)}{\lambda_{\max}(P)},$$

$$\theta_n \triangleq 4\theta_{\max}^2 + 4\sigma_b^2 + (\omega_{\max} - \omega_{\min})^2 + \frac{4\sigma_b d_\sigma}{\alpha},$$

where $V(t)$ is the Lyapunov function (72) [4, Lemma 2.2.5]. Notice that this bound contains an exponentially decaying term and a constant component. In the limiting case, when the exponential term diminishes, this bound reduces to the one in (74), that is,

$$\lim_{t\to\infty} \rho(t) = \frac{\gamma_0}{\sqrt{\Gamma}}.$$

Using the bound on the prediction error in (S11) in the presence of nonzero initialization error, we obtain the performance bounds [4, Thm. 2.2.3]

$$\|x_{\text{ref}}(t) - x(t)\|_\infty \leq \gamma_3(t),$$

$$\|u_{\text{ref}}(t) - u(t)\|_\infty \leq \frac{1}{\omega}\Psi_{H_1}(t) * (\rho(t) + \|\tilde{x}_{\text{in}}(t)\|) + \Psi_{H_3}(t) * \gamma_3(t),$$

which hold for all $t \geq 0$, and all $c_0 \in \mathbb{R}^n$ resulting in minimum-phase and relative-degree-one $c_0^\top H(s)$, where

$$\gamma_3(t) \triangleq \Psi_{H_2}(t) * (\rho(t) + \|\tilde{x}_{\text{in}}(t)\|),$$

$$H_1(s) = \frac{C(s)c_0^\top}{c_0^\top H(s)}, \quad H_2(s) = (\mathbb{I} - G(s)\theta^{\mathsf{T}})^{-1}C(s), \quad H_3(s) = -\frac{C(s)\theta^\top}{\omega},$$

and $\tilde{x}_{\text{in}}(t)$ is the inverse Laplace transform of $\tilde{x}_{\text{in}}(s) \triangleq (s\mathbb{I} - A_m)^{-1}(\hat{x}_0 - x_0)$.

The conclusion is that, for linear time-invariant plants, arbitrary nonzero trajectory initialization errors lead to exponentially decaying transient errors in the input and output signals of the control system.

The next theorem [3] quantifies the time-delay margin at the plant input.

THEOREM S1

Consider plant (50)–(51) with constant uncertain parameters $\theta(t) = \theta$, subject to the bounds (52)–(53) on the uncertainties. Furthermore, consider the state predictor (65)–(66) whose initial conditions differ from the initial conditions of the plant, that is, $\hat{x}(0) = \hat{x}_0 \neq x_0$, and the adaptation laws (69)–(71). Let the adaptive controller be defined according to (77) with $D(s) = 1/s$. Further, let $\mathcal{T}$ be the time-delay margin of the linear time-invariant system with the loop transfer function given by

$$L_o(s) = \frac{C(s)}{1 - C(s)}(1 + \theta^\top \bar{H}(s))$$

and

$$\bar{H}(s) \triangleq (s\mathbb{I} - A_m - b\theta^\top)^{-1}b.$$

If the $\mathcal{L}_1$-norm condition in (85) holds, then for each input time-delay τ satisfying

$$\tau < \mathcal{T},$$

there exist the projection bound σ_b and the adaptation gain Γ such that the closed-loop system is bounded-input, bounded-output stable.

This result is semiglobal in the sense that for each bound $\|x_0\| \leq \rho_0$ on the initial conditions there exists a projection bound $\Delta(\rho_0)$ that ensures that the closed-loop system has time-delay margin τ.

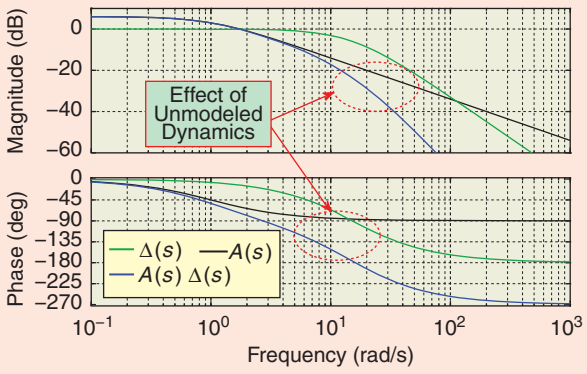

FIGURE 8 Impact of the unmodeled dynamics. The poles of the unmodeled dynamics are much faster than the pole of the plant. Therefore, the unmodeled dynamics start significantly affecting the Bode diagram of the plant in the region where the magnitude of the plant's frequency response is less than −20 dB.

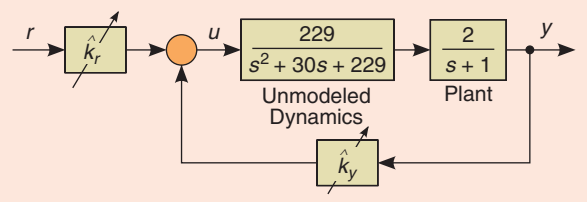

FIGURE 9 Rohrs's example. Closed-loop model reference adaptive-control system with fast, overdamped unmodeled dynamics. The estimates $\hat{k}_r$ and $\hat{k}_y$ are driven by the adaptation laws (93), (94).

$$y(s) = A(s)\mu(s), \quad A(s) = \frac{2}{s+1}, \tag{90}$$

$$\mu(s) = \Delta(s)u(s), \quad \Delta(s) = \frac{229}{s^2 + 30s + 229}. \tag{91}$$

The plant has a gain-crossover frequency of $\omega_{gc} = 1.70$ rad/s and a phase margin of $\phi_m = 107.67°$. Its phase-crossover frequency and the gain margin are $\omega_{\phi c} = 16.09$ rad/s and $g_m = 24.62$ dB, respectively. The control objective in [63] is given by the exponentially stable reference model

$$y_m(s) = \frac{3}{s+3} r(s).$$

Notice that the poles of the unmodeled dynamics are faster than poles of the plant and are separated from the plant dynamics in their frequency range. The Bode plot given in Figure 8 illustrates this separation. We see that the unmodeled dynamics affect the plant's Bode diagram in the region with less than −20 dB magnitude, where the input signals are attenuated. Usually, a properly designed control system does not attempt to act in the frequency range beyond the plant dynamics, where the level of uncertainty is usually high. Thus, from a classical control point of view, it is not difficult to handle unmodeled dynamics (91).

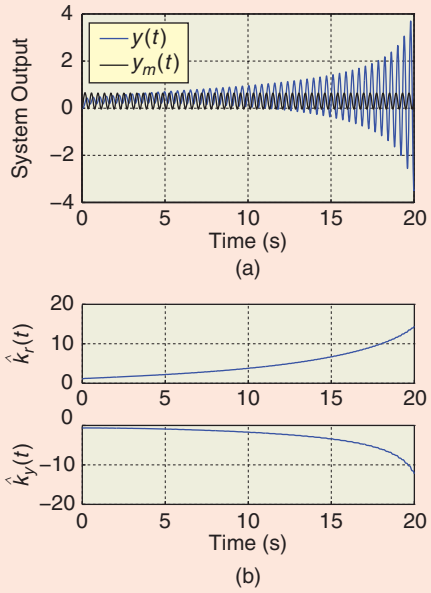

FIGURE 10 Closed-loop model reference adaptive-control response to $r_1(t)$, whose frequency is the phase-crossover frequency of the plant. The adaptive estimates in (b) experience parameter drift, which leads to instability and unbounded growth of the system output. (a) System output $y(t)$, $y_m(t)$ and (b) controller parameters $\hat{k}_r(t)$, $\hat{k}_y(t)$.

MRAC. Parameter Drift

The MRAC controller for plant (90) takes the form

$$u(t) = \hat{k}_y(t)y(t) + \hat{k}_r(t)r(t), \tag{92}$$

$$\dot{\hat{k}}_y(t) = -e(t)y(t), \quad \hat{k}_y(0) = \hat{k}_{y0}, \tag{93}$$

$$\dot{\hat{k}}_r(t) = -e(t)r(t), \quad \hat{k}_r(0) = \hat{k}_{r0}, \tag{94}$$

where $e(t) = y(t) - y_m(t)$. The corresponding feedback loop of the MRAC architecture is shown in Figure 9.

For simulations we consider the same reference inputs as in [63]. The first reference input

$$r_1(t) = 0.3 + 1.85\sin(16.1t) \tag{95}$$

has the frequency equal to the phase-crossover frequency of the plant with the unmodeled dynamics (90)–(91), while the second reference input

$$r_2(t) = 0.3 + 2\sin(8t) \tag{96}$$

is also a sinusoidal reference signal but at a frequency that is approximately half of the phase-crossover frequency of (90)–(91). We use the same initial conditions as in [63], namely, $y(0) = 0$, $\hat{k}_r(0) = 1.14$, and $\hat{k}_y(0) = -0.65$. The simulation results from [63] are reproduced in figures 10 and

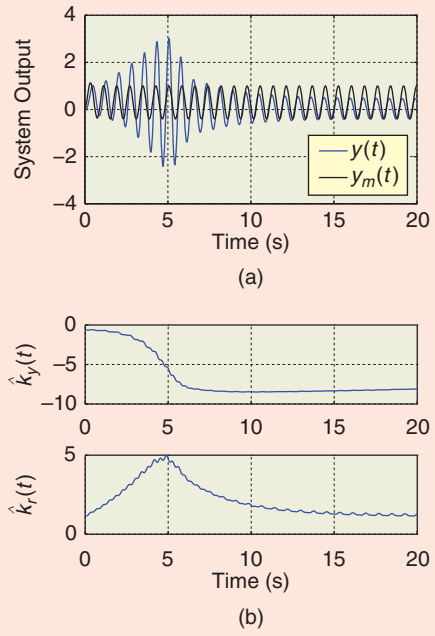

FIGURE 11 Closed-loop model reference adaptive-control (MRAC) response to $r_2(t)$, whose frequency is approximately half of the phase-crossover frequency of the plant. The parameter estimates for a short period of time move to the set for which the controller with frozen parameters is unstable. This behavior of the estimates results in temporary instability of the closed-loop MRAC and causes bursting of the system output $y(t)$, $y_m(t)$ shown in (a).

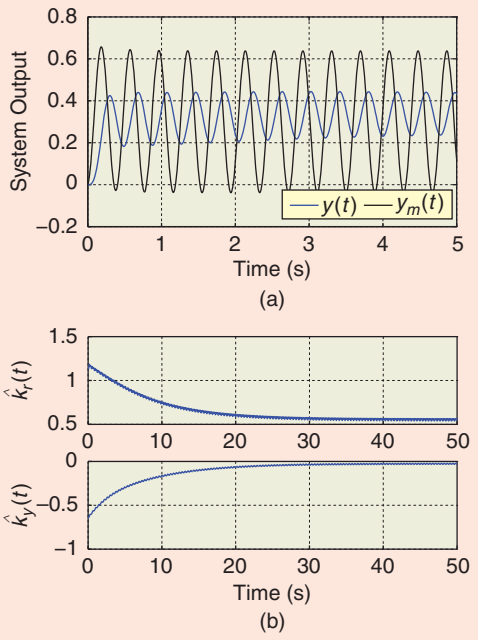

FIGURE 12 Closed-loop model reference adaptive control with the σ-modification response to $r_1(t)$. The damping term is set to $\sigma_m = 0.2$. The parameter estimates and system output remain bounded. (a) System output $y(t)$, $y_m(t)$ and (b) controller parameters $\hat{k}_r(t)$, $\hat{k}_y(t)$.

11. In Figure 10, we can see that, while tracking $r_1(t)$, the closed-loop system is unstable due to parameter drift. In Figure 11, bursting occurs in the response of the closed-loop adaptive system to the reference signal $r_2(t)$. Next we consider the σ-modification of the adaptation laws, which recovers stability of the adaptive-control system.

MRAC with the σ-Modification

The adaptation laws for MRAC with the σ-modification are obtained from (93), (94) by adding damping terms, which leads to

$$\dot{\hat{k}}_y(t) = -e(t)y(t) - \sigma_m \hat{k}_y(t), \quad \hat{k}_y(0) = \hat{k}_{y0}, \tag{97}$$

$$\dot{\hat{k}}_r(t) = -e(t)r(t) - \sigma_m \hat{k}_r(t), \quad \hat{k}_r(0) = \hat{k}_{r0}, \tag{98}$$

where $\sigma_m \in (0, \infty)$ is a constant damping parameter. The control law remains unchanged and is given by (92).

For the simulations we use the same parameters for MRAC as in the previous section, and we consider the same reference signal as in (95). Figure 12 presents the simulation results for $\sigma_m = 0.2$. In this case the parameter estimates converge, and we do not observe parameter drift. However, the simulation results for $\sigma_m = 0.1$ in Figure 13 show that the parameter estimates experience drift, although the divergence rate is slower as compared to the results in Figure 10. This can be explained by the fact that

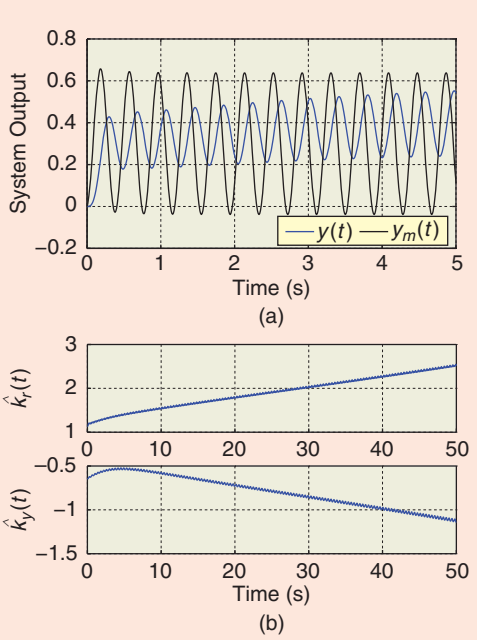

FIGURE 13 Closed-loop model reference adaptive control with the σ-modification response to $r_1(t)$. The damping term is set to $\sigma_m = 0.1$. The value of σ_m is insufficient to ensure robustness to the given unmodeled dynamics. Therefore, the adaptive estimates in (b) experience parameter drift, which leads to instability and unbounded growth of the system output in (a). (a) System output $y(t)$, $y_m(t)$ and (b) controller parameters $\hat{k}_r(t)$, $\hat{k}_y(t)$.

$\mathcal{L}_1$ Adaptive Controller for Systems with Unmodeled Actuator Dynamics

Consider the system with multiplicative unmodeled dynamics located at the plant input [S6] given by

$$\dot{x}(t) = A_m x(t) + b\big(\mu(t) + \theta^\top(t)x(t) + \sigma_0(t)\big), \quad x(0) = x_0, \tag{S12}$$

$$y(t) = c^\top x(t), \tag{S13}$$

where the state vector $x(t) \in \mathbb{R}^n$ is assumed to be measured; $y(t) \in \mathbb{R}$ is the regulated system output; $A_m \in \mathbb{R}^{n\times n}$ is a known Hurwitz matrix specifying the desired closed-loop dynamics; b, $c \in \mathbb{R}^n$ are known constant vectors; $\theta(t) \in \mathbb{R}^n$ is a vector of time-varying unknown parameters; $\sigma_0(t) \in \mathbb{R}$ is a time-varying disturbance; and $\mu(t) \in \mathbb{R}$ is the output of the system

$$\mu(s) = F(s)u(s),$$

where $u(t) \in \mathbb{R}$ is the control input, and $F(s)$ is an unknown exponentially stable transfer function whose dc gain has known sign.

Let $\theta(t)$ and $\sigma_0(t)$, for all $t \geq 0$, satisfy

$$\theta(t) \in \Theta, \quad \sigma_0(t) \in \Delta = [-\sigma_b, \sigma_b], \tag{S14}$$

$$\|\dot{\theta}(t)\| \leq d_\theta < \infty, \quad |\dot{\sigma}_0(t)| \leq d_\sigma < \infty, \tag{S15}$$

where Θ is a known convex compact set, and σ_b, d_θ, $d_\sigma \in (0, \infty)$ are known bounds. Also assume that there exists known $L_F > 0$ verifying $\|F(s)\|_{\mathcal{L}_1} \leq L_F$, and known constants ω_l, $\omega_u \in \mathbb{R}$ satisfying

$$0 < \omega_l \leq F(0) \leq \omega_u, \tag{S16}$$

where, without loss of generality, we assume $F(0) > 0$. Finally, for design purposes, we assume that we know a set $\mathbb{F}_\Delta$ of all admissible actuator dynamics.

The design of the $\mathcal{L}_1$ adaptive controller proceeds by considering a positive feedback gain $k > 0$ and a strictly proper, stable transfer function $D(s)$, such that

$$C(s) \triangleq \frac{kF(s)D(s)}{1 + kF(s)D(s)} \tag{S17}$$

is strictly proper exponentially stable transfer function with dc gain $C(0) = 1$ for all $F(s) \in \mathbb{F}_\Delta$.

Next we present the elements of the $\mathcal{L}_1$ adaptive-control architecture for the class of systems with unmodeled dynamics at the plant input. The state predictor is given by

$$\dot{\hat{x}}(t) = A_m\hat{x}(t) + b\big(\hat{\omega}(t)u(t) + \hat{\theta}^\top(t)x(t) + \hat{\sigma}(t)\big), \quad \hat{x}(0) = x_0, \tag{S18}$$

$$\hat{y}(t) = c^\top\hat{x}(t), \tag{S19}$$

where $\hat{x}(t) \in \mathbb{R}^n$ is the predictor state, while $\hat{\omega}(t)$, $\hat{\sigma}(t) \in \mathbb{R}$ and $\hat{\theta}(t) \in \mathbb{R}^n$ are the adaptive estimates driven by the adaptation laws, given by

$$\dot{\hat{\omega}}(t) = \Gamma\text{Proj}(\hat{\omega}(t), -\tilde{x}^\top(t)Pbu(t)), \quad \hat{\omega}(0) = \hat{\omega}_0, \tag{S20}$$

$$\dot{\hat{\theta}}(t) = \Gamma\text{Proj}(\hat{\theta}(t), -\tilde{x}^\top(t)Pbx(t)), \quad \hat{\theta}(0) = \hat{\theta}_0, \tag{S21}$$

$$\dot{\hat{\sigma}}(t) = \Gamma\text{Proj}(\hat{\sigma}(t), -\tilde{x}^\top(t)Pb), \quad \hat{\sigma}(0) = \hat{\sigma}_0, \tag{S22}$$

where $\tilde{x}(t) \triangleq \hat{x}(t) - x(t)$, $\Gamma \in (0, \infty)$ is the adaptation gain, and the symmetric positive-definite matrix $P = P^\top > 0$ solves the

the value of σ_m is not chosen sufficiently large to prevent the parameter drift. Therefore, we see that the damping term affects the robustness of the closed-loop system, and thus the value of the damping term must be chosen large enough to ensure stability in the presence of unmodeled dynamics.

We notice that the goal of the σ-modification is to recover stability. To analyze its performance we show simulations of the MRAC with the σ-modification for step reference signals with different sizes. We perform tuning of the system for the case $r(t) = 1$, which suggests the choice $\sigma_m = 0.2$. Figure 14 shows that, for the step reference commands $r(t) = 1$, $r(t) = 2$, and $r(t) = 3$, the system transient changes dramatically. The performance of the closed-loop system is thus unpredictable for different reference commands.

$\mathcal{L}_1$ Adaptive Controller

Next we apply the $\mathcal{L}_1$ adaptive controller from "$\mathcal{L}_1$ Adaptive Controller for Systems with Unmodeled Actuator Dynamics" to Rohrs's example. For this purpose, we rewrite this example in state-space form as

$$\dot{x}(t) = -3x(t) + 2(\mu(t) + x(t)), \quad x(0) = x_0,$$
$$y(t) = x(t),$$

where

$$\mu(s) = \frac{229}{s^2 + 30s + 229}\,u(s).$$

Then, the state predictor takes the form

$$\dot{\hat{x}}(t) = -3\hat{x}(t) + 2(\hat{\omega}(t)u(t) + \hat{\theta}(t)x(t) + \hat{\sigma}(t)), \quad \hat{x}(0) = x_0,$$
$$\hat{y}(t) = \hat{x}(t),$$

with $\hat{\omega}(t)$, $\hat{\theta}(t)$ and $\hat{\sigma}(t)$ governed by

$$\dot{\hat{\omega}}(t) = \Gamma\text{Proj}(\hat{\omega}(t), -\tilde{x}(t)u(t)), \quad \hat{\omega}(0) = \hat{\omega}_0, \tag{99}$$

$$\dot{\hat{\theta}}(t) = \Gamma\text{Proj}(\hat{\theta}(t), -x(t)\tilde{x}(t)), \quad \hat{\theta}(0) = \hat{\theta}_0, \tag{100}$$

$$\dot{\hat{\sigma}}(t) = \Gamma\text{Proj}(\hat{\sigma}(t), -\tilde{x}(t)), \quad \hat{\sigma}(0) = \hat{\sigma}_0. \tag{101}$$

The $\mathcal{L}_1$ control law is given by

$$u(s) = -kD(s)(\hat{\eta}(s) - k_g r(s)),$$

Lyapunov equation $A_m^{\top}P + PA_m = -Q$ for arbitrary $Q = Q^{\top} > 0$. The adaptive control law is given by

$$u(s) = -kD(s)(\hat{\eta}(s) - k_g r(s)), \tag{S23}$$

where $k_g \triangleq -1/(c^{\top}A_m^{-1}b)$; $r(s)$ and $\hat{\eta}(s)$ are the Laplace transforms of $r(t)$, and

$$\hat{\eta}(t) \triangleq \hat{\omega}(t)u(t) + \hat{\theta}^{\top}(t)x(t) + \hat{\sigma}(t).$$

The $\mathcal{L}_1$ reference system for this architecture is given by

$$\dot{x}_{\text{ref}}(t) = A_m x_{\text{ref}}(t) + b\big(\mu_{\text{ref}}(t) + \theta^{\top}(t)x_{\text{ref}}(t) + \sigma_0(t)\big), \quad x_{\text{ref}}(0) = x_0, \tag{S24}$$

$$\mu_{\text{ref}}(s) = F(s)u_{\text{ref}}(s), \tag{S25}$$

$$u_{\text{ref}}(s) = \frac{C(s)}{F(s)}(k_g r(s) - \eta_{\text{ref}}(s)), \tag{S26}$$

$$y_{\text{ref}}(t) = c^{\top}x_{\text{ref}}(t), \tag{S27}$$

where $x_{\text{ref}}(t) \in \mathbb{R}^n$ is the reference system state vector, and $\eta_{\text{ref}}(s)$ is the Laplace transform of $\eta_{\text{ref}}(t) \triangleq \theta^{\top}(t)x_{\text{ref}}(t) + \sigma_0(t)$.

The next theorem summarizes the main result for this adaptive architecture.

THEOREM S2 [S6, THEOREM 1]

Assume that k and $D(s)$ are chosen such that

$$\|G(s)\|_{\mathcal{L}_1} L < 1, \tag{S28}$$

where

$$G(s) \triangleq (1 - C(s))H(s), \quad H(s) \triangleq (s\mathbb{I} - A_m)^{-1}b, \quad L \triangleq \max_{\theta \in \Theta} \|\theta\|_1.$$

Then for all $c_0 \in \mathbb{R}^n$ such that $c_0^{\top}H(s)$ is minimum phase and relative degree one,

$$\|\tilde{x}\|_{\mathcal{L}_\infty} \le \gamma_0,$$
$$\|x_{\text{ref}} - x\|_{\mathcal{L}_\infty} \le \gamma_1,$$
$$\|u_{\text{ref}} - u\|_{\mathcal{L}_\infty} \le \gamma_2,$$

where

$$\gamma_0 \triangleq \sqrt{\frac{\theta_m}{\lambda_{\min}(P)\Gamma}},$$

$$\gamma_1 \triangleq \frac{\|C(s)\|_{\mathcal{L}_1}}{1 - \|G(s)\|_{\mathcal{L}_1} L}\gamma_0 + \beta,$$

$$\gamma_2 \triangleq \left\|\frac{C(s)}{F(s)}\right\| L\gamma_1 + \left\|\frac{C(s)c_0^{\top}}{c_0^{\top}H(s)}\right\|_{\mathcal{L}_1}\gamma_0,$$

and $\theta_m \in (0, \infty)$ is a constant depending on the plant uncertainty bounds, and $\beta \in (0, \infty)$ is an arbitrary constant.

The value of the constant θ_m depends on the known uncertainty bounds (S14)–(S16) and the adaptive control system parameters. The expression for θ_m is given in [S6].

REFERENCE

[S6] C. Cao and N. Hovakimyan, "$\mathcal{L}_1$ adaptive controller for systems in the presence of unmodelled actuator dynamics," in *Proc. IEEE Conf. Decision and Control*, New Orleans, LA, 2007, pp. 891–896.

where $\hat{\eta}(t) \triangleq \hat{\omega}(t)u(t) + \hat{\theta}(t)x(t) + \hat{\sigma}(t)$ and $k_g = 3/2$. The block diagram of the $\mathcal{L}_1$ adaptive-control system is given in Figure 15.

The simulation plots for the inputs $r_1(t)$ and $r_2(t)$, given by (95)–(96), using the $\mathcal{L}_1$ adaptive controller with $k = 5$, $D(s) = 1/s$, and $\Gamma = 1000$, are given in figures 16–18. The initial conditions are set to $x_0 = 0$, $\hat{\omega}_0 = 1.14$, $\hat{\theta}_0 = 0.65$, and $\hat{\sigma}_0 = 0$. The projection bounds are set to $\Theta = [-10, 10]$, $\Delta = 10$, and $\Omega = [0.5, 5.5]$. Figures 16–18 show that the $\mathcal{L}_1$ adaptive controller guarantees that both the plant output and the parameters remain bounded.

Next we simulate the $\mathcal{L}_1$ adaptive controller for step reference commands. Figure 19 shows the simulation results for $r(t) = 1$, $r(t) = 2$, and $r(t) = 3$. We see that the response both for plant output and the control signal scales by the value of the step reference command $r(t)$ despite the nonlinear nature of the adaptation laws. The $\mathcal{L}_1$ adaptive controller has predictable performance in the presence of unmodeled multiplicative dynamics.

For further insight into the $\mathcal{L}_1$ adaptive controller we analyze the implementation block diagram in Figure 15 from a classical control perspective. While the feedback gain $\hat{\theta}(t)$ plays a similar role as the feedback gain $\hat{k}_y(t)$ in MRAC, the adaptive parameter $\hat{\omega}(t)$ appears in the feedforward path as a feedback gain around the integrator k/s and thus has the ability to adjust the bandwidth of the lowpass filter, the output of which is the feedback signal of the closed-loop adaptive system. Recall that in MRAC the feedforward gain $\hat{k}_r(t)$ in (92) is not engaged in the stabilization process and scales only the reference input. Note that the σ-modification and the e-modification are used only to ensure boundedness of the parameter estimates, and thus avoid the parameter drift, but do not affect the phase in the system, as $\hat{\omega}(t)$ does in the $\mathcal{L}_1$ architecture. Instead, with the $\mathcal{L}_1$ adaptive controller, the open-loop system bandwidth changes as both $\hat{\omega}(t)$ and $\hat{\theta}(t)$ adapt, which leads to simultaneous adaptation on the loop gain and the phase of the closed-loop system.

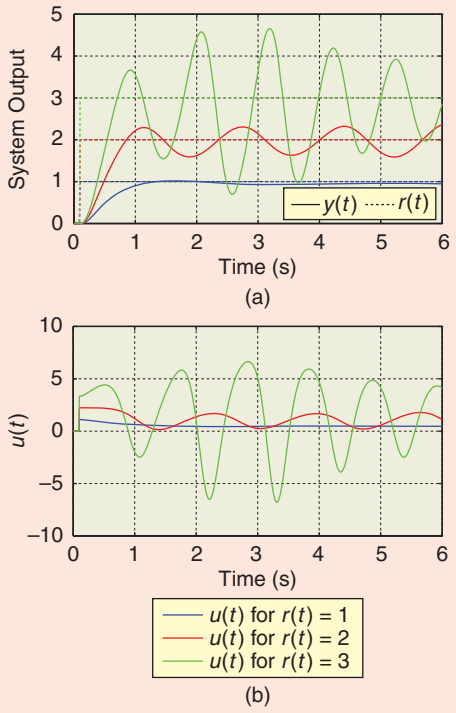

FIGURE 14 Closed-loop model reference adaptive control with the σ-modification response to $r_1(t)$. The damping term is set to $\sigma_m = 0.2$. The performance of the control system is different for different step reference commands. The transient behavior of the system is unpredictable. (a) System output $y(t)$ (solid) for various step reference commands $r(t)$ (dashed) and (b) controller history $u(t)$.

PIECEWISE CONSTANT ADAPTATION LAWS FOR $\mathcal{L}_1$ CONTROLLER

In this section we present the $\mathcal{L}_1$ adaptive output feedback controller using piecewise constant adaptation laws. For a brief review of this control architecture, applicable to non-SPR reference systems, see "$\mathcal{L}_1$ Adaptive Output-Feedback Controller with Piecewise Constant Adaptation Law." We use a first-order system to elucidate the features of this adaptation law. Thus, let the plant dynamics be given by

$$\dot{x}(t) = -ax(t) + b(u(t) + d(t)), \quad x(0) = x_0, \tag{102}$$

where $x(t) \in \mathbb{R}$ is the measured state, $a \in \mathbb{R}$ is the unknown plant parameter with known conservative bounds, $b > 0$ is a known plant parameter; $d(t) \in \mathbb{R}$ is the input disturbance. The adaptive controller must ensure that the output $x(t)$ tracks the bounded reference signal $r(t)$ with desired transient specifications given by the ideal system

$$\dot{x}_m(t) = -a_m x_m(t) + bk_g r(t), \quad x_m(0) = x_0, \tag{103}$$

where $a_m > 0$ is a known system parameter, and $k_g \triangleq a_m/b$.

Plant (102) can be written as

$$\dot{x}(t) = -a_m x(t) + b(u(t) + \sigma(t)), \tag{104}$$

where

$$\sigma(t) \triangleq \frac{a_m - a}{b} x(t) + d(t).$$

The state predictor for this example takes the form

$$\dot{\hat{x}}(t) = -a_m \hat{x}(t) + bu(t) + \hat{\sigma}(t), \tag{105}$$

where $\hat{\sigma}(t)$ is the parameter estimate generated by the sampled-data update law

$$\hat{\sigma}(t) = -\Phi^{-1}(T_s)\mu(T_s)\tilde{x}(iT_s), \quad t \in [iT_s, (i+1)T_s), \tag{106}$$

with $T_s > 0$ the adaptation sampling period, $\tilde{x}(t) \triangleq \hat{x}(t) - x(t)$, and

$$\Phi(T_s) \triangleq \int_0^{T_s} \mathrm{e}^{-a_m(T_s-\tau)} d\tau = \left[\frac{1}{a_m}\mathrm{e}^{-a_m(T_s-\tau)}\right]\Big|_0^{T_s} = \frac{1}{a_m}(1 - \mathrm{e}^{-a_m T_s}), \tag{107}$$

$$\mu(T_s) \triangleq \mathrm{e}^{-a_m T_s}. \tag{108}$$

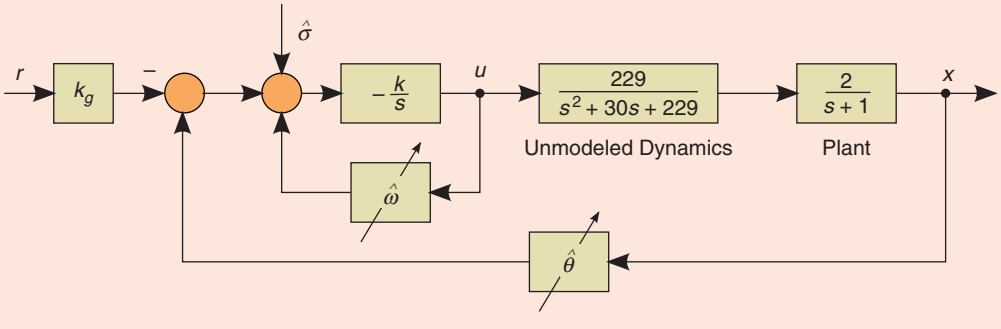

FIGURE 15 Rohrs's example. Closed-loop $\mathcal{L}_1$ control system with fast, overdamped unmodeled dynamics. The estimates $\hat{\omega}$, $\hat{\theta}$, and $\hat{\sigma}$ are driven by the adaptation laws (99)–(101).

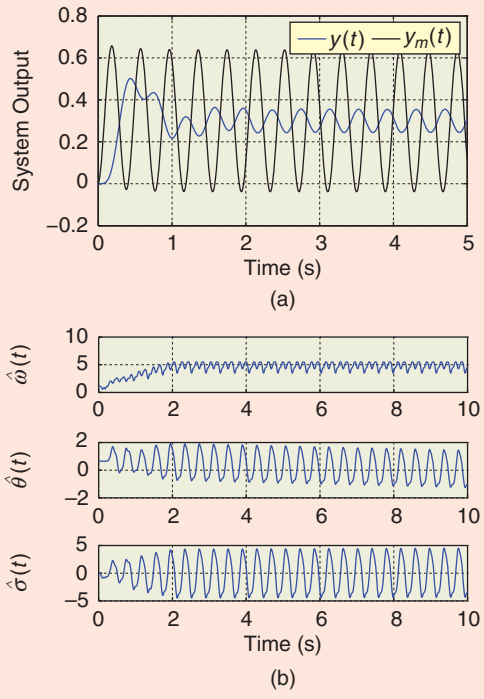

FIGURE 16 Closed-loop response of the $\mathcal{L}_1$ adaptive control system to $r_1(t)$. The projection operator helps to avoid parameter drift. Therefore, the system output and parameter estimates remain bounded. (a) System output $y(t)$, $y_m(t)$ and (b) controller parameters $\hat{\omega}(t)$, $\hat{\theta}(t)$, $\hat{\sigma}(t)$.

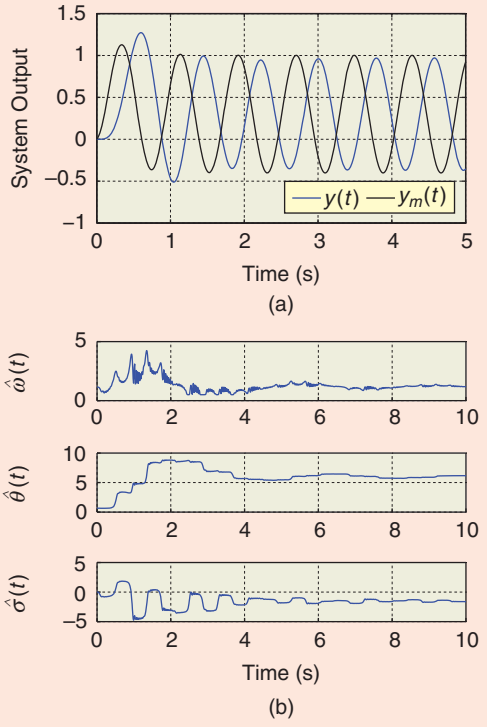

FIGURE 17 Closed-loop response of the $\mathcal{L}_1$ adaptive control system to $r_2(t)$. The parameter estimates remain bounded, and the control system does not experience bursting. (a) System output $y(t)$, $y_m(t)$ and (b) controller parameters $\hat{\omega}_t$, $\hat{\theta}_t$, $\hat{\sigma}_t$,.

The control signal, which is computed as the output of the lowpass filter $C(s)$ with unit dc gain $C(0) = 1$, is given by

$$u(s) = C(s)\left(k_r r(s) - \frac{1}{b}\hat{\sigma}(s)\right), \tag{109}$$

where $r(s)$ and $\hat{\sigma}(s)$ are the Laplace transforms of $r(t)$ and $\hat{\sigma}(t)$, respectively.

To demonstrate the role of the sampling and the inversion of $\Phi(T_s)$ in the update law, we rewrite the plant (104) in frequency domain as

$$x(s) = \frac{b}{s + a_m}(u(s) + \sigma(s)), \tag{110}$$

where $\sigma(s)$ is the Laplace transform of $\sigma(t)$. The state predictor (105) can be similarly rewritten as

$$\hat{x}(s) = \frac{b}{s + a_m}\left(u(s) + \frac{1}{b}\hat{\sigma}(s)\right). \tag{111}$$

Subtracting (110) from (111), we obtain the prediction error dynamics

$$\begin{aligned}\tilde{x}(s) &= \frac{b}{s + a_m}\left(u(s) + \frac{1}{b}\hat{\sigma}(s)\right) - \frac{b}{s + a_m}(u(s) + \sigma(s)) \\ &= \frac{b}{s + a_m}\left(\frac{1}{b}\hat{\sigma}(s) - \sigma(s)\right).\end{aligned} \tag{112}$$

Assume that during $t \in [0, t_0)$ for some $t_0 > 0$ the plant (104) is affected by the disturbance $\sigma(t)$, which results in $\tilde{x}(t_0) = \tilde{x}_0 \neq 0$. Next we check how the closed-loop system reacts to the accumulated prediction error $\tilde{x}_0$. For this purpose, we set the disturbance during the next time interval $t \in [t_0, t_0 + T_s]$ to zero. The solution to (112) on the time interval $t \in [t_0, t_0 + T_s]$ for $\sigma(t) = 0$ is given by

$$\tilde{x}(t) = \tilde{x}_0 \mathrm{e}^{-a_m(t - t_0)} + \frac{1}{a_m}\hat{\sigma}(t_0)(1 - \mathrm{e}^{-a_m(t - t_0)}).$$

At the end of the sampling interval we have

$$\tilde{x}(t_0 + T_s) = \tilde{x}_0 \mathrm{e}^{-a_m T_s} + \frac{1}{a_m}\hat{\sigma}(t_0)(1 - \mathrm{e}^{-a_m T_s}).$$

Substituting the value of the adaptive estimate given by (106) yields

$$\begin{aligned}\tilde{x}(t_0 + T_s) &= \tilde{x}_0 \mathrm{e}^{-a_m T_s} - \frac{1}{a_m}\hat{\Phi}^{-1}(T_s)\mu(T_s)\tilde{x}(t_0)(1 - \mathrm{e}^{-a_m T_s}) \\ &= \tilde{x}_0 \mathrm{e}^{-a_m T_s} - \mathrm{e}^{-a_m T_s}\tilde{x}(t_0) \\ &= 0.\end{aligned} \tag{113}$$

Thus, we observe that the update law at each sampling time generates an estimate that perfectly compensates for the prediction error accumulated during the previous sampling period of the adaptation loop. However, in reality, the disturbance $\sigma(t)$ is not zero during $t \in [t_0, t_0 + T_s]$.

$\mathcal{L}_1$ Adaptive Output-Feedback Controller with Piecewise Constant Adaptation Law

Consider the single-input, single-output (SISO) plant

$$y(s) = A(s)(u(s) + d(s)), \tag{S29}$$

where $u(t) \in \mathbb{R}$ is the control input; $y(t) \in \mathbb{R}$ is the output; $A(s)$ is a strictly proper unknown transfer function of unknown relative degree n_r, for which only a known lower bound $1 < d_r \leq n_r$ is available; and $d(s)$ is the Laplace transform of the time-varying uncertainty and disturbance $d(t) = f(t, y(t))$. We assume that there exist constants $L > 0$ and $L_0 > 0$ such that, for all time $t \geq 0$ and all y, y_1, y_2

$$|f(t, y_1) - f(t, y_2)| \leq L|y_1 - y_2|, \quad |f(t, y)| \leq L|y| + L_0. \tag{S30}$$

Let the desired performance specifications be given by the exponentially stable minimum-phase transfer function $M(s)$ of relative degree d_r, which is not necessarily strictly positive real (SPR). Then plant (S29) in terms of the ideal system can be rewritten as

$$y(s) = M(s)(u(s) + \sigma(s)), \tag{S31}$$

$$\sigma(s) = \frac{(A(s) - M(s))u(s) + A(s)d(s)}{M(s)}. \tag{S32}$$

Let $(A_m, b, c^\top)$ be a minimal realization of $M(s)$, so that A_m is Hurwitz. Then the plant (S31) can be rewritten as

$$\dot{x}(t) = A_m x(t) + b(u(t) + \sigma(t)), \quad x(0) = 0, \tag{S33}$$

$$y(t) = c^\top x(t). \tag{S34}$$

The elements of $\mathcal{L}_1$ adaptive output-feedback controller are introduced next. The state predictor is given by

$$\dot{\hat{x}}(t) = A_m \hat{x}(t) + bu(t) + \hat{\sigma}(t), \quad \hat{x}(0) = 0, \tag{S35}$$

$$\hat{y}(t) = c^\top \hat{x}(t), \tag{S36}$$

where $\hat{\sigma}(t) \in \mathbb{R}^n$ is the vector of adaptive parameters. Notice that while $\sigma(t) \in \mathbb{R}$ in (S33) is matched, the uncertainty estimate $\hat{\sigma}(t)$ in (S35) is unmatched because its dimension $n > 1$ is higher than dimension of the scalar control input.

The adaptation laws for this $\mathcal{L}_1$ architecture are sampled in time. The sampling period T_s is the fixed time-step during which the adaptive parameters in $\hat{\sigma}(t)$ take constant values during $[iT_s, (i+1)T_s)$ for every $i = 0, 1, \ldots$. Letting $\tilde{y}(t) \triangleq \hat{y}(t) - y(t)$ be the prediction error, and $\tilde{y}(iT_s)$, $i = 1, 2, \ldots$ be the sampled values of the prediction error, the piecewise constant update law for $\hat{\sigma}(t)$ is given by

$$\hat{\sigma}(t) = -\Phi^{-1}(T_s)\mu(T_s)\tilde{y}(iT_s), \quad t \in [iT_s, (i+1)T_s), \tag{S37}$$

where $\Phi^{-1}(T_s)\mu(T_s)$ represents the update law gain, with

$$\Phi(T_s) \triangleq \Lambda \int_0^{T_s} e^{A_m(T_s - \tau)} d\tau = (e^{A_m T_s} - \mathbb{I}), \tag{S38}$$

$$\mu(T_s) \triangleq \Lambda e^{A_m T_s} \Lambda^{-1} 1_1. \tag{S39}$$

Here $1_1 \triangleq [1, 0, \ldots, 0]^\top \in \mathbb{R}^n$, and

$$\Lambda \triangleq \begin{bmatrix} c^\top \\ D\sqrt{P} \end{bmatrix},$$

where $P = P^\top > 0$ satisfies the algebraic Lyapunov equation

$$A_m^\top P + PA_m = -Q,$$

where $Q = Q^\top > 0$ is arbitrary, and D is a $(n-1) \times n$ matrix that contains the null space of $c^\top(\sqrt{P})^{-1}$, that is,

$$D(c^\top(\sqrt{P})^{-1})^\top = 0.$$

Notice that reducing T_s increases the values of the adaptation gains in $\Phi^{-1}(T_s)$, which imposes hardware requirements. Also, substituting (S38) and (S39) in (S37) leads to the simplified form of adaptation

$$\hat{\sigma}(t) = -(e^{A_m T_s} - \mathbb{I})^{-1} A_m e^{A_m T_s} \Lambda^{-1} 1_1 \tilde{y}(iT_s), \quad t \in [iT_s, (i+1)T_s).$$

Therefore, the value of $\tilde{x}(t_0 + T_s)$ is usually not zero since the error dynamics are also affected by the additive disturbance. By setting the adaptation sampling time T_s small enough, the value of $\tilde{x}(t)$ can be kept small and arbitrary performance improvement can be achieved in the presence of disturbances. The proof of this result is given in [66].

To further clarify the nature of this compensation, consider the definition of $\Phi(T_s)$ in (107). We notice that $\Phi(T_s)$ is equal to the plant state at the time T_s for a constant unit control signal, zero initial conditions, and in the absence of the disturbance, that is,

$$\Phi(T_s) = x(T_s), \quad u(t) \equiv 1, \quad \sigma \equiv 0, \quad x(0) = 0.$$

From (113) we see that $\Phi^{-1}(T_s)$ inverts the error dynamics in a discretized manner. Namely, $\Phi^{-1}(T_s)$ cancels the effect of the error dynamics at fixed sampling times iT_s, $i = 1, 2, 3, \ldots$, thus making the error dynamics response equal to

The control law is given by

$$u(s) = C(s)r(s) - \frac{C(s)}{c^\top(s\mathbb{I} - A_m)^{-1}b}\, c^\top(s\mathbb{I} - A_m)^{-1}\hat{\sigma}(s), \quad \text{(S40)}$$

where $r(s)$ is the Laplace transform of a bounded reference signal, and $C(s)$ is a strictly proper system of relative degree d_r, with $C(0) = 1$.

Similar to the state feedback case, we consider the ideal control signal

$$u_{\text{id}}(t) = r(t) - \sigma(t),$$

which is the input that leads to the desired system response

$$y_{\text{id}}(s) = M(s)r(s)$$

by exactly canceling the uncertainty.

Next we define a filtered version of the ideal control law. This control law cancels the uncertainty within the bandwidth of the filter $C(s)$ compatible with the control channel specifications and leads to the $\mathcal{L}_1$ reference system

$$y_{\text{ref}}(s) = M(s)(u_{\text{ref}}(s) + \sigma_{\text{ref}}(s)), \quad \text{(S41)}$$

$$u_{\text{ref}}(s) = C(s)(r(s) - \sigma_{\text{ref}}(s)), \quad \text{(S42)}$$

where

$$\sigma_{\text{ref}}(s) \triangleq \frac{(A(s) - M(s))u_{\text{ref}}(s) + A(s)d_{\text{ref}}(s)}{M(s)},$$

and $d_{\text{ref}}(t) \triangleq f(t, y_{\text{ref}}(t))$.

By using the ideas discussed in "Bridging Adaptive and Robust Control," we can rewrite the equations for the $\mathcal{L}_1$ reference system in (S41)–(S42) to obtain the reference controller in the form

$$u_{\text{ref}}(s) = \frac{C(s)M(s)}{1 - C(s)}(M(s)r(s) - y_{\text{ref}}(s)).$$

This control law is similar to (S4), and its structure allows the use of robust control for designing the filter for verification of the $\mathcal{L}_1$-norm stability condition in (S43) [S4].

The next theorem summarizes the main result for this adaptive architecture.

THEOREM S3 [66, THEOREM 1]
Assume that the lowpass filter $C(s)$ for the given $M(s)$ is chosen such that

$$H(s) \triangleq \frac{A(s)M(s)}{C(s)A(s) + (1 - C(s))M(s)}$$

is exponentially stable and satisfies the $\mathcal{L}_1$-norm condition

$$\|G(s)\|_{\mathcal{L}_1} L < 1, \quad \text{(S43)}$$

where $G(s) \triangleq H(s)(1 - C(s))$, and L is defined in (S30). Then the reference system in (S41)–(S42) is bounded-input, bounded-output stable. Furthermore, there exist a sampling time T_s such that

$$\|\tilde{y}\|_{\mathcal{L}_\infty} \leq \gamma_0(T_s),$$

$$\|y_{\text{ref}} - y\|_{\mathcal{L}_\infty} \leq \gamma_1(T_s),$$

$$\|u_{\text{ref}} - u\|_{\mathcal{L}_\infty} \leq \gamma_2(T_s),$$

where $\gamma_0(T_s)$, $\gamma_1(T_s)$, and $\gamma_2(T_s)$ are known class $\mathcal{K}$ functions of T_s.

Thus, the tracking error between $y(t)$ and $y_{\text{ref}}(t)$, as well between $u(t)$ and $u_{\text{ref}}(t)$, is uniformly bounded by a constant proportional to T_s. This fact implies that during the transient phase, it is possible to achieve arbitrary improvement of tracking performance by uniformly reducing T_s. These results are consistent with the results in the section "Adaptive Control in the Presence of Unknown Input Gain," where improvement of the transient performance is achieved by increasing the adaptation rate in the projection-based integral adaptation laws.

Notice that the functions $\gamma_0(T_s)$, $\gamma_1(T_s)$, and $\gamma_2(T_s)$ can be constructed based on the uncertainty bounds and adaptive control system parameters. For details, see [66].

$$\tilde{x}((i+1)T_s) = \tilde{x}(iT_s)\mathrm{e}^{-a_m T_s} - \mu(T_s)\tilde{x}(iT_s).$$

The role of $\mu(T_s)\tilde{x}(iT_s)$ is to compensate for the prediction error accumulated since the previous sample period of the adaptation loop. Furthermore, notice that, for each $T_s > 0$, the quantity $\Phi(T_s)$, given by (107), is not equal zero. This fact implies that the inverse of $\Phi(T_s)$ exists for every $T_s > 0$. The same holds also for systems of arbitrary dimension, including nonstrictly positive real systems, as proved in [66] and [67], where $\Phi(T_s)$ is a nonsingular matrix. However, because $\Phi(T_s)$ approaches zero as $T_s \to 0$, the adaption law (106) cannot be written for the case of continuous-time systems. Despite this fact, the control signal is continuous since the control signal is defined as the output of a lowpass filter. We notice that the output-feedback $\mathcal{L}_1$ adaptive-control architecture for a minimum-phase, nonstrictly positive real system can also be defined using standard projection-based adaptation laws. The details on this adaptive architecture with stability and performance proofs can be found in [68].

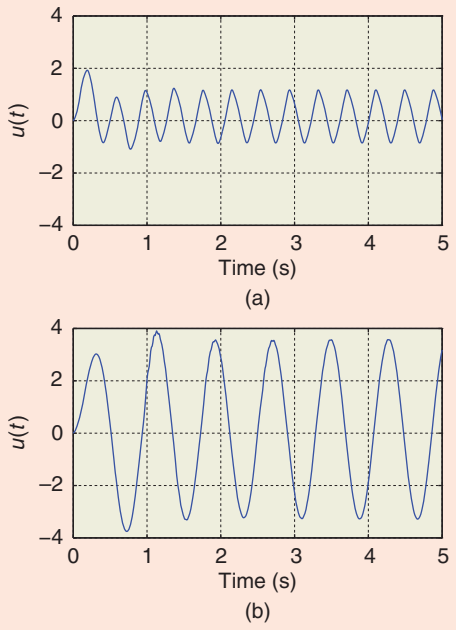

FIGURE 18 Control signal time-history for the $\mathcal{L}_1$ adaptive control system. The control signal remains bounded and does not present high-frequency content. (a) $u(t)$ for $r_1(t)$ and (b) $u(t)$ for $r_2(t)$.

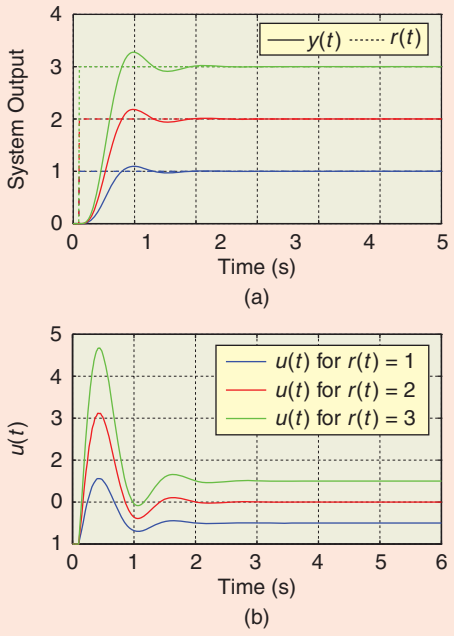

FIGURE 19 Closed-loop $\mathcal{L}_1$ adaptive controller response to several step reference commands. The closed-loop response is scaled in accordance with the step reference commands. (a) System output $y(t)$ (solid) for various step reference commands $r(t)$ (dashed) and (b) control history $u(t)$.

Illustrative Example

To demonstrate the interpretation of the $\mathcal{L}_1$ adaptive controller with piecewise constant adaptation laws (105)–(109), we consider the first-order plant (102). Let the system parameters be given by $a = a_m = b = 1$. We set the sampling time $T_s = 0.01$ s, which results in

$$\Phi(T_s) = \frac{1}{a_m}(1-\mathrm{e}^{-a_m T_s}) = 0.01$$

and

$$\mu(T_s) = \mathrm{e}^{-a_m T_s} = 0.99.$$

For the control design we choose the first-order lowpass filter

$$C(s) = \frac{1}{0.1s+1}.$$

Let the disturbance be given by

$$\begin{aligned} d(t) = {} & 100(\mathrm{u}(t-0.01) - \mathrm{u}(t-0.02)) \\ & + (300 + 500\sin(500t))(\mathrm{u}(t-0.04) - \mathrm{u}(t-0.05)) \\ & + (500\sin(1000t) - 500)(\mathrm{u}(t-0.07) - \mathrm{u}(t-0.08)), \end{aligned} \tag{114}$$

where $\mathrm{u}(t)$ denotes the unit step function. The disturbance $d(t)$ is zero everywhere except for three intervals of duration T_s separated by intervals of duration $2T_s$. During the first interval, the disturbance is constant, while, during the second and the third intervals (114), the disturbance contains sine waves with different frequencies and bias.

Figure 20 shows simulation results for the system without the plant uncertainty and the disturbance $d(t)$. In Figure 20, the plot of the prediction error given by (c) along with the plot for the parameter estimates given by (d) show that the $\mathcal{L}_1$ controller does not respond to the disturbance during the sampling period, when the disturbance occurs. However, at the beginning of the following sampling period, the controller generates a parameter estimate, which cancels the prediction error, accumulated during the previous sampling period. During other sampling periods both the prediction error and the parameter estimate remain zero.

The perfect cancellation of the error caused by the disturbance $d(t)$ in one sample step, as observed in Figure 20(c), is possible if the plant pole in (102) is the same as the pole of the desired dynamics (103), that is, $a = a_m$. Otherwise, if $a \neq a_m$, the ideal plant dynamics (103) used by the inversion-based update law (106) are different from the true plant dynamics (102), which results in additional prediction error. This error is treated by the $\mathcal{L}_1$ controller the same way as the error resulting from the disturbance.

Figure 21 shows the simulation results for the unstable plant with the parameters $a = -0.5$, $b = 0.5$ and the same $\mathcal{L}_1$ controller. While the controller tends to cancel the

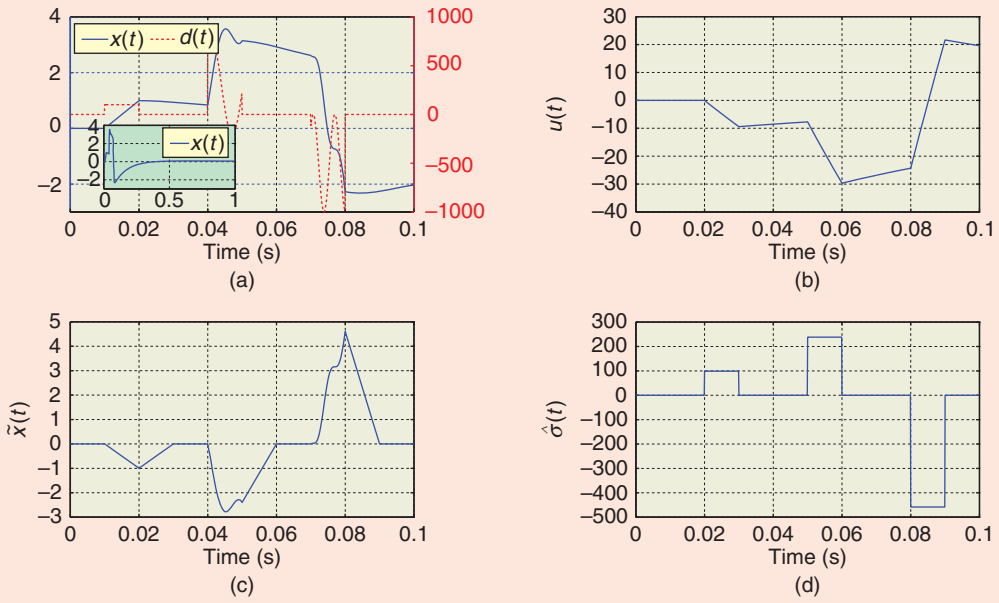

FIGURE 20 System response to the disturbance $d(t)$. The plots show that, at the beginning of the sampling period, the $\mathcal{L}_1$ adaptive controller generates a parameter estimate that cancels the prediction error accumulated during the previous sampling period. In the absence of the prediction error the controller generates a zero control input. (a) State transient $x(t)$, (b) control history $u(t)$, (c) prediction error $\tilde{x}(t)$, and (d) parameter estimate $\hat{\sigma}(t)$.

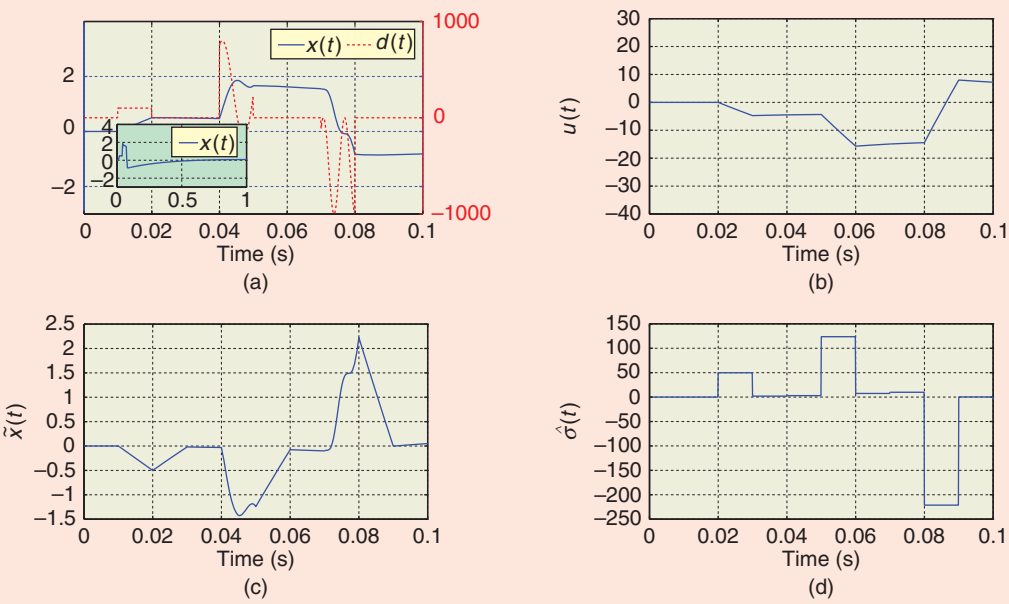

FIGURE 21 System response to the disturbance $d(t)$. The plant uncertainty prevents compensation of the prediction error during each sampling period. However, choosing a smaller sampling period T_s helps to keep the prediction error small. (a) State transient $x(t)$, (b) control history $u(t)$, (c) prediction error $\tilde{x}(t)$, and (d) parameter estimate $\hat{\sigma}(t)$.

prediction error, the controller cannot compensate for the prediction error completely due to the uncertain plant dynamics. However, a small value of the sampling time, namely, $T_s = 0.01$ s, makes this error small, as predicted in [66] and [67].

BENCHMARK PROBLEM: TWO CARTS

The two-cart mass-spring-damper (MSD) example is a benchmark problem for robust control design. In [69], a slightly modified version of the original two-cart system is used to illustrate the design methodology and performance

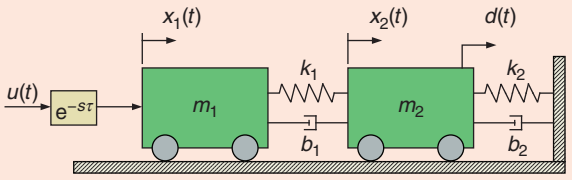

FIGURE 22 The two-cart mass-spring-damper system. The states $x_1(t)$ and $x_2(t)$ represent the positions of the two carts, whose masses are m_1 and m_2, respectively. Only $x_2(t)$ is measured. The carts are mechanically connected between each other and the rigid surface by means of spring-damper couples k_1–b_1 and k_2–b_2, respectively. The masses of the carts and the parameters b_1, b_2, and k_2 are known. Only the spring stiffness coefficient k_1 is unknown; however, lower and upper bounds for k_1 are known. The signal $d(t)$ is a random colored disturbance force, and $u(t)$ is the control force. The block with $e^{-s\tau}$ represents the delay time τ.

of the robust multiple model adaptive control. Next, we revisit the two-cart example with the $\mathcal{L}_1$ output feedback adaptive controller presented in "$\mathcal{L}_1$ Adaptive Output-Feedback Controller with Piecewise Constant Adaptation Law." Additional explanations and simulations can be found in [6].

The two-cart system is shown in Figure 22. The states $x_1(t)$ and $x_2(t)$ represent the absolute position of the two carts, whose masses are m_1 and m_2, respectively. Only $x_2(t)$ is measured. The signal $d(t)$ is a random colored disturbance force acting on the mass m_2, and $u(t)$ is the control force, which acts on the mass m_1. The disturbance force $d(t)$ is modeled as a first-order colored stochastic process generated by driving a lowpass filter with continuous-time white noise $\xi(s)$, with zero-mean and unit intensity, that is, $\Xi = 1$, and

$$d(s) = \frac{\alpha}{s+\alpha}\xi(s), \quad \alpha > 0.$$

The state-space representation is given by

$$\dot{x}(t) = Ax(t) + Bu(t) + L\xi(t),$$
$$y(t) = Cx(t) + \theta(t),$$

where the state vector is

$$x^{\top}(t) = [x_1(t) \;\; x_2(t) \;\; \dot{x}_1(t) \;\; \dot{x}_2(t) \;\; d(t)]^{\top}$$

and

$$A = \begin{bmatrix} 0 & 0 & 1 & 0 & 0 \\ 0 & 0 & 0 & 1 & 0 \\ -\frac{k_1}{m_1} & \frac{k_1}{m_1} & -\frac{b_1}{m_1} & \frac{b_1}{m_1} & 0 \\ \frac{k_1}{m_2} & -\frac{k_1+k_2}{m_2} & \frac{b_2}{m_2} & -\frac{b_1+b_2}{m_2} & \frac{1}{m_2} \\ 0 & 0 & 0 & 0 & -\alpha \end{bmatrix}, \tag{115}$$

$$B^{\top} = \begin{bmatrix} 0 & 0 & \frac{1}{m_1} & 0 & 0 \end{bmatrix}, \quad L^{\top} = \begin{bmatrix} 0 & 0 & 0 & 0 & \alpha \end{bmatrix}, \tag{116}$$

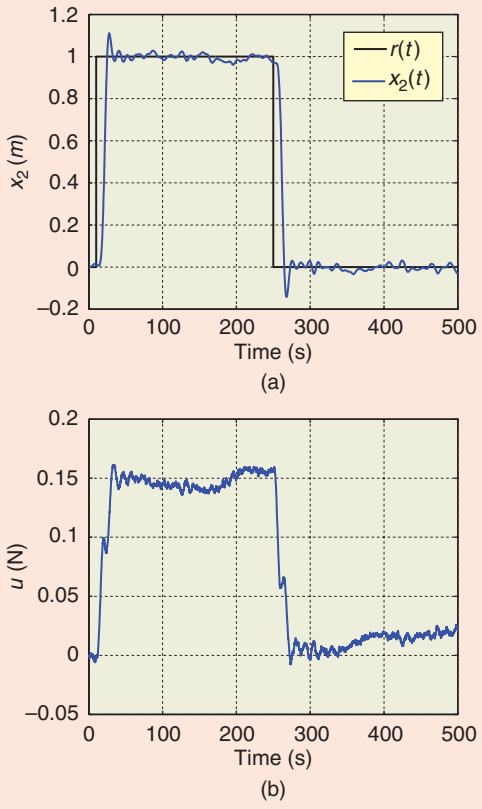

FIGURE 23 Closed-loop response to a step input of 1 m with $k_1 = 0.25$ and $\tau = 0.05$ s. The system output tracks the reference commands with the desired control specifications. The control signal remains bounded and does not exhibit high-frequency oscillations. (a) System output $x_2(t)$ and (b) control history $u(t)$.

$$C = \begin{bmatrix} 0 & 1 & 0 & 0 & 0 \end{bmatrix}, \tag{117}$$

while $\theta(t)$ is an additive sensor noise affecting the single measurement, and $\theta(t)$ is modeled as white noise, independent of $\xi(t)$, defined by

$$\mathrm{E}\{\theta(t)\} = 0, \;\; \mathrm{E}\{\theta(t)\theta(\tau)\} = 10^{-6}\delta(t-\tau).$$

The parameters in (115)–(117), which are constant and known, are given by

$$m_1 = m_2 = 1\text{kg}, \;\; k_2 = 0.15 \text{ N/m},$$
$$b_1 = b_2 = 0.1 \;\; \text{N-s/m}, \;\; \alpha = 0.1,$$

while the spring constant k_1 is unknown with known bounds given by

$$0.25 \le k_1 \le 1.75.$$

The control objective is to design a control law $u(t)$ so that the mass m_2 tracks the reference step signal $r(t)$ following

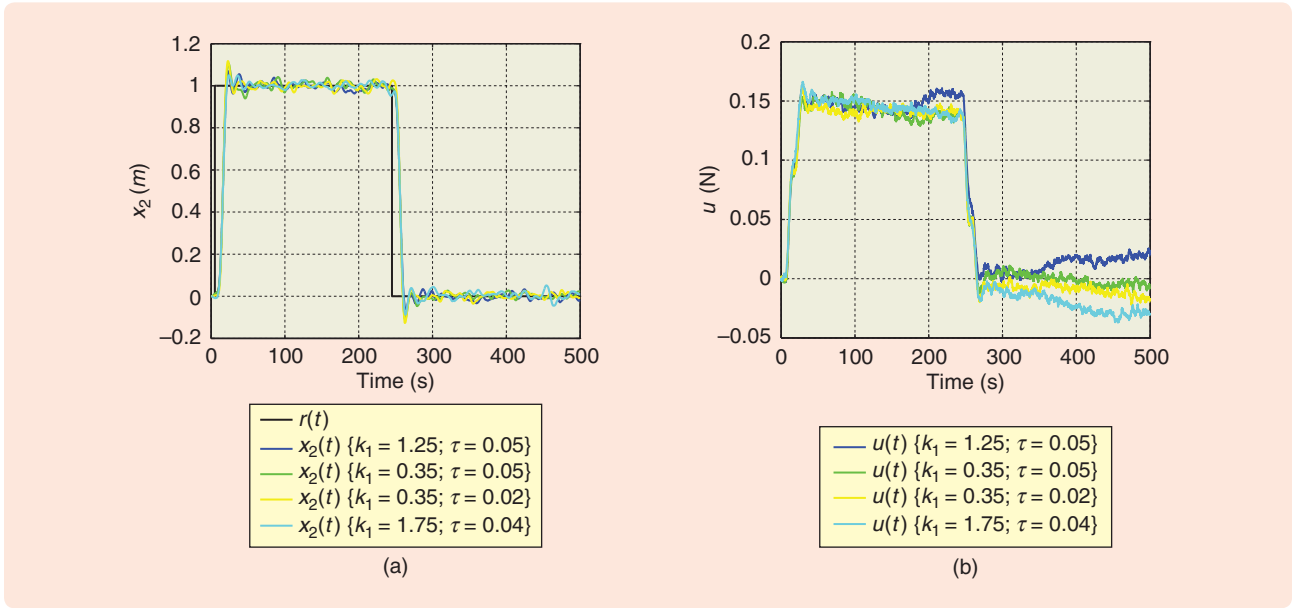

FIGURE 24 Closed-loop response to a 1-m step input for various values of the unknown parameters k_1 and τ. For all cases of the unknown parameters, the closed-loop system has similar response. The control signal changes with different values of the parameters, however, the control signal remains bounded and does not exhibit high-frequency oscillations.(a) System output $x_2(t)$ and (b) control signal $u(t)$.

a desired model, while minimizing the effects of the disturbance $d(t)$ and the sensor noise $\theta(t)$.

The control problem is challenging because the control signal $u(t)$ is applied through the uncertain spring, which makes the amount of force exerted through the spring to the mass m_2 uncertain. Taking into account the fact that only x_2 is measurable, we have a noncolocated actuator problem [69]. Moreover the model contains the unknown time delay τ in the control channel, whose maximum possible value is 0.05 s.

For application of the $\mathcal{L}_1$ adaptive output feedback controller to the two-cart example, the design procedure described in [70] leads to

$$M(s) = \frac{1}{s^3 + 1.4s^2 + 0.17s + 0.052},$$

$$C(s) = \frac{0.18s + 0.19}{s^5 + 2.8s^4 + 3.3s^2 + 2.0s^2 + 0.66s + 0.19},$$

while the sample time for the adaptation loop is set to $T_s = 1$ ms.

Figures 23 and 24 show the response of the closed-loop system with the $\mathcal{L}_1$ adaptive output feedback controller to step reference inputs of different amplitudes and for different values of the unknown parameters k_1 and τ. As we can see, the $\mathcal{L}_1$ adaptive controller drives the mass m_2 to the desired position in about 15 s for arbitrary values of the unknown parameters within given bounds, while minimizing the effects of both the disturbance and the sensor noise present in the system.

SAFETY-CRITICAL FLIGHT CONTROL APPLICATION

During 2007–2010, the NASA Aviation Safety Program created the Integrated Resilient Aircraft Control (IRAC) Project, one of whose primary objectives is to advance and transition adaptive flight control technologies as a means of increasing safety. In fact, adaptive control has long been seen as an appealing technology with the potential to reduce loss-of-control (LOC) accidents and improve aircraft performance by reducing pilot workload during challenging flight conditions and in the event of severe failures or vehicle damage. As part of this project, an $\mathcal{L}_1$ adaptive-control law was flown in a series of remotely piloted flight tests on the NASA AirSTAR Generic Transport Model (GTM) aircraft, a twin-turbine-powered and dynamically scaled model of a civil transport aircraft, designed to provide a flexible research environment with the ability to conduct rapid prototyping and testing for control algorithms in extremely adverse flight conditions, such as in-flight failure emulation and flight at high risk upset conditions. For further details on the program and the GTM aircraft, see "NASA's AirSTAR." This section provides an overview of the results from these flight tests; for additional details see [7] and [8].

Flight Control Law Design

The flight control system (FCS) developed for the GTM aircraft has as its primary objective achieving tracking for a variety of tasks with guaranteed stability and robustness in the presence of uncertain dynamics, such as changes due

NASA's AirSTAR

Loss of control (LOC) is one of the leading contributors to the fatal accident rate of large commercial transport airplanes. LOC accidents are of great concern because they are usually catastrophic, involving loss of aircraft and lives. These accidents are complex in that they typically have many causal factors and precursors, and they are difficult to analyze because often involve excursions beyond the normal flight envelope. For example, LOC accidents are known to exhibit post-stall angles of attack or steep pitch and bank attitudes, which can make recovery to normal flight difficult.

Flight validation of control technologies aimed at the LOC problem is recognized as a significant challenge due to the difficulties and risks associated with full-scale testing of transport airplanes in abnormal flight regimes. The AirSTAR is a state-of-the-art facility designed for the purpose of investigating and validating high-payoff technologies aimed at the LOC problem using subscale flight vehicles without excessive risk [S7], [S8]. The AirSTAR infrastructure is designed to support aeronautics research under adverse conditions. These conditions include upsets, such as unusual attitudes and post-stall flight, control-surface faults, structural damage such as missing wing segments, and sensor failures. Some of the key research areas are adaptive flight control technologies, system identification, flight dynamics modeling, data mining, and fault-detection methods. AirSTAR vehicles are designed for testing in regimes beyond the normal flight envelope or with degraded control characteristics, such as hardware failures or system faults.

The AirSTAR infrastructure is comprised of the research flight vehicle shown in Figure S4 and the mobile operation station (MOS). The primary AirSTAR flight test vehicle, the Generic Transport Model (GTM) tail number T2, is a remotely piloted, twin-turbine-powered, and 5.5% dynamically-scaled civil transport aircraft. Dynamic scaling allows subscale flight test results to be applied to full-scale aircraft. The GTM T2 model has a

(a) (b)

FIGURE S4 AirSTAR flight test vehicle with tail number T2 performing (a) takeoff and (b) landing. The test aircraft is a 5.5% dynamically scaled, twin-turbine-powered generic transport model. The model has a 6.5-ft wingspan, weighs 54 lb at takeoff, and has a flight time of approximately 18 min. The aircraft is outfitted with full flight test instrumentation, including angle-of-attack and angle-of-sideslip vanes, static and dynamic pressure sensors, and a 6DOF INS/GPS package including rate gyros and accelerometers. Engine speed is also measured through an engine control unit, while potentiometers mounted on the rotation axes of all control surfaces measure control-surface deflections. Downlink data update rates vary from 5 Hz on the GPS data to 200 Hz on the data from analog sensors, while uplink commands are transmitted at 200 Hz. (Photos courtesy of Irene Gregory/NASA Langley Sean Smith.)

to rapidly varying flight conditions during standard maneuvers and unexpected failures. All of these requirements are expected to be achieved while providing Level 1 handling qualities [71], [72] under nominal flight conditions with graceful degradation under significant adversity. For more information on handling qualities, see "Aircraft Handling Qualities and Their Specifications." In particular, one essential objective for safe flight under adverse conditions is for the aircraft to remain within the extended flight envelope since no guarantees for recovery can be made once outside the boundary as discussed in this article; see Figure 1. Consequently, the adaptive controller is expected to learn fast enough to keep the aircraft within the extended flight envelope. This requirement implies that the control law action in the initial 2–3 s after initiation of an adverse condition is the key to safe flight.

The $\mathcal{L}_1$ control system used for this application consists of a nonadaptive stability augmentation system (SAS) for pitch and roll, as well as a three-axis angle-of-attack α, roll-rate p, and sideslip-angle β adaptive command augmentation system (CAS), which is based on the theory presented in "$\mathcal{L}_1$ Adaptive Controller for Systems with Unmatched Uncertainties." Hence, the $\mathcal{L}_1$ adaptive controller provides command-tracking capabilities in both

6.5-ft wingspan, weighs 54 lb at takeoff, and has a flight time of approximately 18 min. The aircraft is outfitted with a 6DOF INS/GPS package, which provides three-axis linear accelerometer measurements, angular-rate measurements, estimated attitude angles, and GPS position and velocity. Additionally, air-data probes mounted on each wingtip measure angle of attack, angle of sideslip, dynamic pressure, and static pressure. Engine speed is also measured through an engine control unit, while potentiometers mounted on the rotation axes of all control surfaces measure control-surface deflections. Aircraft dynamic failures are emulated using software to schedule appropriate actuators to provide desired degradation. For example, longitudinal stability degradation is achieved by commandeering two of the four elevator segments from the control law path and scheduling these segments with angle of attack to adversely change the pitching moment, thus reducing available pitch-control authority by 50% and destabilizing the aircraft by a prescribed amount. Similarly, spoilers scheduled with roll rate are used to degrade lateral stability.

The MOS is an integrated ground station and control room and comprises a research pilot station as well as systems and engineering stations. The MOS is connected to the aircraft through an L-band with 1–2 GHz telemetry uplink and an S-band with 2–4 GHz telemetry downlink and provides real-time telemetry processing and monitoring capabilities. Downlink data update rates vary from 5 Hz on the GPS data to 200 Hz on the data from analog sensors, while uplink commands are transmitted at 200 Hz. The total downlink and uplink closed-loop data latency is estimated to be below 25 ms. The MOS provides also a real-time simulation environment for pilot training, control law testing, and experiment reproduction.

For each flight, the AirSTAR concept of operations distinguishes three sequential phases, namely, takeoff, research flight, and landing. Takeoff and landing are accomplished by a safety pilot using direct visual contact and conventional radio control equipment. In the research flight phase, a research pilot executes flight test maneuvers from a research cockpit located in the pilot station inside the MOS, while keeping the aircraft within visual range of the safety pilot. Head-up and head-down synthetic vision displays drawn from aircraft sensor data and a local terrain database support the research pilot during this phase. Computers in the MOS execute research flight control laws and interface with the research pilot station using a direct connection by cable. Actuator commands from research pilot inputs and the ground-based flight control computer are transmitted to the aircraft by the telemetry uplink. While the model is being controlled from the research pilot station, a reversionary flight control capability is provided by a safety pilot. If a problem were to arise, the safety pilot can override the research pilot control inputs and fly using a hobbyist radio-control interface. This design provides a flexible environment to conduct flight research and evaluate research flight control laws with minimal risk.

The vehicles and operational concept used by AirSTAR present unique challenges. First and foremost, dynamically scaling an aircraft results in increased model airspeed, angular rates, wind loading, as well as increased pilot workload relative to a model that is only geometrically scaled. These factors make a dynamically scaled model more challenging to fly and less forgiving of mistakes. Second, under the current AirSTAR concept of operations, the aircraft must remain within visual range of the safety pilot, which limits the test volume to an approximately 1/2-mi radius circle around the safety pilot, extending to approximately 2000 ft in altitude. Limited test volume combined with the high airspeeds of the test aircraft add to the pilot's workload. Third, the primary purpose of AirSTAR is to perform flight research and flight validation of multiple research control laws in adverse flight conditions, which presents unique challenges to flight testing in an efficient and safe manner.

REFERENCES

[S7] K. Cunningham, J. V. Foster, E. A. Morelli, and A. M. Murch, "Practical application of a subscale transport aircraft for flight research in control upset and failure conditions," in *Proc. AIAA Guidance, Navigation and Control Conf.*, Honolulu, HI, AIAA-2008-6200, 2008.

[S8] A. M. Murch, "A flight control system architecture for the NASA AirSTAR flight test infrastructure," in *Proc. AIAA Guidance, Navigation and Control Conf.*, Honolulu, HI, AIAA-2008-6990, 2008.

nominal and off-nominal conditions without the presence of a nonadaptive CAS. Moreover, the adaptive controller provides automatic compensation for the undesirable effects of unmatched uncertainty on the output of the system, which is essential for achieving desired performance, reducing a pilot's workload, and improving the aircraft's handling qualities. In fact, the effects of unregulated variables, such as airspeed and bank angle, unmodeled nonlinearities, cross-coupling between axes, and dynamic asymmetries, may appear as an unmatched component in the inner-loop aircraft dynamics being controlled. Further details on aircraft flight dynamics can be found in [73]. For subscale platforms, these dynamics may have time scales comparable to the time scale of the pilot dynamics as well as the dynamics that the pilot is trying to control. Therefore, if the design of the inner-loop FCS does not account for this uncertainty, then its undesirable effects in the inner-loop dynamics may require excessive pilot compensation or may lead to adverse aircraft-pilot interactions, such as pilot-induced oscillations.

The $\mathcal{L}_1$ adaptive FCS is designed to satisfy the same requirements as any standard classical flight control system, namely, good flying qualities, precision tracking, reduced control-surface activity, and graceful degradation

Aircraft Handling Qualities and Their Specifications

Handling qualities involves the study and evaluation of the stability and control characteristics of an aircraft [S9]. Handling qualities have a critical bearing on the safety of flight and on the ease of controlling an airplane in steady flight and in maneuvers. The stability characteristics of airplanes can be separated into longitudinal and lateral groups with the corresponding modes of motion. The longitudinal modes of a statically stable airplane following a disturbance consist of a long-period oscillation called the phugoid oscillation, usually with a period in seconds of about one-quarter of the airspeed in miles per hour, and a short-period oscillation, with a period of only a few seconds. The lateral motion has three modes of motion, namely, an aperiodic mode called the spiral mode, which can be a divergence or subsidence, a heavily damped aperiodic mode called the roll subsidence, and a short-period oscillation, usually lightly damped, called the Dutch-roll mode.

Guidelines for stability and control of an aircraft, whether an open-loop airframe, one with a feedback stability augmentation system, or one with full-authority command augmentation, are described in the U.S. Military Specifications (Mil-Spec) [72]. These specifications establish the relationships between pilot ratings, phases of flight, aircraft class, flight envelopes, and aircraft states. Moreover, these specifications provide specific guidelines on the desired dynamics for specific longitudinal and lateral motions of the aircraft as well as the simplified dynamics that can express these dynamics, known as low-order equivalent systems. These Mil-Spec guidelines are used in both civilian and military aircraft to shape dynamics associated with good handling qualities for both piloted and unmanned aircraft.

The evaluation of how well a piloted aircraft behavior follows these guidelines is based on the Cooper-Harper scale. The Cooper-Harper scale is universally used to enable the pilot to award a number to an aircraft to allow comparison with other aircraft or to show compliance with specifications. The scale has ten points, where one indicates excellent and ten the worst qualities possible, namely, an uncontrollable aircraft resulting in a crash. The scale is dichotomous, which results in improved repeatability by leading the evaluation pilot through a series of decisions regarding the task performance and pilot workload. The latter is subjective but the task performance is reasonably repeatable provided that the task is well defined. Note that the rating is task specific, which implies that, although the aircraft may be controllable and flyable, the specific task rating might be poor. Such a result would indicate a constraint on the aircraft performance and maneuverability and would typically be a result of a fault or failure.

REFERENCE

[S9] J. Hodgkinson, *Aircraft Handling Qualities (AIAA Educational Series)*. Reston, VA: AIAA, 1999.

in the presence of faults and failures. Specifically, the design of the $\mathcal{L}_1$ adaptive FCS for the GTM is based on the linearized dynamics of the aircraft at a nominal flight condition corresponding to an equivalent airspeed of 80 kt and an altitude of 1000 ft. For design purposes, these linear dynamics are further simplified to include only short-period dynamics for the longitudinal axis, thus neglecting velocity and pitch attitude, and roll rate, sideslip angle, and yaw rate for the lateral-directional dynamics. Since the airplane is Level 1 at this flight condition, the nominal desired dynamics of the linear state predictor are chosen to be similar to the linearized dynamics of the airplane. Some additional damping is added to both longitudinal and directional dynamics of the state predictor, while the lateral dynamics are set to be faster than the original dynamics to satisfy performance specifications and to enforce MIL-standard requirements [72]. The state predictor of the $\mathcal{L}_1$ control law is scheduled to specify different performance requirements at special flight regimes, such as high speed above the allowable research envelope and post-stall high angle of attack. To improve the handling qualities of the airplane, a linear prefilter is added to the adaptive flight control law to ensure desired decoupling properties as well as desired command-tracking performance. Overdamped second-order lowpass filters with unity dc gain are used in all control channels, while their bandwidths are set to ensure a time-delay margin of at least 0.125 s and a gain margin of at least 6 dB. Finally, the adaptation sampling time is set to $T_s = 1/600$ s, which corresponds to the execution speed of the AirSTAR flight control computer. Recall that $\mathcal{L}_1$ adaptive controller takes full advantage of the available computation speeds to improve the performance bounds. We notice that the same control parameters for the prefilter, lowpass filters, and adaptation rate are used across the entire flight envelope, including the post-stall high angle-of-attack region, with no scheduling or reconfiguration. The $\mathcal{L}_1$ control law with its main elements is represented in Figure 25. Further details about the design and robustness properties of the $\mathcal{L}_1$ adaptive flight control law for the GTM can be found in [74] and [75].

Flight Control Law Evaluation

The $\mathcal{L}_1$ adaptive flight control law was evaluated on a twin-turbine-powered, dynamically scaled GTM aircraft with tail number T2 during a series of flight tests conducted on

$\mathcal{L}_1$ Adaptive Controller for Systems with Unmatched Uncertainties

The flight control system developed for the AirSTAR flight test vehicle uses an $\mathcal{L}_1$ adaptive controller designed for a class of multi-input, multi-output uncertain plants in the presence of uncertain system input gain and time- and state-dependent unknown nonlinearities, without enforcing matching conditions [S10]. Next, we present an overview of this $\mathcal{L}_1$ control architecture. In particular, the class of systems considered includes general unmatched uncertainty that cannot be addressed by recursive design methods developed for strict-feedback systems, semi-strict-feedback systems, pure-feedback systems, and block-strict-feedback systems [S11], [S12].

Consider the system with unmatched nonlinear uncertainty and with unmodeled dynamics given by

$$\dot{x}(t) = A_m x(t) + B_m \omega u(t) + f(t, x(t), z(t)), \quad x(0) = x_0, \tag{S44}$$

$$y(t) = Cx(t), \tag{S45}$$

where $x(t) \in \mathbb{R}^n$ is the state vector (measured); $u(t) \in \mathbb{R}^m$ is the control signal; $y(t) \in \mathbb{R}^m$ is the regulated output; $A_m \in \mathbb{R}^{n\times n}$ is a known Hurwitz matrix that defines the desired dynamics for the closed-loop system; $B_m \in \mathbb{R}^{n\times m}$ and $C \in \mathbb{R}^{m\times n}$ are known full-rank constant matrices; $\omega \in \mathbb{R}^{m\times m}$ is the uncertain plant input gain matrix; $f : \mathbb{R} \times \mathbb{R}^n \times \mathbb{R}^p \to \mathbb{R}^n$ is an unknown nonlinear function. The initial condition x_0 is assumed to be inside a known set, that is, $\|x_0\|_\infty \le \rho_0 < \infty$ for some $\rho_0 > 0$. The signal $z(t) \in \mathbb{R}^p$ is the output of the unmodeled dynamics

$$\dot{x}_z(t) = g(t, x_z(t), x(t)), \quad x_z(0) = x_{z0}, \tag{S46}$$

$$z(t) = g_o(t, x_z(t)), \tag{S47}$$

where $x_z(t) \in \mathbb{R}^l$ is the state vector of internal unmodeled dynamics; $g_o : \mathbb{R} \times \mathbb{R}^l \to \mathbb{R}^p$, and $g : \mathbb{R} \times \mathbb{R}^l \times \mathbb{R}^n \to \mathbb{R}^l$ are unknown nonlinear functions such that the standard assumptions on existence and uniqueness of solutions are satisfied.

We rewrite (S44)–(S45) as

$$\dot{x}(t) = A_m x(t) + B_m(\omega u(t) + f_1(t, x(t), z(t))) + B_{um} f_2(t, x(t), z(t)),$$

$$x(0) = x_0, \tag{S48}$$

$$y(t) = Cx(t), \tag{S49}$$

where $B_{um} \in \mathbb{R}^{n\times(n-m)}$ is a constant matrix such that $B_m^\top B_{um} = 0$ and also $\operatorname{rank}([B_m, B_{um}]) = n$, while $f_1 : \mathbb{R} \times \mathbb{R}^n \times \mathbb{R}^p \to \mathbb{R}^m$ and $f_2 : \mathbb{R} \times \mathbb{R}^n \times \mathbb{R}^p \to \mathbb{R}^{(n-m)}$ are unknown nonlinear functions that verify

$$\begin{bmatrix} f_1(t, x(t), z(t)) \\ f_2(t, x(t), z(t)) \end{bmatrix} = B^{-1} f(t, x(t), z(t)), \quad B \triangleq [B_m, B_{um}]. \tag{S50}$$

In this problem formulation, $f_1(\cdot)$ represents the *matched component* of the uncertainty, which is in the span of matrix B_m, whereas $f_2(\cdot)$ represents the *unmatched component*, which enters the plant dynamics orthogonally to the matrix B_m.

Let $X \triangleq [x^\top, z^\top]^\top$, and with a slight abuse of language let $f_i(t, X) \triangleq f_i(t, x, z)$, $i = 1, 2$. Then let $\|f_i(t, 0)\|_{\mathcal{L}_\infty} \le B_{i0}$ for all $t \ge 0$, $i = 1, 2$, where $B_{i0} > 0$ are known bounds. Next, assume that, for each $\delta > 0$, there exist positive K_{1_δ}, K_{2_δ} such that

$$\|f_i(t, X_1) - f_i(t, X_2)\|_\infty \le K_{i_\delta} \|X_1 - X_2\|_\infty, \quad i = 1, 2,$$

for all $\|X_j\|_\infty \le \delta$, $j = 1, 2$, uniformly in t. Furthermore, assume that there exist L_z, $B_z > 0$ such that, for all $t \ge 0$,

$$\|z_t\|_{\mathcal{L}_\infty} \le L_z \|x_t\|_{\mathcal{L}_\infty} + B_z.$$

The uncertain plant input gain matrix ω is assumed to be an unknown, nonsingular, strictly row-diagonally dominant matrix with $\operatorname{sgn}(\omega_{ii})$ known. Also, we assume that there exists a known compact convex set Ω such that $\omega \in \Omega \subset \mathbb{R}^{m\times m}$ and that a nominal plant input gain $\omega_0 \in \Omega$ is known. Finally, we assume that the transmission zeros of the transfer matrix $H_m(s) = C(s\mathbb{I} - A_m)^{-1}B_m$ lie in the open left-half plane.

Before we present the adaptive architecture and give an $\mathcal{L}_1$-norm stability condition, define

$$H_{xm}(s) \triangleq (s\mathbb{I}_n - A_m)^{-1}B_m,$$

$$H_{xum}(s) \triangleq (s\mathbb{I}_n - A_m)^{-1}B_{um},$$

$$H_m(s) \triangleq CH_{xm}(s) = C(s\mathbb{I}_n - A_m)^{-1}B_m,$$

$$H_{um}(s) \triangleq CH_{xum}(s) = C(s\mathbb{I}_n - A_m)^{-1}B_{um},$$

and also define $\rho_{\text{in}} \triangleq \|s(s\mathbb{I} - A_m)^{-1}\|_{\mathcal{L}_1}\rho_0$, where $\rho_0 = \max\|x_0\|_\infty$. Furthermore, let $\bar{\gamma}_1$ be an arbitrary small positive constant and, for each $\delta > 0$, define

$$L_{i\delta} \triangleq \frac{\bar{\delta}(\delta)}{\delta} K_{i\bar{\delta}(\delta)}, \quad \bar{\delta}(\delta) \triangleq \max\{\delta + \bar{\gamma}_1, L_z(\delta + \bar{\gamma}_1) + B_z\}. \tag{S51}$$

The design of the $\mathcal{L}_1$ adaptive controller involves a feedback gain matrix $K \in \mathbb{R}^{m\times m}$ and an $m \times m$ strictly proper transfer matrix $D(s)$, which lead, for all $\omega \in \Omega$, to a strictly proper exponentially stable

$$C(s) \triangleq \omega KD(s)(\mathbb{I}_m + \omega KD(s))^{-1} \tag{S52}$$

with dc gain $C(0) = \mathbb{I}_m$. The choice of K and $D(s)$ must ensure that $C(s)H_m^{-1}(s)$ is a proper exponentially stable transfer matrix and, for a given ρ_0, there exists $\rho_r > \rho_{\text{in}}$ such that the $\mathcal{L}_1$-norm condition

$$\|G_m(s)\|_{\mathcal{L}_1} + \|G_{um}(s)\|_{\mathcal{L}_1}\ell_0 < \frac{\rho_r - \|H_{xm}(s)C(s)K_g(s)\|_{\mathcal{L}_1}\|r\|_{\mathcal{L}_\infty} - \rho_{\text{in}}}{L_{1_\rho}\rho_r + B_0} \tag{S53}$$

is satisfied, where

$$G_m(s) \triangleq H_{xm}(s)(\mathbb{I}_m - C(s)),$$

$$G_{um}(s) \triangleq (\mathbb{I}_n - H_{xm}(s)C(s)H_m^{-1}(s)C)H_{xum}(s),$$

while

$$\ell_0 \triangleq \frac{L_{2\rho_r}}{L_{1\rho_r}},\ B_0 \triangleq \max\left\{B_{10}, \frac{B_{20}}{\ell_0}\right\},$$

and $K_g(s)$ is the exponentially stable feedforward prefilter.

Next, we introduce the elements of the $\mathcal{L}_1$ adaptive control architecture. The state-predictor is given by

$$\dot{\hat{x}}(t) = A_m\hat{x}(t) + B_m(\omega_0 u(t) + \hat{\sigma}_1(t)) + B_{um}\hat{\sigma}_2(t),\ \hat{x}(0) = x_0, \quad \text{(S54)}$$

$$\hat{y}(t) = C\hat{x}(t), \quad \text{(S55)}$$

where $\hat{\sigma}_1(t) \in \mathbb{R}^m$ and $\hat{\sigma}_2(t) \in \mathbb{R}^{n-m}$ are the adaptive estimates of the matched and unmatched uncertainties, respectively. These estimates are driven by the adaptation laws

$$\begin{bmatrix}\hat{\sigma}_1(t)\\ \hat{\sigma}_2(t)\end{bmatrix} = -\begin{bmatrix}\mathbb{I}_m & 0\\ 0 & \mathbb{I}_{n-m}\end{bmatrix}B^{-1}\Phi^{-1}(T_s)\mu(T_s)\tilde{x}(iT_s),$$
$$t \in [iT_s, (i+1)T_s), \quad \text{(S56)}$$

for $i = 0,1,2,\ldots$, where $T_s > 0$ is the *adaptation sampling time*, $\tilde{x}(t) = \hat{x}(t) - x(t)$ is the prediction error, B is introduced in (S50), and

$$\Phi(T_s) \triangleq A_m^{-1}(e^{A_m T_s} - \mathbb{I}),$$

while

$$\mu(T_s) = e^{A_m T_s}.$$

The control law is given by

$$u(s) = -KD(s)\hat{\eta}(s), \quad \text{(S57)}$$

where $\hat{\eta}(s)$ is the Laplace transform of the signal

$$\hat{\eta}(t) \triangleq \omega_0 u(t) + \hat{\eta}_1(t) + \hat{\eta}_{2m}(t) - r_g(t), \quad \text{(S58)}$$

with $r_g(s) \triangleq K_g(s)r(s)$, $\hat{\eta}_{2m}(s) \triangleq H_m^{-1}(s)H_{um}(s)\hat{\eta}_2(s)$ capturing the estimation of the unmatched uncertainty, where $\hat{\eta}_2(t) \triangleq \hat{\sigma}_2(t)$, and with $\hat{\eta}_1(t) \triangleq \hat{\sigma}_1(t)$ estimating the matched uncertainty.

Notice that conventional design methods from multivariable control theory can be used to design the prefilter $K_g(s)$ to achieve desired decoupling properties. As an example, if we choose $K_g(s)$ as the constant matrix $K_g = -(CA_m^{-1}B_m)^{-1}$, then the diagonal entries of the desired transfer matrix $M(s) = C(s\mathbb{I}_n - A_m)^{-1}B_m K_g$ have dc gain equal to one, while the off-diagonal entries have zero dc gain.

The $\mathcal{L}_1$ reference system for this architecture is given by

$$\dot{x}_{\text{ref}}(t) = A_m x_{\text{ref}}(t) + B_m(\omega u_{\text{ref}}(t) + f_1(t, x_{\text{ref}}(t), z(t)))$$
$$+ B_{um}f_2(t, x_{\text{ref}}(t), z(t)),\ x_{\text{ref}}(0) = x_0, \quad \text{(S59)}$$

$$u_{\text{ref}}(s) = -\omega^{-1}C(s)(\eta_{1\text{ref}}(s) + H_m^{-1}(s)H_{um}(s)\eta_{2\text{ref}}(s) - K_g(s)r(s)), \quad \text{(S60)}$$

$$y_{\text{ref}}(t) = Cx_{\text{ref}}(t), \quad \text{(S61)}$$

where $\eta_{i\text{ref}}(s)$ is the Laplace transform of $\eta_{i\text{ref}}(t) \triangleq f_i(t, x_{\text{ref}}(t), z(t))$, $i = 1, 2$.

Again, using the ideas discussed in "Bridging Adaptive and Robust Control," we can derive the reference controller from the equations of the $\mathcal{L}_1$ reference system (S59)–(S60) to arrive at

$$u_{\text{ref}}(s) = kD(s)H_m^{-1}(s)(H_m(s)K_g(s)r(s) - Cx_{\text{ref}}(s)),$$

which is similar to the reference controller for the state feedback with matched uncertainty in (S7). Due to this structural equivalence between the $\mathcal{L}_1$ reference controller and a linear internal model controller, robust control methods can be applied to design a lowpass filter that satisfies the $\mathcal{L}_1$ norm stability condition in (S53).

The next theorem summarizes the main result for this adaptive architecture.

THEOREM 1 [S10, THEOREM 1]

Let the feedback gain K and the filter $D(s)$ be chosen to satisfy the $\mathcal{L}_1$-norm condition in (S53). Then, the reference system in (S59)–(S61) is bounded-input, bounded-output stable. Moreover, there exists an adaptation sampling time T_s such that

$$\|\tilde{x}\|_{\mathcal{L}_\infty} \leq \gamma_0(T_s), \quad \text{(S62)}$$

$$\|x_{\text{ref}} - x\|_{\mathcal{L}_\infty} \leq \gamma_1(T_s), \quad \text{(S63)}$$

$$\|u_{\text{ref}} - u\|_{\mathcal{L}_\infty} \leq \gamma_2(T_s), \quad \text{(S64)}$$

where $\gamma_0(T_s)$, $\gamma_1(T_s)$, and $\gamma_2(T_s)$ are known class $\mathcal{K}$ functions of T_s.

Notice that the functions $\gamma_0(T_s)$, $\gamma_1(T_s)$, and $\gamma_2(T_s)$ can be constructed based on knowledge of the uncertainty bounds and the adaptive control system parameters. For details see [S10].

Thus, the tracking error between $y(t)$ and $y_{\text{ref}}(t)$, as well as $u(t)$ and $u_{\text{ref}}(t)$, is uniformly bounded by a constant that can be arbitrarily reduced by decreasing the adaptation sampling time T_s. Therefore, arbitrarily close tracking performance can be achieved, both in transient and steady state, for both signals simultaneously by adapting sufficiently fast. These results are consistent with the results in "$\mathcal{L}_1$ Adaptive Output-Feedback Controller with Piecewise Constant Adaptation Laws," where we achieve arbitrary performance bounds by choosing an appropriate value of the sampling time T_s.

REFERENCES

[S10] E. Xargay, N. Hovakimyan, and C. Cao, "$\mathcal{L}_1$ adaptive controller for multi-input multi-output systems in the presence of nonlinear unmatched uncertainties," in *Proc. American Control Conf.*, Baltimore, MD, 2010, pp. 874–879.

[S11] M. Krstić, I. Kanellakopoulos, and P. V. Kokotović, *Nonlinear and Adaptive Control Design*. New York: Wiley, 1995.

[S12] B. Yao and M. Tomizuka, "Adaptive robust control of SISO nonlinear systems in a semi-strict feedback form," *Automatica*, vol. 33, no. 5, pp. 893–900, 1997.

June 4, 2010 and September 10, 2010 at Ft. Pickett, Virginia. To place the flight test results into the appropriate context, a summary of the flight test procedures is presented.

The main objective of the flight control law evaluation is to assess the time-delay margin of the adaptive system as a measure of closed-loop robustness, as well as the ability of the adaptive controller to maintain aircraft stability and predictable performance in off-nominal adverse flight conditions as a measure of robust performance. The time-delay margin is determined by progressively increasing the latency in the control channel until instability occurs. The performance of the adaptive controller is evaluated through a series of tasks designed to test the LOC prevention and recovery capabilities of the closed-loop adaptive system. In particular, these tasks include flight under aerodynamic stability degradation, post-stall flight and recovery, and handling qualities assessment based on Cooper-Harper ratings (CHR) as well as subjective pilot comments. In the stability degradation tasks, both the longitudinal and lateral stability of the aircraft are simultaneously degraded, while reducing pitch-control authority by 50%. The flight control law evaluation also includes high angle-of-attack flight and recovery in the stall and post-stall region of the flight envelope. In these tasks, the pilot is asked to hold the aircraft in controlled flight at an

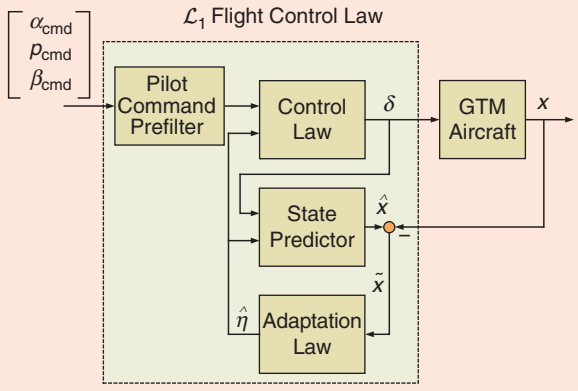

FIGURE 25 Block diagram of the $\mathcal{L}_1$ flight control architecture. The $\mathcal{L}_1$ control law consists of an estimation scheme and a control law. The estimation scheme includes a state predictor and an adaptation law, which are used to generate estimates of the uncertainties present in the plant $\hat{\eta}$. The state predictor generates a prediction $\hat{x}$ of the state x. The difference between these signals yields an error signal $\tilde{x}$ that drives the adaptation process. The adaptation law updates the estimates of the uncertainties present in the plant at a high adaptation rate. Based on the estimates of the uncertainties, the control law uses lowpass filters to generate control-surface deflection commands δ.

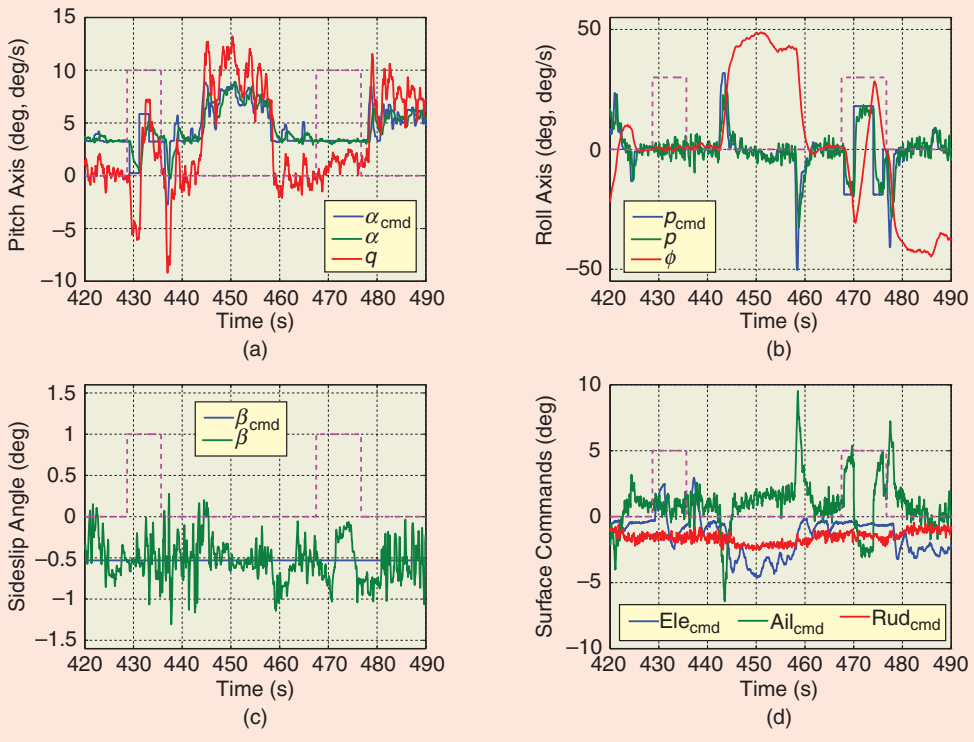

FIGURE 26 Pitch and roll doublets for the nominal aircraft. These plots show 70 s of flight including angle-of-attack and roll-rate wavetrains, one complete turn, and part of another turn. The pitch- and roll-doublet wavetrains, which are superimposed on the pilot's stick commands, are used to excite the closed-loop system dynamics and evaluate tracking performance. This nominal response is considered to have solid Level 1 handling qualities according to pilot ratings and comments. The injection of the wavetrain is indicated in the plots with a purple dashed line. (a) Pitch-axis response, (b) roll-axis response, (c) slideslip-angle tracking, and (d) control surface commands.

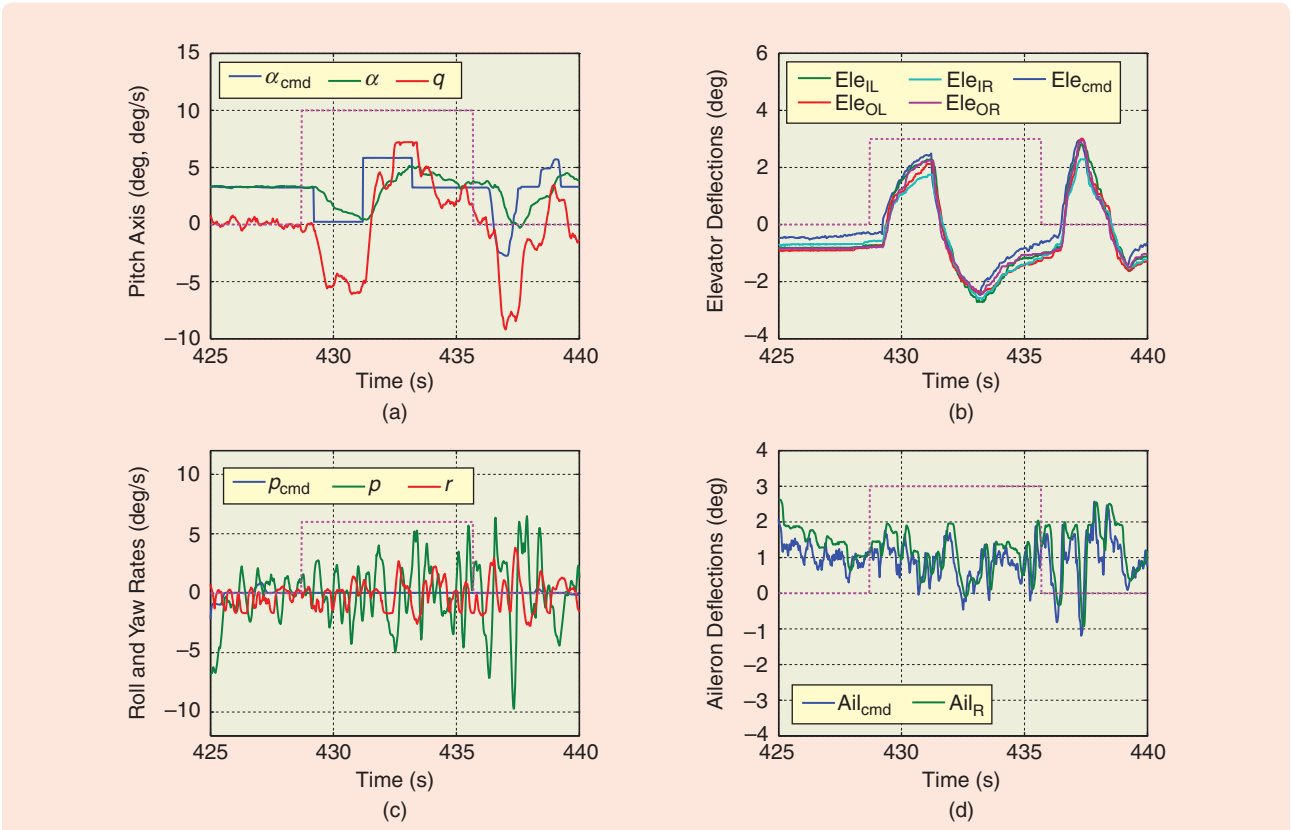

FIGURE 27 Pitch-doublet response for the nominal aircraft. The flight control law, which provides a first-order-like angle-of-attack response, is able to isolate the commanded response to the longitudinal axis, ensuring reduced cross-coupling between channels. In fact, during the injection of the wavetrain, the roll and yaw rates remain within the turbulence level. The injection of the wavetrain is indicated in the plots with a purple dashed line. (a) Pitch-axis response, (b) elevator deflections, (c) lateral-directional response, and (d) right-aileron deflection.

angle of attack above 13° while keeping the bank angle below 45°. Finally, handling qualities assessment involves high-workload offset landing tasks, where the pilot is asked to land the aircraft in a virtual scenario presented on the pilot's head-up display. The initial task condition is a final approach at 80 kt characterized by an offset from the center line of the virtual runway that is 100 ft to the left of the centerline, 100 ft above the runway, and 1800 ft downrange from a desired touchdown box marked on the runway. This particular task is considered to be demanding for a pilot under nominal conditions. To evaluate the performance of an adaptive controller, pilot assessment is also provided for off-nominal cases with simultaneous stability degradation in both longitudinal and lateral axes.

In the following section, a brief overview of representative results from the flight tests conducted in June and September 2010 is presented. References [7] and [8] provide additional data and analysis of the results.

Robustness Evaluation

To determine the time-delay margin of the adaptive closed-loop system, a progressively increasing latency is added to the control channel until the aircraft response becomes unstable or presents sustained high-amplitude oscillations. For this task, the pilot is asked to fly the aircraft in a figure-eight pattern at approximately 900 ft and 80 kt, while pitch and roll doublets are superimposed on the pilot's stick commands to excite the system dynamics. During the flight test evaluation conducted in June 2010, it was determined that the $\mathcal{L}_1$ flight control law is robust to a 0.125-s latency added to the control channel, which, with a nominal system latency of approximately 0.022 s, amounts to a total time-delay margin of approximately 0.147 s. A description of this task with the corresponding flight data can be found in [7].

Flight Under Aerodynamic Stability Degradation

The evaluation conducted in June 2010 was also used to determine the ability of the $\mathcal{L}_1$ flight control law to compensate for simultaneous longitudinal and lateral aerodynamic stability degradation and a 50% reduction in pitch-control authority. The stability degradation task is introduced gradually; starting with a 50% degradation, the stability is reduced in decrements of 25% until the closed-loop system

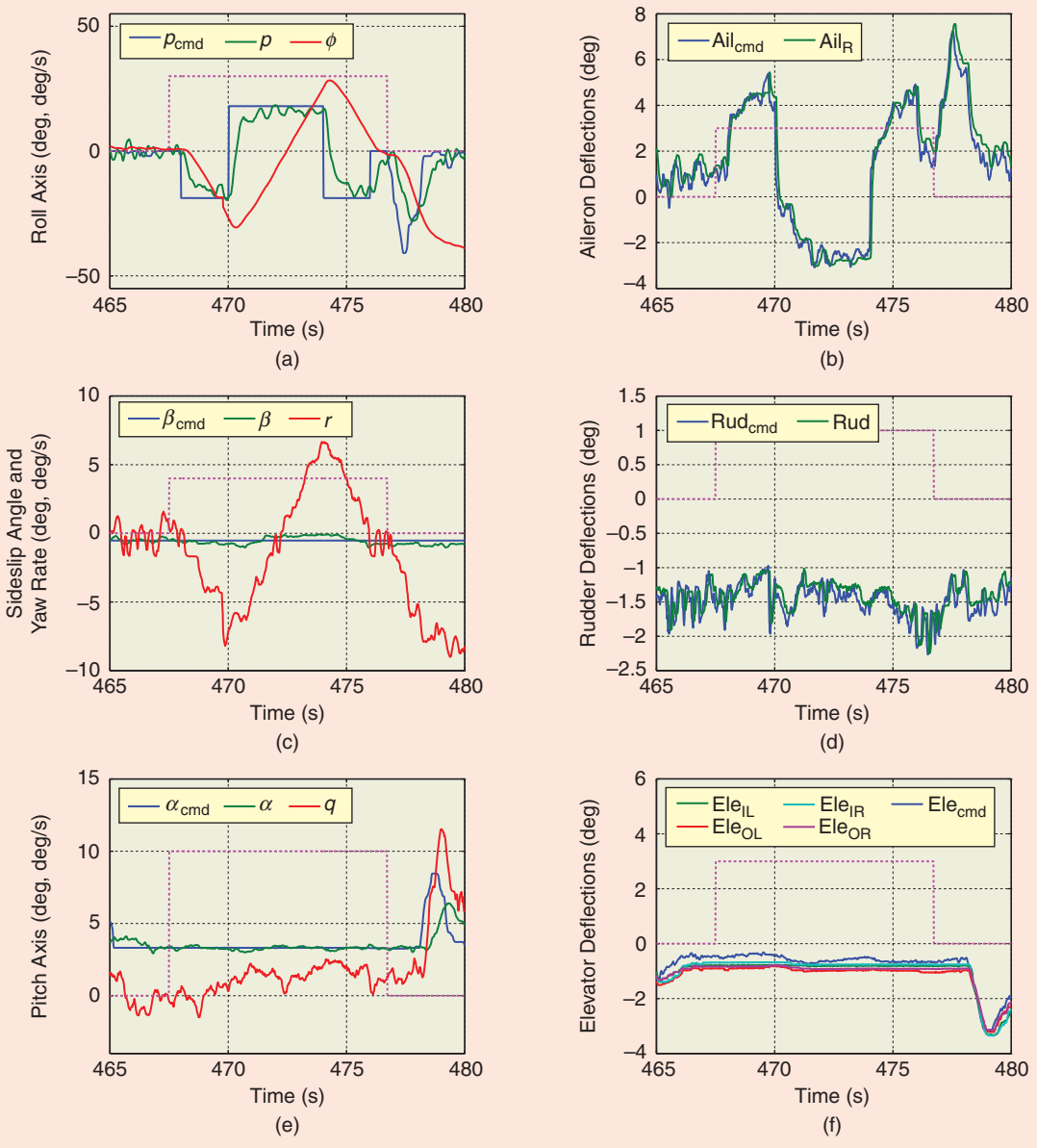

FIGURE 28 Roll-doublet response for the nominal aircraft. The flight control law provides a predictable first-order-like roll-rate response, while maintaining the angle of attack and sideslip angle within $\pm 0.5^\circ$ of the commanded values. The injection of the wavetrain is indicated in the plots with a purple dashed line. (a) Roll-axis response, (b) right-aileron deflection, (c) directional response, (d) rudder deflection, (e) pitch-axis response, and (f) elevator deflections.

with the tested flight controller is unstable. Of particular interest are the cases of 100% and 125% stability degradation, which correspond, respectively, to a neutrally stable aircraft and an unstable aircraft. Similar to the latency-injection task, the pilot is asked to fly the aircraft in a figure-eight pattern at approximately 900 ft and 80 kt, while pitch- and roll-doublet wavetrains are superimposed on the pilot's stick commands during the straight legs of the pattern to excite the system dynamics. The $\mathcal{L}_1$ controller tested in June 2010 was able to maintain aircraft stability for up to 100% simultaneous degradation in longitudinal and lateral aerodynamic stability with an additional 50% reduction in pitch-control authority.

To provide a basis for comparison, the nominal response of the aircraft with the $\mathcal{L}_1$ flight control law, which is considered to have solid Level 1 handling qualities according to pilot ratings and comments, is presented. Figure 26 shows 70 s of flight data including the pitch and roll wavetrains, one complete turn, and part of another turn. The wavetrains can be observed in Figure 26(a) and (b) as precise straight-line

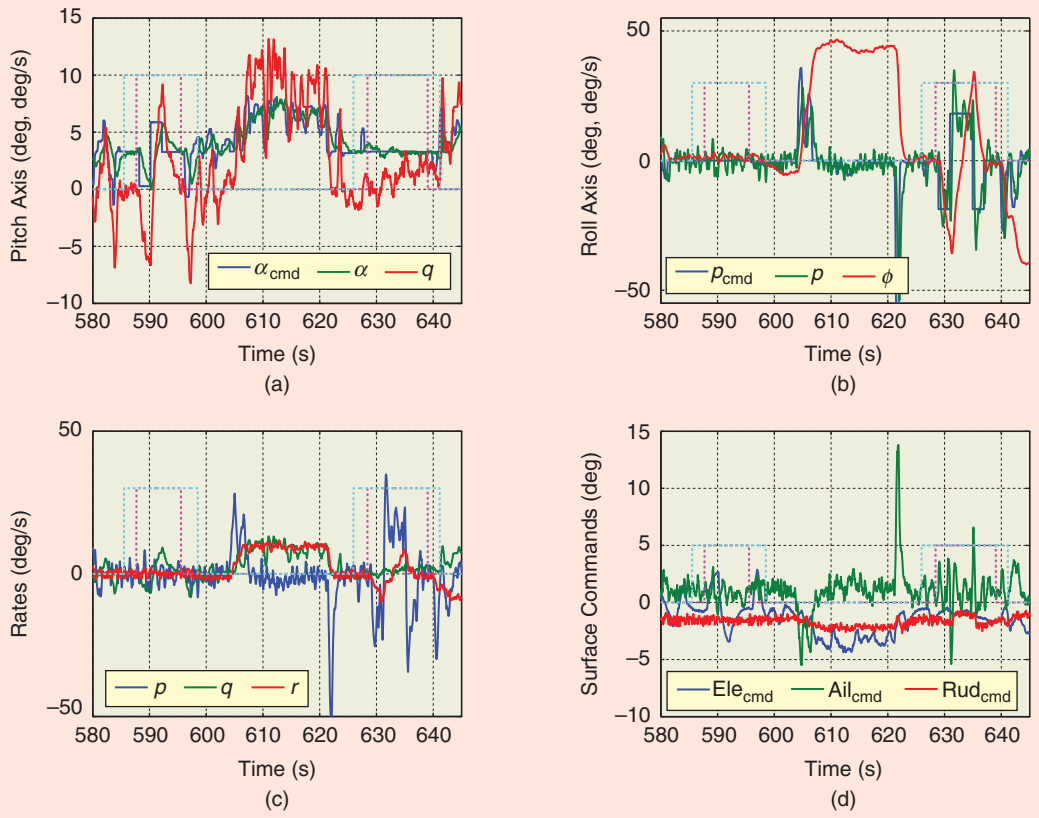

FIGURE 29 Pitch and roll doublets for the case of 75% stability degradation. With respect to the case of nominal aircraft, the closed-loop system experiences a slight degradation in roll-rate tracking performance, while the pitch-axis response remains similar. In addition, there is more aileron activity to compensate for turbulence-induced roll rate. The injection of the wavetrain is indicated in the plots with a purple dashed line, while the injection of the stability degradation is indicated with a cyan dashed line. (a) Pitch-axis response, (b) roll-axis response, (c) body rates, and (d) control-surface commands.

doublets, which indicates that the wavetrain injection is done with the pilot's hands off the stick. Figure 26(c) shows that the $\mathcal{L}_1$ adaptive-control law maintains the sideslip-angle tracking error within $\pm 0.8°$; the constant nonzero sideslip-angle command is due to the vane-calibration bias. The control-surface deflection commands for this flight segment are illustrated in Figure 26(d). The response of the closed-loop system to the pitch and roll wavetrains can be observed in detail in figures 27 and 28. In particular, Figure 27 shows the pitch-axis wavetrain with the corresponding lateral-directional response, while Figure 28 presents the roll-axis wavetrain with the corresponding longitudinal response. The flight control law, which provides a first-order-like response for both channels, is able to isolate the commanded response to the appropriate axis, ensuring reduced cross-coupling between channels. During the injection of the pitch-axis wavetrain, for example, the roll and yaw rates do not exceed ± 5 deg/s, which is considered to be within the turbulence level; see Figure 27(c). Similarly, during the injection of the roll-axis wavetrain, both the angle of attack and sideslip angle are maintained within $\pm 0.5°$ of the commanded values; see Figure 28(c) and (e). The main comment from the pilot during the post-flight debrief is that the $\mathcal{L}_1$ flight control law provides "a nice Level 1 flying airplane for light turbulence conditions."

Next, the performance of the closed-loop adaptive system in the presence of aerodynamic stability degradation is analyzed. Recall that the stability degradation is applied simultaneously in the longitudinal and lateral axes while the elevator effectiveness is reduced by 50%. The reduction in longitudinal stability is obtained by closing a destabilizing feedback loop from angle of attack to inboard elevators, while the spoilers are used asymmetrically to reduce lateral stability through roll damping. The results for the case of 50% stability degradation are similar to the results for the nominal aircraft shown in figures 26–28. The main difference is a higher control surface activity to compensate for turbulence, especially in the roll channel. The pilot, however, reported that he did not detect a perceptible difference from flying the nominal aircraft. The results for the 50% degradation case can be found in [7]. The case of 75% stability degradation, which is considered a severe failure, is illustrated in figures 29–31. As shown in the figures, the closed-loop system

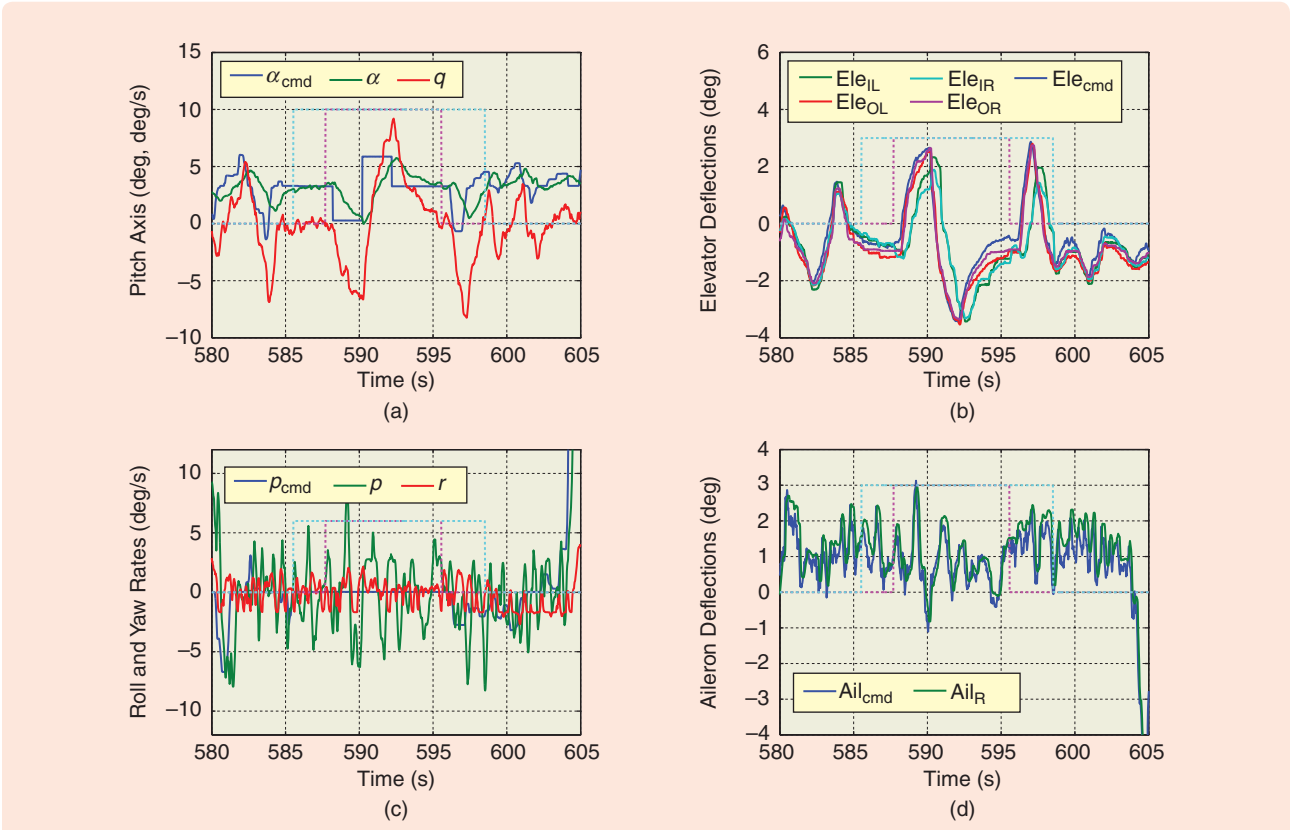

FIGURE 30 Pitch-doublet response for the case of 75% stability degradation. The flight control law provides a first-order-like angle-of-attack response similar to the response of the nominal aircraft. Due to the reduction in roll damping, there is more aileron activity to compensate for turbulence-induced roll rate. The left and right inboard elevators do not track the elevator command provided by the $\mathcal{L}_1$ control law, since they are used to produce the 75% longitudinal stability degradation. The injection of the wavetrain is indicated in the plots with a purple dashed line, while the injection of the stability degradation is indicated with a cyan dashed line. (a) Pitch-axis response, (b) elevator deflections, (c) lateral-directional response, and (d) right-aileron deflection.

experiences a slight degradation in roll-rate tracking performance, while the pitch-axis response remains similar to the response of the nominal aircraft. In addition, there is more aileron activity to compensate for the turbulence-induced roll rate.

For the case of 100% stability degradation, the $\mathcal{L}_1$ flight control law is not able to maintain prescribed performance. Figure 32 shows angle-of-attack and roll-rate tracking as well as the angular-rate response and the corresponding actuator commands through the entire segment of flight. The roll response exhibits oscillatory behavior as well as increased aileron activity, resulting in an evident deterioration in the closed-loop system performance. The response of the aircraft to the pitch and roll wavetrains are isolated in figures 33 and 34, respectively. In particular, Figure 33 shows that the pitch-axis closed-loop damping is reduced, as evidenced by overshoot in the angle-of-attack response and larger amplitudes in pitch rate. Moreover, as shown in Figure 33(c), the pitch-axis doublet induces ±15-deg/s oscillations in roll rate. The pilot observed roll ratcheting during the injection of the pitch-axis wavetrain. In Figure 33(b), the use of the inboard elevators to produce the 100% longitudinal stability degradation is evident; in fact, as mentioned above, the inboard elevators are scheduled with angle of attack to create a destabilizing feedback loop and thus do not follow the elevator command generated by the $\mathcal{L}_1$ flight control law. During the injection of the roll-axis wavetrain, the closed-loop system exhibits large overshoot and ±20-deg/s sustained oscillations in roll rate, which seems to indicate that the controller is reaching the limit of its ability to provide robust performance in the roll channel; see Figure 34. Also, despite the controller performance degradation in the roll axis, the angle-of-attack and sideslip-angle tracking errors are maintained within ±1 deg/s.

The $\mathcal{L}_1$ flight control law flown during the June 2010 deployment was not able to handle the case of 125% stability degradation. Flight test results for this case can be found in [7].

Stall and Post-Stall Flight

From the perspective of the IRAC project, interest in stall and post-stall flight is twofold. First, there is an interest

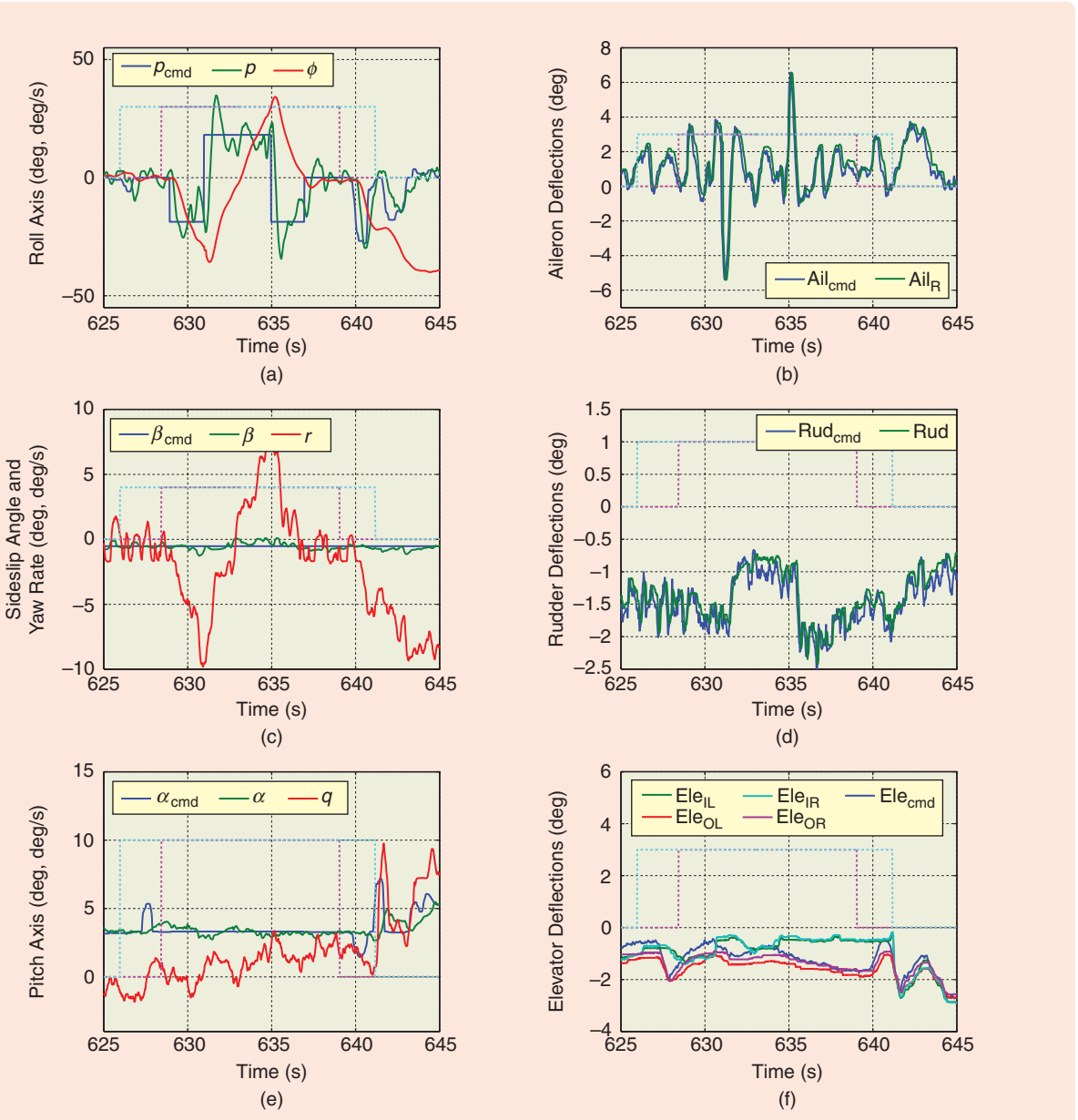

FIGURE 31 Roll-doublet response for the case of 75% stability degradation. These plots illustrate the degradation in roll-rate tracking performance caused by the reduction in roll damping. The roll-rate response exhibits an overshoot, which reduces the predictability of the closed-loop response. The injection of the wavetrain is indicated in the plots with a purple dashed line, while the injection of the stability degradation is indicated with a cyan dashed line. (a) Roll-axis response, (b) right-aileron deflection, (c) directional response, (d) rudder deflection, (e) pitch-axis response, and (f) elevator deflections.

in exploiting the AirSTAR facility as a flying wind tunnel to model unsteady nonlinear aerodynamics encountered at post-stall flight regimes. Second, high angle-of-attack flight provides a challenging scenario for adaptive controllers in which the dynamics of the aircraft experience significant changes and are characterized by uncertain nonlinear phenomena. The primary challenge associated with post-stall high angle of attack is rapidly changing roll damping characteristics and an abrupt wing drop due to asymmetric wing stall. Roll asymmetry with an abrupt wing drop is expected to occur at an angle of attack of about 13°. Also, roll damping characteristics are expected to rapidly change from stable to unstable in the 10–12° angle-of-attack range. At angles of attack above stall, roll damping is expected to improve and aerodynamic asymmetry is expected to decrease. The defining stall characteristic is expected to be an unstable pitch break occurring at an angle of attack of 13°; moreover, at post-stall 15° angle of attack, static and dynamic longitudinal stability is expected to be low.

Fast and robust adaptation is the key feature of the $\mathcal{L}_1$ adaptive control that leads to a priori quantifiable transient and steady-state performance.

Figure 35 presents flight test results for a post-stall angle-of-attack acquisition task, which illustrates some of the stall phenomena described above. In particular, Figure 35 shows the result of three unsuccessful attempts to capture an angle of attack of 18° without exceeding 45° of bank angle. In all three attempts, there is an abrupt roll-rate response exceeding 40 deg/s, while the bank angle exceeds the 45° limit.

Based on the performance and predictability of the $\mathcal{L}_1$ flight control law observed in the stability degradation tasks, the pilot had the confidence to take the GTM into post-stall flight during the June 2010 deployment. Figure 36 shows the results of two attempts to capture an angle of attack of 18° without exceeding the prescribed limit of 45° of bank angle. During these attempts, the $\mathcal{L}_1$ flight control law exhibits a predictable and repeatable behavior, maintaining the roll rate within ±20 deg/s and the bank angle within ±15°. The time-history response for one of these attempts is illustrated in Figure 36(c). For this particular attempt, the bank-angle excursion lasts for less than 2 s before returning to a 5° offset. The pilot captures and maintains the angle of attack at 18° for more than 7 s. Moreover, the combination of power setting and pilot command saturates all elevator segments from 849 to 854 s without observable ill effects on the FCS or aircraft dynamics; see Figure 36(d). At 854 s, the pilot initiates post-stall recovery, recovers by 856 s and initiates a turn by 858 s. To date, the $\mathcal{L}_1$ flight control law is the only control law that has flown in the high angle-of-attack, post-stall regime on the GTM aircraft.

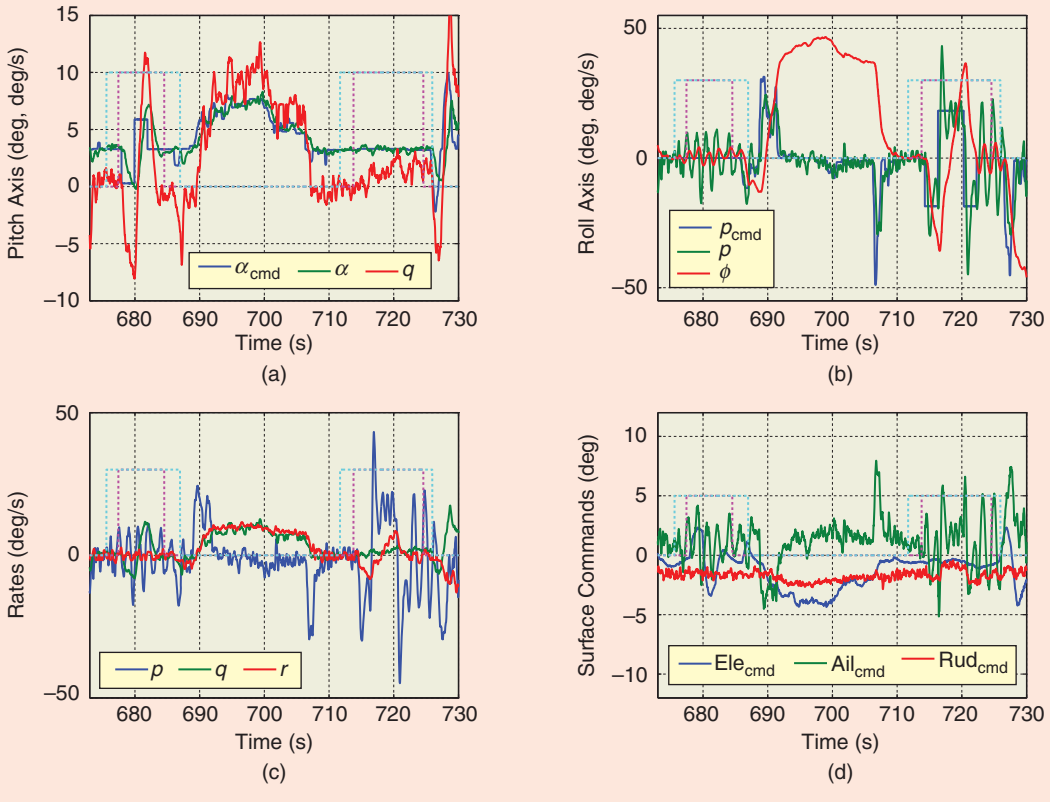

FIGURE 32 Pitch and roll doublets for the case of 100% stability degradation. The roll response exhibits oscillatory behavior as well as increased aileron activity, resulting in an evident deterioration in closed-loop system performance. The injection of the wavetrain is indicated in the plots with a purple dashed line, while the injection of the stability degradation is indicated with a cyan dashed line. (a) Pitch-axis response, (b) roll-axis response, (c) body rates, and (d) control-surface commands.

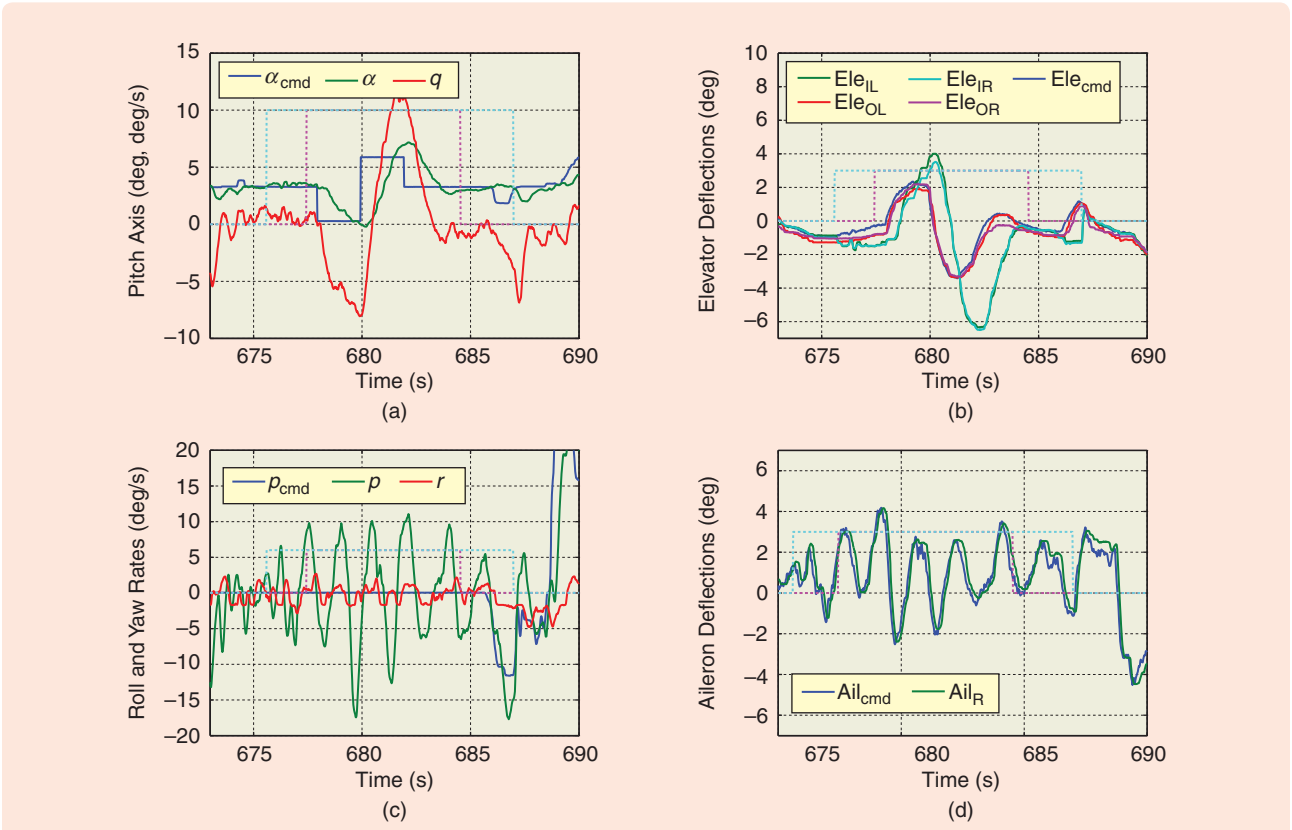

FIGURE 33 Pitch-doublet response for the case of 100% stability degradation. These plots show that the pitch-axis closed-loop damping is reduced, as evidenced by an overshoot in the angle-of-attack response and larger amplitudes in pitch rate. The injection of the pitch-axis wavetrain induces ±15-deg/s oscillations in roll rate. (b) also illustrates the use of the left and right inboard elevators to produce the 100% longitudinal stability degradation. The injection of the wavetrain is indicated in the plots with a purple dashed line, while the injection of the stability degradation is indicated with a cyan dashed line. (a) Pitch-axis response, (b) elevator deflections, (c) lateral-directional response, and (d) right-aileron deflection.

Offset Landings

The $\mathcal{L}_1$ flight control law was evaluated in a series of offset landing tasks, which were conducted during the September 2010 deployment. The offset landing task is considered to be a high workload task in which the pilot tries to put the aircraft down in a desired touchdown spot on the runway. During the flight test, the task requirements are set on aircraft attitude, flight-path angle, and touchdown position on the runway. Moreover, as mentioned above, to evaluate the ability of the adaptive controller, the task is performed not only for the nominal aircraft but also for the cases of 100% and 125% stability degradation with an additional 50% reduction in pitch-control authority. To place the results in an appropriate context, note that the GTM, without any feedback FCS, is rated CHR 3, Level 1 flying qualities; this rating deteriorates to CHR 4, Level 2 flying qualities for the offset landing task of a nominal aircraft. Furthermore, for the neutral stability case, 100% roll- and pitch-axis stability degradation, the pilot rated the task as CHR 10, that is, aircraft uncontrollable with catastrophic landing expected.

The offset landing task was flown under light turbulence conditions, which typically exacerbates stability degradation especially in roll axis since the destabilizing feedback loop responds to turbulence induced roll rate. Hence, the implication of turbulence is that the control surface deflections required to make aircraft neutrally stable, 100% stability degradation, would, in reality, be larger and make the aircraft slightly unstable. Under nominal aircraft stability, the $\mathcal{L}_1$ control law is rated CHR 3, Level 1 handling qualities. For the case of 100% stability degradation, the $\mathcal{L}_1$ controller experiences some handling qualities degradation and is rated CHR 5, Level 2. Finally, for the case of 125% stability degradation, the pilot achieves a safe landing with CHR 7, Level 3 handling qualities. The $\mathcal{L}_1$ flight control law provided a graceful degradation in terms of flying qualities rating for each of the stability degradation cases, that is, nominal CHR 3, neutrally stable CHR 5, and unstable CHR 7. We refer to [8] for the flight test data of these offset landing tasks. A summary of comments and CHRs that the AirSTAR research pilot

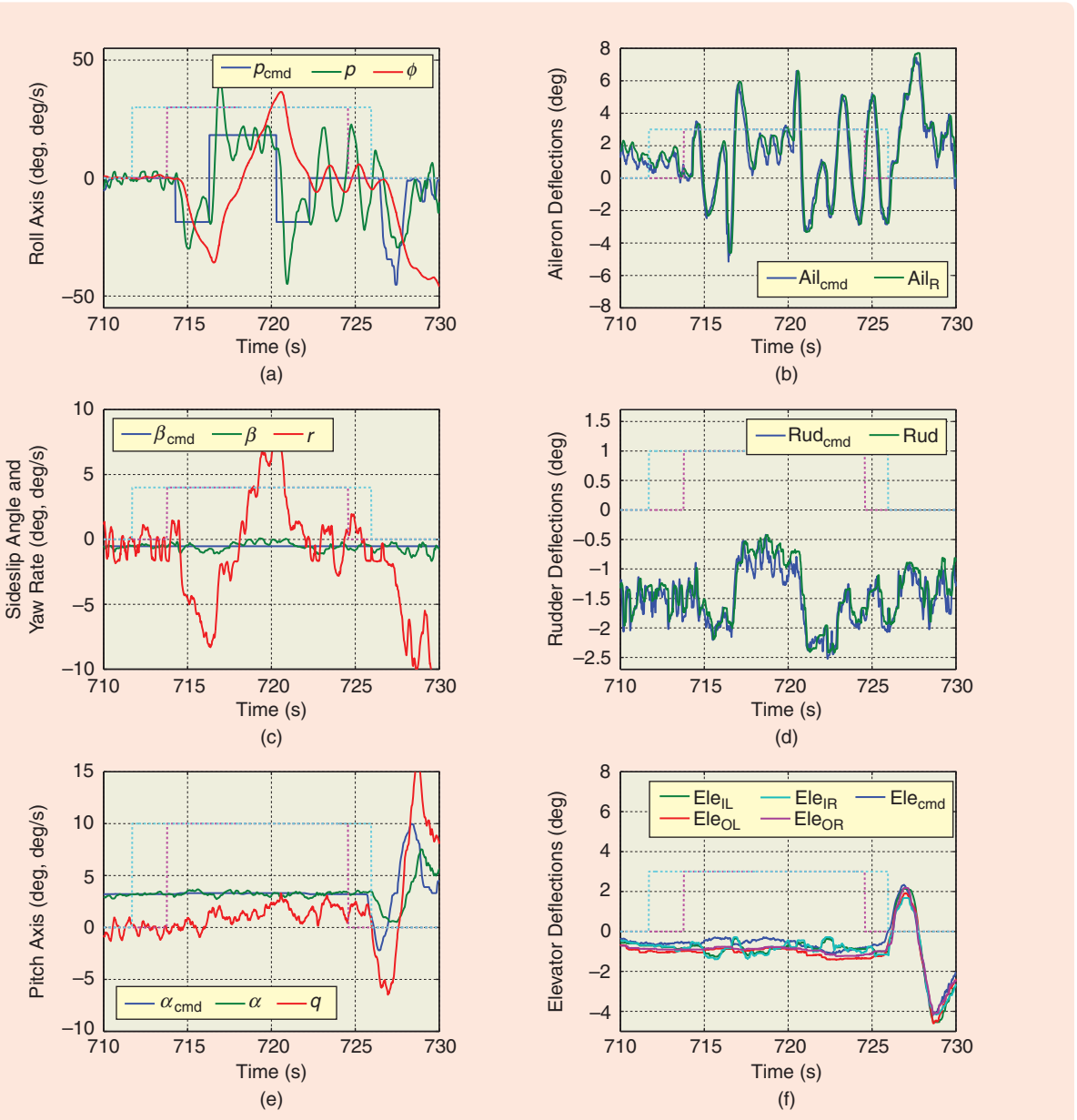

FIGURE 34 Roll-doublet response for the case of 100% stability degradation. During the injection of the roll-axis wavetrain, the system response exhibits overshoots and sustained oscillations in roll rate, which seems to indicate that the controller is reaching the limit of its ability to provide robust performance in the roll channel. The injection of the wavetrain is indicated in the plots with a purple dashed line, while the injection of the stability degradation is indicated with a cyan dashed line. (a) Roll-axis response, (b) right-aileron deflection, (c) directional response, (d) rudder deflection, (e) pitch-axis response, and (f) elevator deflections.

provided for the offset landing task evaluation can be found in [78].

$\mathcal{L}_1$ Flight Control Law in Support of Unsteady Aerodynamic Modeling Work

By the September 2010 deployment, the $\mathcal{L}_1$ adaptive flight control law had established itself as a reliable and predictable tool to be used in support of other research tasks to reduce the pilot's workload and provide tighter acquisition of target flight conditions. One of the research tasks flown during the September 2010 deployment was the calibration of the two air-data vanes placed on each wingtip of the GTM aircraft. The precise calibration of the angle-of-attack and angle-of-sideslip vanes is critical for system identification and nonlinear aerodynamic modeling. Significantly, the control law demonstrates a precision tracking capability at the edge of aircraft controllability even with persistently saturated control surfaces. Moreover, the $\mathcal{L}_1$ control law provides predictable response to the pilot when the control authority for different axes is divided between a

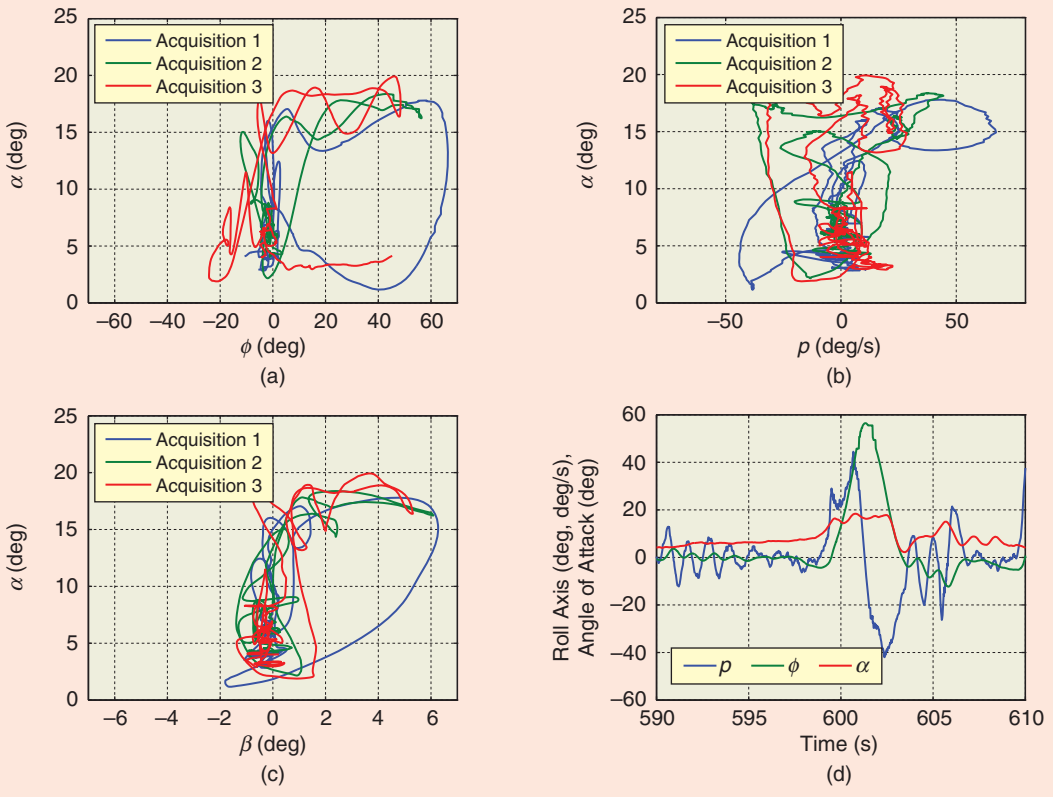

FIGURE 35 Stick-to-surface post-stall angle-of-attack acquisition task. The primary challenge associated with post-stall high angle of attack is rapidly changing roll damping characteristics and an abrupt wing drop due to asymmetric wing stall, which occurs at about 13° angle of attack. These plots show the result of three unsuccessful attempts to capture an 18° angle of attack without exceeding 45° of bank angle. In all three attempts, the roll rate experiences an abrupt departure and exceeds 40 deg/s, while the bank angle exceeds the 45° limit. (a) Bank angle, (b) roll rate, (c) sideslip angle, and (d) time-history response (single attempt).

pilot and an automatic command. The results of these flight tests are presented in [76].

In addition, during the September 2010 deployment, the $\mathcal{L}_1$ flight control law was used to support unsteady aerodynamic modeling work at post-stall. For this modeling work, the main objective of the control law is to stabilize the aircraft at an angle of attack of 18° and, once the desired angle of attack is reached, track a predetermined input wavetrain with the pilot's hands off the stick. To improve tracking performance at high angles of attack to better support these modeling tasks, it was necessary to increase the bandwidth of the $\mathcal{L}_1$ lowpass filter in the longitudinal channel. As predicted by $\mathcal{L}_1$ adaptive-control theory, the tradeoff for increased performance led to a decrease in closed-loop latency robustness, which decreased from the 0.147 s mentioned above to 0.117 s. Flight test results for two of these modeling tasks are shown in Figure 37. In particular, Figure 37(a) illustrates a precision tracking task in which the GTM is required to track a multistep wavetrain in the post-stall regime, while Figure 37(b) presents the response of the system to a Schroeder sweep, also in the post-stall regime. As shown in Figure 37(b), the $\mathcal{L}_1$ flight control law provides high angle-of-attack tracking capabilities and ensures a safe recovery once the post-stall maneuver is completed. Further description of the performance of the $\mathcal{L}_1$ adaptive flight control law on these and other supporting tasks can be found in [8].

Finally, during the May 2011 deployment, the $\mathcal{L}_1$ adaptive-control law continued to enable exploration of departure-prone edges of the flight envelope and support nonlinear unsteady aerodynamic modeling beyond the linear flight regime. The $\mathcal{L}_1$ adaptive flight control law was used as a means to maintain departure resistance and to reduce pilot workload during test-point acquisition. The $\mathcal{L}_1$ control law allowed the research pilot to operate the aircraft in precarious flight conditions near stall and departure for longer periods of time, which provided time for the optimized multi-input wavetrains to excite the aircraft dynamics in all 6DOF to collect the data needed for real-time dynamic modeling. The $\mathcal{L}_1$ control operated without introducing high correlations in the states and controls during the maneuvers. Note that the maneuvers were implemented by adding wavetrain perturbation inputs directly to the actuator commands from the control law, just upstream of the rate and position limiting. Moreover, the $\mathcal{L}_1$ adaptive flight control law was

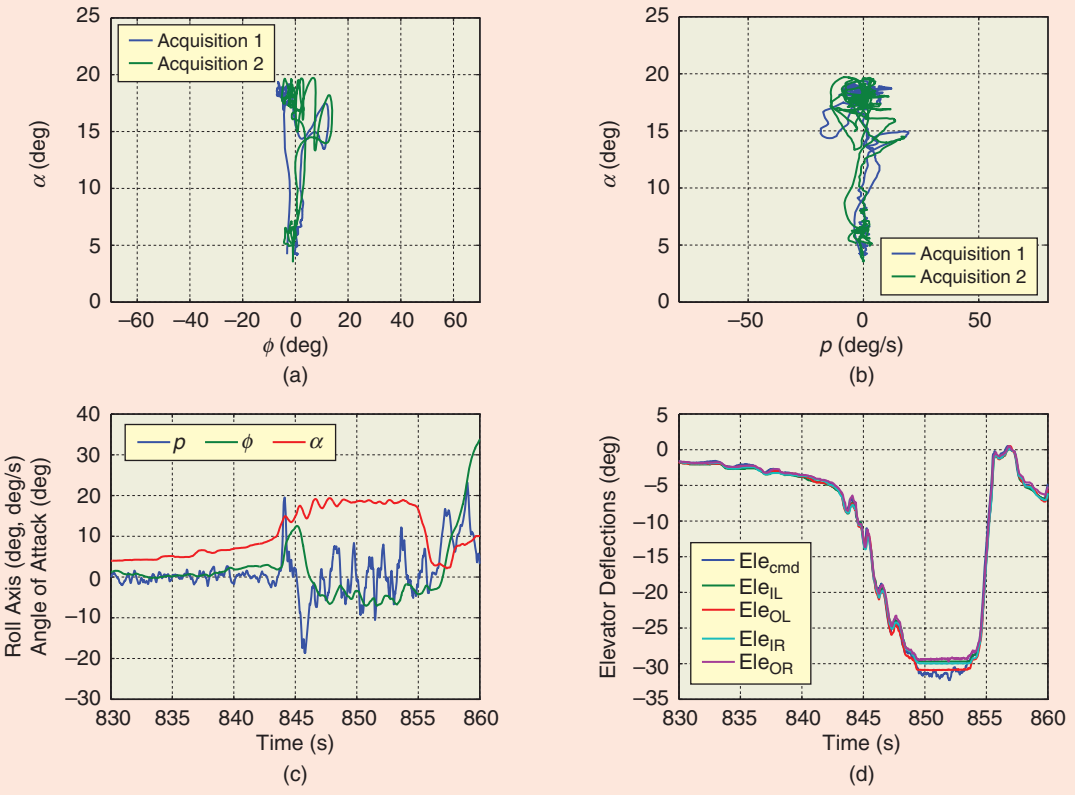

FIGURE 36 Post-stall angle-of-attack acquisition task with the $\mathcal{L}_1$ adaptive flight control law. During these attempts, the $\mathcal{L}_1$ flight control law exhibits a predictable repeatable behavior, maintaining the roll rate within ± 20 deg/s and the bank angle within $\pm 15°$. The combination of power setting and pilot command saturates all of the elevator segments from 849 to 854 s without observable ill effects on the control system or aircraft dynamics. (a) Bank angle, (b) roll rate, (c) time-history response (single attempt), and (d) elevator deflections.

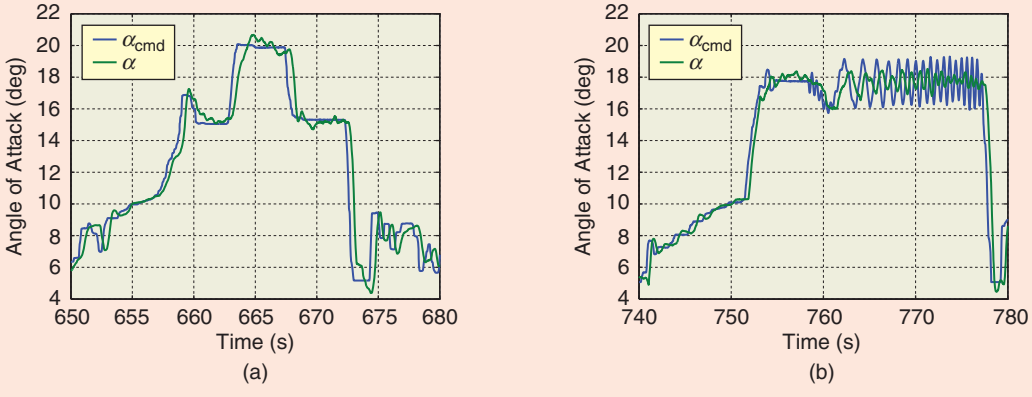

FIGURE 37 $\mathcal{L}_1$ flight control law in support of unsteady aerodynamic modeling work in post-stall regimes. In these modeling tasks, the main objective of the control law is to track an angle of attack of 18° and, once the desired angle of attack is reached, track a predetermined input wavetrain with the pilot's hands off the stick. These plots illustrate two precision tracking tasks, in which the aircraft is required to track, respectively, (a) a multistep wavetrain and (b) a Schroeder sweep.

used to support an unsteady aerodynamics modeling investigation at aerodynamic stall. The control law was used to track roll-axis excitation waveforms in flight conditions near and post stall. The purpose of this maneuver was to validate unsteady aerodynamic behavior, which was identified in wind-tunnel tests using a forced-oscillation test technique. Flight tests results for these research tasks are reported in [8].

Flight Test Summary

The series of flight tests on the GTM remotely piloted aircraft conducted with an $\mathcal{L}_1$ adaptive-control law provides a challenging, real-world environment that stresses the control law to its limits, exposes its behavior in various demanding scenarios, and verifies the theoretical predictions of its behavior. The results show that the $\mathcal{L}_1$ flight control law provides predictable behavior both in the neighborhood of the design point as well as at other operating points of the flight envelope, such as stall and post-stall regimes. Fast adaptation is critical for ensuring safe operation and providing predictable aircraft behavior for the pilot, even as significant changes in aircraft dynamics happen unexpectedly. Moreover, the $\mathcal{L}_1$ controller enables modeling of unsteady nonlinear aerodynamic phenomena at challenging flight conditions, such as stall and post-stall, and also enables real-time dynamic modeling of the departure-prone edges of the flight envelope. In this sense, the $\mathcal{L}_1$ flight control provides a reliable tool for enhancing the experimental capabilities of the GTM aircraft, by facilitating precision tracking with reduced pilot workload.

CONCLUSIONS

This article presents the development of $\mathcal{L}_1$ adaptive-control theory and its application to safety critical FCS development. Several architectures of the theory and benchmark examples are analyzed. The key feature of $\mathcal{L}_1$ adaptive-control architectures is the decoupling of estimation and control, which enables the use of arbitrarily fast estimation rates without sacrificing robustness. Rohrs's example and the two-cart system are used as benchmark problems for illustration. NASA's flight tests on subscale commercial jet verify the theoretical claims in a set of safety-critical test flights.

ACKNOWLEDGMENTS

The development of $\mathcal{L}_1$ adaptive-control theory was supported by U.S Air Force Office of Scientific Research and was leveraged by the U.S. Army Research Office and U.S. Office of Naval Research. The flight test program was supported by NASA's Aviation Safety Program. The authors would like to thank the anonymous reviewers whose comments helped to improve the presentation.

AUTHOR INFORMATION

Naira Hovakimyan (nhovakim@illinois.edu) received her M.S. in theoretical mechanics and applied mathematics in 1988 from Yerevan State University in Armenia. She received her Ph.D. in physics and mathematics in 1992, in Moscow, from the Institute of Applied Mathematics of Russian Academy of Sciences, majoring in optimal control and differential games. In 1997 she was awarded a governmental postdoctoral scholarship to work in INRIA, France. In 1998 she was invited to the School of Aerospace Engineering of Georgia Tech, where she worked as a research faculty member until 2003. In 2003 she joined the Department of Aerospace and Ocean Engineering of Virginia Tech, and in 2008 she moved to the University of Illinois at Urbana-Champaign, where she is a professor and Schaller faculty scholar. She is the 2011 recipient of the AIAA Mechanics and Control of Flight Award. She has coauthored one book and more than 250 refereed publications. Her research interests are in the theory of robust adaptive control and estimation with an emphasis on aerospace applications, control in the presence of limited information, networks of autonomous systems and game theory. She is an associate fellow and life member of AIAA, a Senior Member of IEEE, and a member of AMS and ISDG. She can be contacted at 223 Mechanical Engineering Building, University of Illinois at Urbana-Champaign, 1206 West Green Street, Urbana, IL 61801 USA.

Chengyu Cao has been an assistant professor of mechanical engineering at the University of Connecticut since 2008. Prior to that, he was a research scientist in the Department of Aerospace and Ocean Engineering at Virginia Polytechnic Institute and State University. He received his Ph.D. in mechanical engineering from the Massachusetts Institute of Technology in 2004. He earned his B.S. degree in electronics and information engineering from Xi'an Jiaotong University, China, and M.S. in manufacturing engineering from Boston University in 1995 and 1999, respectively. His research interests are in the areas of dynamics and control, adaptive and intelligent systems, and mechatronics, with a focus on unmanned systems and aerospace applications. He is the author of more than 100 publications.

Evgeny Kharisov is a Ph.D. candidate at the Department of Aerospace Engineering at the University of Illinois at Urbana-Champaign. He received the bachelor's and master's from the Department of Informatics and Control Systems at Bauman Moscow State Technical University in 2004 and 2007, respectively. His research interests include adaptive control, robust control, multiagent systems, and automatic control in aerospace system.

Enric Xargay is a Ph.D. candidate in the Department of Aerospace Engineering at the University of Illinois at Urbana-Champaign. He received an M.S. in control engineering from the Technical University of Catalonia and an M.S. in aerospace engineering from the Politecnico di Torino, both in 2007. His research interests include aircraft flight control, nonlinear systems, adaptive control, robust control, and cooperative control of autonomous systems.

Irene M. Gregory is a senior research engineer at NASA Langley Research Center, Dynamic Systems and Control Branch. She received a B.S. in aeronautics and astronautics from the Massachusetts Institute of Technology in 1988, an M.S. in 1990, and a Ph.D. in control and dynamical systems from the California Institute of Technology in 2004. Her research includes advanced

flight control for hypersonic, supersonic, subsonic flight regimes, aircraft, launch vehicles, and unmanned aerial vehicles. Her current interests are adaptive, nonlinear control, their robustness and performance measures for real systems as well as autonomy and safe flight in next generation national aerospace system. She is an Associate Fellow of AIAA and a Member of IEEE.

REFERENCES

[1] S. A. Jacklin, "Closing certification gaps in adaptive flight control software," in *Proc. AIAA Guidance, Navigation and Control Conf.*, Honolulu, HI, AIAA-2008-6988, 2008.

[2] H. K. Khalil, *Nonlinear Systems*. Englewood Cliffs, NJ: Prentice-Hall, 2002.

[3] C. Cao and N. Hovakimyan, "Stability margins of $\mathcal{L}_1$ adaptive control architecture," *IEEE Trans. Automat. Contr.*, vol. 55, no. 2, pp. 480–487, 2010.

[4] N. Hovakimyan and C. Cao, $\mathcal{L}_1$ *Adaptive Control Theory*. Philadelphia, PA: Society for Industrial and Applied Mathematics, 2010.

[5] E. Kharisov, N. Hovakimyan, and K. J. Åström, "Comparison of several adaptive controllers according to their robustness metrics," in *Proc. AIAA Guidance, Navigation, and Control Conf.*, Toronto, Canada, AIAA-2010-8047, 2010.

[6] E. Xargay, N. Hovakimyan, and C. Cao, "Benchmark problems of adaptive control revisited by $\mathcal{L}_1$ adaptive control," in *Proc. Mediterranean Conf. Control and Automation*, Thessaloniki, Greece, 2009, pp. 31–36.

[7] I. M. Gregory, E. Xargay, C. Cao, and N. Hovakimyan, "Flight test of $\mathcal{L}_1$ adaptive controller on the NASA AirSTAR flight test vehicle," in *Proc. AIAA Guidance, Navigation and Control Conf.*, Toronto, AIAA-2010-8015, 2010.

[8] I. M. Gregory, E. Xargay, C. Cao, and N. Hovakimyan, "Flight test of an $\mathcal{L}_1$ adaptive control law: Offset landings and large flight envelope modeling work," in *Proc. AIAA Guidance, Navigation and Control Conf.*, Portland, OR, AIAA-2011-6608, 2011.

[9] P. C. Gregory, "Air research and development command plans and programs," in *Proc. Self Adaptive Flight Control Symp.*, P. C. Gregory, Ed. OH: Wright-Patterson Air Force Base, 1959, pp. 8–15.

[10] E. Mishkin and L. Braun, *Adaptive Control Systems*. New York: McGraw-Hill, 1961.

[11] K. J. Åström, "Adaptive control around 1960," in *Proc. 34th IEEE Conf. Decision and Control*, New Orleans, LA, 1995, pp. 2784–2789.

[12] L. W. Taylor, Jr. and E. J. Adkins, "Adaptive control and the X-15," in *Proc. Princeton University Conf. Aircraft Flying Qualities*, Princeton, NJ, 1965.

[13] L. Ljung, *System Identification—Theory for the User*. Englewood Cliffs, NJ: Prentice-Hall, 1987.

[14] R. Kalman, "Design of self-optimizing control systems," *ASME Trans.*, vol. 80, pp. 468–478, 1958.

[15] K. J. Åström and B. Wittenmark, "On self-tuning regulators," *Automatica*, vol. 9, no. 2, pp. 185–199, 1973.

[16] B. Egardt, *Stability of Adaptive Controllers*. New York: Springer-Verlag, 1979.

[17] G. C. Goodwin and K. S. Sin, *Adaptive Filtering Prediction and Control*. Englewood Cliffs, NJ: Prentice-Hall, 1984.

[18] S. Sastry and M. Bodson, *Adaptive Control: Stability, Convergence and Robustness*. Englewood Cliffs, NJ: Prentice-Hall, 1989.

[19] S. Sastry, *Nonlinear Systems: Analysis, Stability, and Control (Interdisciplinary Applied Mathematics)*. New York: Springer-Verlag, 1999.

[20] J.-J. E. Slotine and W. Li, *Applied Nonlinear Control*. Englewood Cliffs, NJ: Prentice-Hall, 1991.

[21] P. R. Kumar and P. P. Varaiya, *Stochastic Systems: Estimation, Identification, and Adaptive Control*. Englewood Cliffs, NJ: Prentice-Hall, 1986.

[22] K. J. Åström and B. Wittenmark, *Adaptive Control*, 2nd ed. New York: Dover, 2008. Originally published by Addison Wesley, 1995.

[23] R. E. Bellman, *Adaptive Control Processes—A Guided Tour*. Princeton, NJ: Princeton Univ. Press, 1961.

[24] Y. D. Landau, *Adaptive Control: The Model Reference Approach (Control and Systems Theory)*. New York: Marcel Dekker, 1979.

[25] A. S. Morse, "Global stability of parameter-adaptive control systems," *IEEE Trans. Automat. Contr.*, vol. 25, no. 3, pp. 433–439, 1980.

[26] K. S. Narendra, Y.-H. Lin, and L. S. Valavani, "Stable adaptive controller design, part II: Proof of stability," *IEEE Trans. Automat. Contr.*, vol. 25, no. 3, pp. 440–448, 1980.

[27] C. E. Rohrs, L. S. Valavani, M. Athans, and G. Stein, "Robustness of continuous-time adaptive control algorithms in the presence of unmodeled dynamics," *IEEE Trans. Automat. Contr.*, vol. 30, no. 9, pp. 881–889, 1985.

[28] K. J. Åström, "Interactions between excitation and unmodeled dynamics in adaptive control," in *Proc. IEEE Conf. Decision and Control*, Las Vegas, NV, 1984, pp. 1276–1281.

[29] B. D. O. Anderson, "Failures of adaptive control theory and their resolution," *Commun. Inform. Syst.*, vol. 5, no. 1, pp. 1–20, 2005.

[30] P. A. Ioannou and P. V. Kokotović, "An asymptotic error analysis of identifiers and adaptive observers in the presence of parasitics," *IEEE Trans. Automat. Contr.*, vol. 27, no. 4, pp. 921–927, 1982.

[31] P. A. Ioannou and P. V. Kokotović, *Adaptive Systems with Reduced Models*. Secaucus, NJ: Springer-Verlag, 1983.

[32] P. A. Ioannou and P. V. Kokotović, "Robust redesign of adaptive control," *IEEE Trans. Automat. Contr.*, vol. 29, no. 3, pp. 202–211, 1984.

[33] B. B. Peterson and K. S. Narendra, "Bounded error adaptive control," *IEEE Trans. Automat. Contr.*, vol. 27, no. 6, pp. 1161–1168, 1982.

[34] G. Kresselmeier and K. S. Narendra, "Stable model reference adaptive control in the presence of bounded disturbances," *IEEE Trans. Automat. Contr.*, vol. 27, no. 6, pp. 1169–1175, 1982.

[35] K. S. Narendra and A. M. Annaswamy, "A new adaptive law for robust adaptation without persistent excitation," *IEEE Trans. Automat. Contr.*, vol. 32, no. 2, pp. 134–145, 1987.

[36] P. A. Ioannou and J. Sun, *Robust Adaptive Control*. Upper Saddle River, NJ: Prentice-Hall, 1996.

[37] K. S. Tsakalis, "Performance limitations of adaptive parameter estimation and system identification algorithms in the absence of excitation," *Automatica*, vol. 32, no. 4, pp. 549–560, 1996.

[38] K. A. Wise, E. Lavretsky, J. Zimmerman, J. Francis, D. Dixon, and B. Whitehead, "Adaptive flight control of a sensor guided munition," in *Proc. AIAA Guidance, Navigation and Control Conf.*, San Francisco, CA, AIAA-2005-6385, 2005.

[39] K. A. Wise, E. Lavretsky, and N. Hovakimyan, "Adaptive control in flight: Theory, application, and open problems," in *Proc. American Control Conf.*, Minneapolis, MN, 2006, pp. 5966–5971.

[40] R. W. Beard, N. B. Knoebel, C. Cao, N. Hovakimyan, and J. S. Matthews, "An $\mathcal{L}_1$ adaptive pitch controller for miniature air vehicles," in *Proc. AIAA Guidance, Navigation and Control Conf.*, Keystone, CO, AIAA-2006-6777, 2006.

[41] C. Cao, N. Hovakimyan, I. Kaminer, V. V. Patel, and V. Dobrokhodov, "Stabilization of cascaded systems via $\mathcal{L}_1$ adaptive controller with application to a UAV path following problem and flight test results," in *Proc. American Control Conf.*, New York, 2007, pp. 1787–1792.

[42] C. Cao, N. Hovakimyan, and E. Lavretsky, "Application of $\mathcal{L}_1$ adaptive controller to wing rock," in *Proc. AIAA Guidance, Navigation and Control Conf.*, Keystone, CO, AIAA-2006-6426, 2006.

[43] V. V. Patel, C. Cao, N. Hovakimyan, K. A. Wise, and E. Lavretsky, "$\mathcal{L}_1$ adaptive controller for tailless unstable aircraft," in *Proc. American Control Conf.*, New York, 2007, pp. 5272–5277.

[44] V. V. Patel, C. Cao, N. Hovakimyan, K. A. Wise, and E. Lavretsky, "$\mathcal{L}_1$ adaptive controller for tailless unstable aircraft in the presence of unknown actuator failures," in *Proc. AIAA Guidance, Navigation and Control Conf.*, Hilton Head, SC, AIAA-2006-6314, 2007.

[45] J. Wang, C. Cao, V. V. Patel, N. Hovakimyan, and E. Lavretsky, "$\mathcal{L}_1$ adaptive neural network controller for autonomous aerial refueling with guaranteed transient performance," in *Proc. AIAA Guidance, Navigation and Control Conf.*, Keystone, CO, AIAA-2006-6206, 2006.

[46] J. Wang, V. V. Patel, C. Cao, N. Hovakimyan, and E. Lavretsky, "$\mathcal{L}_1$ adaptive neural network controller for autonomous aerial refueling in the presence of unknown actuator failures," in *Proc. AIAA Guidance, Navigation and Control Conf.*, Hilton Head, SC, AIAA-2006-6313, 2007.

[47] I. M. Gregory, C. Cao, V. V. Patel, and N. Hovakimyan, "Adaptive control laws for flexible semi-span wind tunnel model of high-aspect ratio flying wing," in *Proc. AIAA Guidance, Navigation and Control Conf.*, Hilton Head, SC, AIAA-2007-6525, 2007.

[48] R. Hindman, C. Cao, and N. Hovakimyan, "Designing a high performance, stable $\mathcal{L}_1$ adaptive output feedback controller," in *Proc. AIAA Guidance, Navigation and Control Conf.*, Hilton Head, SC, AIAA-2007-6644, 2007.

[49] I. Kaminer, O. A. Yakimenko, V. Dobrokhodov, A. M. Pascoal, N. Hovakimyan, V. V. Patel, C. Cao, and A. Young, "Coordinated path following for time-critical missions of multiple UAVs via $\mathcal{L}_1$ adaptive output feedback controllers," in *Proc. AIAA Guidance, Navigation and Control Conf.*, Hilton Head, SC, AIAA-2007-6409, 2007.

[50] Y. Lei, C. Cao, E. M. Cliff, N. Hovakimyan, and A. J. Kurdila, "Design of an $\mathcal{L}_1$ adaptive controller for air-breathing hypersonic vehicle model in the presence of unmodeled dynamics," in *Proc. AIAA Guidance, Navigation and Control Conf.*, Hilton Head, SC, AIAA-2006-6527, 2007.

[51] E. Kharisov, I. M. Gregory, C. Cao, and N. Hovakimyan, "$\mathcal{L}_1$ adaptive control for flexible space launch vehicle and proposed plan for flight validation," in *Proc. AIAA Guidance, Navigation and Control Conf.*, Honolulu, HI, AIAA-2008-7128, 2008.

[52] V. Dobrokhodov, I. Kitsios, I. Kaminer, K. D. Jones, E. Xargay, N. Hovakimyan, C. Cao, M. I. Lizárraga, and I. M. Gregory, "Flight validation of metrics driven $\mathcal{L}_1$ adaptive control," in *Proc. AIAA Guidance, Navigation and Control Conf.*, Honolulu, HI, AIAA-2008-6987, 2008.

[53] I. Kitsios, V. Dobrokhodov, I. Kaminer, K. D. Jones, E. Xargay, N. Hovakimyan, C. Cao, M. I. Lizárraga, I. M. Gregory, N. T. Nguyen, and K. S. Krishnakumar, "Experimental validation of a metrics driven $\mathcal{L}_1$ adaptive control in the presence of generalized unmodeled dynamics," in *Proc. AIAA Guidance, Navigation and Control Conf.*, Chicago, IL, AIAA-2009-6188, 2009.

[54] I. M. Gregory, C. Cao, E. Xargay, N. Hovakimyan, and X. Zou, "$\mathcal{L}_1$ adaptive control design for NASA AirSTAR flight test vehicle," in *Proc. AIAA Guidance, Navigation and Control Conf.*, Chicago, IL, AIAA-2009-5738, 2009.

[55] T. Leman, E. Xargay, G. Dullerud, and N. Hovakimyan, "$\mathcal{L}_1$ adaptive control augmentation system for the X-48B aircraft," in *Proc. AIAA Guidance, Navigation and Control Conf.*, Chicago, IL, AIAA-2009-5619, 2009.

[56] Z. Li, V. Dobrokhodov, E. Xargay, N. Hovakimyan, and I. Kaminer, "Development and implementation of $\mathcal{L}_1$ gimbal tracking loop onboard of small UAV," in *Proc. AIAA Guidance, Navigation and Control Conf.*, Chicago, IL, AIAA-2009-5681, 2009.

[57] Y. Lei, C. Cao, E. M. Cliff, N. Hovakimyan, A. J. Kurdila, and K. A. Wise, "$\mathcal{L}_1$ adaptive controller for air-breathing hypersonic vehicle with flexible body dynamics," in *Proc. American Control Conf.*, St. Louis, MO, 2009, pp. 3166–3171.

[58] B. Michini and J. How, "$\mathcal{L}_1$ adaptive control for indoor autonomous vehicles: Design process and flight testing," in *Proc. AIAA Guidance, Navigation and Control Conf.*, Chicago, IL, AIAA-2009-5754, 2009.

[59] I. Kaminer, A. Pascoal, E. Xargay, N. Hovakimyan, C. Cao, and V. Dobrokhodov, "Path following for unmanned aerial vehicles using $\mathcal{L}_1$ adaptive augmentation of commercial autopilots," *J. Guid. Control Dyn.*, vol. 33, no. 2, pp. 550–564, 2010.

[60] X. Fan and R. C. Smith, "Model-based $\mathcal{L}_1$ adaptive control of hysteresis in smart materials," in *Proc. IEEE Conf. Decision and Control*, Cancun, Mexico, 2008, pp. 3251–3256.

[61] C. Cao and N. Hovakimyan, "Design and analysis of a novel $\mathcal{L}_1$ adaptive control architecture with guaranteed transient performance," *IEEE Trans. Automat. Contr.*, vol. 53, no. 2, pp. 586–591, 2008.

[62] K. J. Åström and B. Wittenmark, *Adaptive Control*. Boston, MA: Addison-Wesley, 1994.

[63] C. E. Rohrs, L. S. Valavani, M. Athans, and G. Stein, "Robustness of adaptive control algorithms in the presence of unmodeled dynamics," in *Proc. IEEE Conf. Decision and Control*, Orlando, FL, 1982, vol. 1, pp. 3–11.

[64] J.-B. Pomet and L. Praly, "Adaptive nonlinear regulation: Estimation from the Lyapunov equation," *IEEE Trans. Automat. Contr.*, vol. 37, no. 6, pp. 729–740, 1992.

[65] T. T. Georgiou and M. C. Smith, "Robustness analysis of nonlinear feedback systems: An input-output approach," *IEEE Trans. Automat. Control*, vol. 42, no. 9, pp. 1200–1221, 1997.

[66] C. Cao and N. Hovakimyan, "$\mathcal{L}_1$ adaptive output-feedback controller for non-strictly-positive-real reference systems: Missile longitudinal autopilot design," *AIAA J. Guid. Contr. Dyn.*, vol. 32, no. 3, pp. 717–726, 2009.

[67] E. Xargay, N. Hovakimyan, and C. Cao, "$\mathcal{L}_1$ adaptive controller for multi-input multi-output systems in the presence of nonlinear unmatched uncertainties," in *Proc. American Control Conf.*, Baltimore, MD, 2010, pp. 874–879.

[68] E. Kharisov and N. Hovakimyan, "$\mathcal{L}_1$ adaptive output feedback controller for minimum phase systems," in *Proc. American Control Conf.*, San Francisco, CA, 2011, pp. 1182–1187.

[69] S. Fekri, M. Athans, and A. M. Pascoal, "Issues, progress and new results in robust adaptive control," *Int. J. Adapt. Control Signal Process.*, vol. 20, no. 10, pp. 519–579, 2006.

[70] J. Wang, C. Cao, N. Hovakimyan, R. Hindman, and D. B. Ridgely, "$\mathcal{L}_1$ adaptive controller for a missile longitudinal autopilot design," in *Proc. AIAA Guidance, Navigation and Control Conf.*, Honolulu, HI, AIAA-2008-6282, 2008.

[71] G. E. Cooper and R. P. Harper, Jr., "The use of pilot rating in the evaluation of aircraft handling qualities," *NASA, Tech. Note D–5153*, Moffett Field, CA: Ames Research Center, 1969.

[72] MIL-STD-1797B. (2006). Flying qualities of piloted aircraft, Interface Standard (Limited circulation). U.S. Department of Defense Military Specification. [Online]. Available: http://www.assistdocs.com/search/document_details.cfm?ident_number=70037&StartRow=1&PaginatorPageNumber=1&doc_id=MIL–STD–1797&search_method=BASIC

[73] B. L. Stevens and F. L. Lewis, *Aircraft Control and Simulation*. New York: Wiley, 1992.

[74] E. Xargay, V. Dobrokhodov, I. Kaminer, N. Hovakimyan, C. Cao, I. M. Gregory, and R. B. Statnikov, "$\mathcal{L}_1$ adaptive flight control system: Systematic design and verification and validation of control metrics," in *Proc. AIAA Guidance, Navigation and Control Conf.*, Toronto, Canada, AIAA-2010-7773, 2010.

[75] P. Seiler, A. Dorobantu, and G. J. Balas, "Robustness analysis of an $\mathcal{L}_1$ adaptive controller," in *Proc. AIAA Guidance, Navigation and Control Conf.*, Toronto, Canada, AIAA-2010-8407, 2010.

[76] I. M. Gregory, E. Xargay, C. Cao, and N. Hovakimyan, "$\mathcal{L}_1$ adaptive control law in support of large flight envelope modeling work," in *Proc. CEAS Conf. Guidance, Navigation and Control*, Munich, Germany, 2011.

[77] J. V. Foster, K. Cunningham, C. M. Fremaux, G. H. Shah, E. C. Stewart, R. A. Rivers, J. E. Wilborn, and W. Gato, "Dynamics modeling and simulation of large transport airplanes in upset conditions," in *Proc. AIAA Guidance, Navigation and Control Conf.*, San Francisco, CA, 2005 AIAA-2005-533.

[78] K. Cunningham, D. E. Cox, D. G. Murri, and S. E. Riddick, "A piloted evaluation of damage accommodating flight control using a remotely piloted vehicle," in *Proc. AIAA Guidance, Navigation, and Control Conf.*, Portland, OR, AIAA-2011-6451, Aug. 2011.